Development of New Nanostructurally Engineered Polymer Semiconductors for Organic Electronics

by

Amani Alsam

A thesis

presented to the University of Waterloo

in fulfillment of the

thesis requirement for the degree of

Master of Applied Science

in

Chemical Engineering (Nanotechnology)

Waterloo, Ontario, Canada, 2014

AUTHOR'S DECLARATION

I hereby declare that I am the sole author of this thesis. This is a true copy of the thesis, including any required final revisions, as accepted by my examiners.

I understand that my thesis may be made electronically available to the public.

Abstract

The research presented in this thesis was focused on organic semiconductors and has resulted in the development of novel printable polymer semiconductors that can be used in organic thin film transistors (OTFTs) and organic photovoltaics (OPVs), or solar cells. Polymers used in OTFT applications must have particular characteristics, such as a highly ordered or crystalline structure, favoured molecular orientation, and appropriate energy levels for either hole transport (p-type semiconductors) or electron transport (n-type semiconductors). Achieving these properties requires control of the design and synthesis of the polymers through the choice of appropriate building blocks and side chain substituents. In contrast, for OPV applications, the band gap, thin film morphology, and balance of the donor's hole mobility and the acceptor's electron mobility must be finely tuned for optimal photovoltaic performance. The specific focus of the research was on a new type of donor-acceptor copolymers that have alternating electron-accepting azo units and common electron donor units (e.g., thiophene). These polymers are expected to have strong intermolecular interactions due to the donor-acceptor effect, which could lead to improved molecular organization for efficient charge carrier transport in OTFT devices. The donor-acceptor effect also creates narrow band gap polymers, which are preferred for optimum light harvesting. The polymer materials developed in this research are evaluated as channel semiconductors in OTFTs and can also be used as donors in polymer solar cells.

Zs discovery of which complemented previous work conducted by the same research group. These innovative building blocks would be valuable in numerous applications, including OTFTs and OPVs. Five polymers have been created, three of which show the most promising potential for OTFT and OPV applications: **P1-DTA-BTV**, **P5-DTAE-BT**, and **P6-DTAE-TT**. All of these copolymers have been synthesized via Stille coupling reaction. The first copolymer, **P1-DTA-BTV**, which exhibits a small band gap of 1.13 eV, with HOMO and LUMO energy levels of -5.21 eV and - 4.08 eV, respectively, is suitable for both OTFT devices and OPV applications. **P5-DTAE-BT** and **P6-DTAE-TT**, on the other hand, are characterized by broader band gaps of 1.29 eV and 1.32 eV, respectively, and their average HOMO and LUMO energy levels are -5.43 eV, -4.20 eV, and -5.40 eV, -4.00 eV, respectively. It has been experimentally demonstrated that the presence of an ester group in the (E)-1,2-di(thiazol-2-yl)diazene **DTA** monomer helps lower the LUMO energy level, creating the broad band gap revealed in the (*E*)-bis(2-octyldodecyl) 2,2'-(diazene-1,2-diyl)bis(thiazole-4-carboxylate) **DTAE** copolymer results, and making the **P5-**

DTAE-BT D-A copolymer an n-type semiconductor, which is very useful for the applications mentioned above. The polymers were characterized by Differential Scanning Calorimetry DSC, Thermal Gravimetric Analysis TGA, Ultraviolet-Visible Spectrometry UV-Vis, Cyclic Voltammetry CV, Atomic Force Microscopy AFM, and X-Ray Diffraction XRD.

Acknowledgements

I would like to thank my supervisor, Professor Yuning Li, for his encouragement, guidance, and invaluable assistance during my studies.

I would also like to express my gratitude to Wei Hong, Chang Guo, and Bin Sun for their help with the characterizations and device performance.

Many thanks go to Jesse Quinn, who has had great contributions to some parts of this project and provided extensive assistance in the laboratory.

I am likewise very appreciative of my review committee, Professor Neil McManus, and Professor Aiping Yu.

A own particular gratitude to my parents specially my father, a natural giver, who encouraged me to complete my studies, as well as to my brothers, Majed and Fahad, who stood by me all the way through my study and challenges, endowing me with love, confidence, and unlimited support.

I give heartfelt thanks for my family; to whom I owe more gratitude than I can ever put into words.

Among my sincere acknowledgements, the financial support I have received from the Saudi Arabian Ministry of Higher Education is highly appreciated.

I would also like to thank the other members of Professor Li's group: Mylene Le Borgne, Jane Yan, Yinghui He, and Xiang Li.

Table of Contents

List of figures

List of Schemes

List of Tables

List of Abbreviations, Symbols and Nomenclature

AFM: Atomic force microscopy

Ag: Silver

AgCl: Silver chloride

BGBC: Bottom-gate, bottom contact

BGTC: Bottom-gate, top contact

B3LYP: Becke, 3-parameter, Lee-Yang-Parr

BT: 5,5'-bis(trimethylstannyl)-2,2'-bithiophene

BT-Br: 5,5'-dibromo-2,2'-bithiophene

BTV: (*E*)-1,2-bis(3-dodecyl-5-(trimethylstannyl)thiophen-2-yl)ethene

CV: Cyclic voltammetry

D-A: Donor-acceptor

DArP: Direct Arylation Polymerization

DFT: Density functional theory

DMSO: Dimethyl sulfoxide

DPP: Diketopyrrolopyrrole

DSC: Differential scanning calorimetry

DTA: (E)-1,2-di(thiazol-2-yl)diazene

DTA-Br: (*E*)-1,2-bis(5-bromo-4-undecylthiazol-2-yl)diazene

DTAE: (*E*)-bis(2-octyldodecyl) 2,2'-(diazene-1,2-diyl)bis(thiazole-4-carboxylate)

DTAE-Br: (*E*)-bis(2-octyldodecyl) 2,2'-(diazene-1,2-diyl)bis(5-bromothiazole-4-carboxylate)

DTS: Dodecyltrichlorosilane

e^-: Electron

FET: Field-effect transistor

HOMO: Highest occupied molecular orbital

HT-GPC: High-temperature gel permeation chromatography

I_{DS}: Drain-source current

$I_{on/off}$: Current on-and-off ratio

LUMO: Lowest unoccupied molecular orbital

M_n: Number average molecular weight

M_w: Weight average molecular weight

NIR: Near infrared

NMR: Nuclear magnetic resonance

OLED: Organic light emitting diode

OPV: Organic photovoltaic

OTFT: Organic thin film transistor

PDI: Poly index

PMMA: Poly(methyl methacrylate)

RB: Round-bottom

TCE: 1,1,2,2-tetrachloroethane

TGA: Thermal gravimetric analysis

THF: Tetrahydrofuran

TT: 2,5-bis(trimethylstannyl)thieno[3,2-*b*]thiophene

UV-Vis: Ultraviolet-visible spectrometry

V_{DS}*:* Drain-source voltage

V_{GS}*:* Gate voltage

V_T*:* Threshold voltage

XRD: X-ray diffraction

λ_{max}*:* Maximum absorption (nm)

μ: Mobility ($cm^2V^{-1}s^{-1}$)

μ_e: Electron mobility ($cm^2V^{-1}s^{-1}$)

μ_h: Hole mobility ($cm^2V^{-1}s^{-1}$)

Chapter 1

1. Introduction

The development of polymers has revolutionized the Materials Science and Engineering field and has transformed chemical manufacturing processes. Recent progress in this area has led to the creation of organic electronics, which have a wide range of applications, especially in items like solar cells, sensors, memory devices, radio frequency identification (RFID) tags, and flexible displays because they can be manufactured at ultra-low costs using high-speed roll-to-roll printing technologies (Guo 2012). Organic materials offer significant opportunities for providing an impressive number of elements that can be used and/or transformed in the production of this type of electronics. The materials most critical for enabling organic electronics are organic semiconductors, which differ from inorganic materials with respect to the attractive features they provide: solution processability, low cost, light weight, and mechanical robustness (Guo 2012).

The research presented in this thesis was focused on organic semiconductors and has resulted in the development of two major building blocks that could be used in numerous applications, the most notable of which are organic thin film transistors (OTFTs) and photovoltaic (OPV) devices. These new building blocks are known as (*E*)-1,2-di(thiazol-2-yl)diazene (**DTA**) and (*E*)-bis(2-octyldodecyl) 2,2'-(diazene-1,2-diyl)bis(thiazole-4-carboxylate) (**DTAE**) and represent new electron acceptor monomers for organic electronic devices. Their structures are shown in Scheme 1.

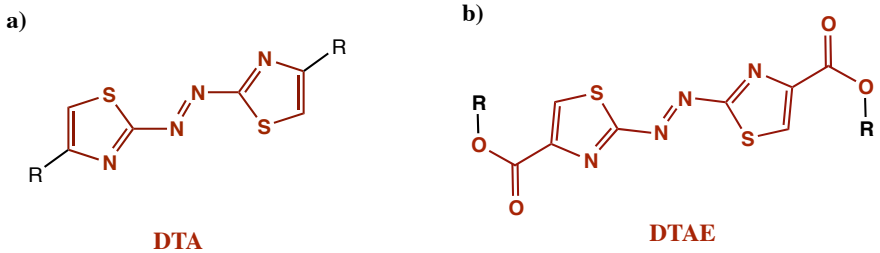

Scheme 1: Structures of a) **DTA**- and b) **DTAE**-based accepting monomers.

This thesis explains how these two new monomers have been copolymerized with common electron donors, in this case, thiophene and its derivatives, to form new polymer semiconductors that could be used as channels in transistor applications. Transistors are fundamental components of all modern electronics; those based on organic semiconductors as the active layer are referred to as organic thin film transistors (OTFTs), such as the one presented in (Li. F. 2011).

2. Organic Electronics

Organic electronics and their electrical behaviour were first investigated in the 1960s (Facchetti 2011). The term refers to electronics comprised of carbon-based materials (Li 2012). Organic electronics have their advantages and disadvantages. The disadvantages include poor crystallinity; low mobility, which translates into decreased device speeds; and possible degradation under environmental influences. However, significant advantages of organic electronics that are worth mentioning are their lightweight, mechanical flexibility, their ability to be chemically modified, and the ease and low cost of their processing for inkjet printing and spin coating. The use of organic electronics encompasses a vast range of applications, including transistors, be chemically modified (Li. F. 2011). Figure 1 illustrates the broad scope of products and technologies in which organic electronics could be used, demonstrating the importance of these elements in today's technologically advanced society.

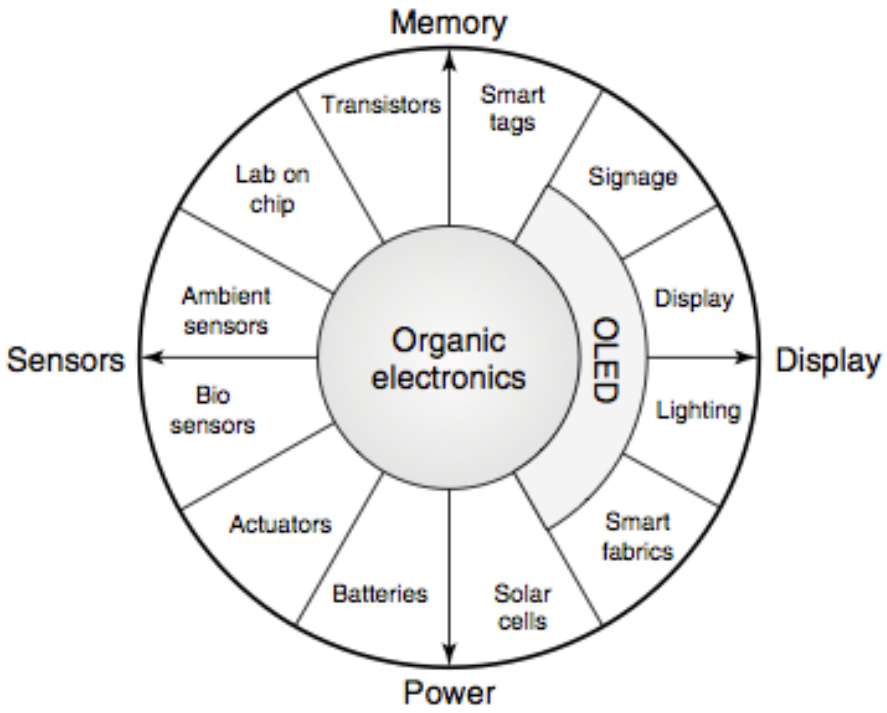

Figure 1: Broad range of products and technologies developed from organic electronics (Li. F. 2011)

The polymers produced for this thesis work are suitable for transistor applications, which is the primary research focus. However, the properties of some of these polymers also make them suitable for other applications such as organic photovoltaics (OPVs).

Organic electronics can be categorized according to two different groups; small-molecular materials such as pentacene or anthracene and polymers such as polythiophene or polyphenyen-vinylene (Li. F. 2011). This research was focused on polymer organic electronics, which can be prepared by means of solution processing, such as spin coating or inkjet printing techniques.

Several techniques are employed for printing electronics; however, the most commonly used and most popular are spin coating techniques. Since organic semiconductors are characterized by excellent printability, a spin-coating technique can be used for printing polymer semiconductors (Dimitrakopoulos 2001). Such polymers are π-conjugated polymers that consist of at least one backbone chain of alternating double and single bonds (Mehta 2011).

2.1 π -Conjugated Polymers

π - conjugated polymers can be described as organic macromolecules that have p_z-orbitals of the carbon atoms that are responsible for forming the π-orbitals of the alternating double and single bonds (Facchetti 2011). Figure 2 shows the isolated and conjugated π-bonds, which indicates that having a long π-bonds conjugated building block (red colour) facilitates an electron hopping through one bond to another in more rapid way making conjugated polymers one-dimensional semiconductors (Facchetti 2011).

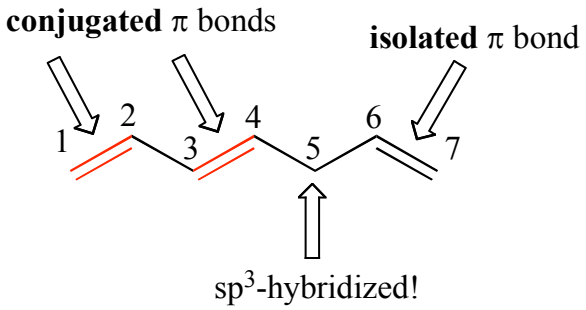

Figure 2: Conjugated and isolated π-bonds (Soderberg 2010)

2.2 The Electron Donor

Obtaining high-performance polymer materials requires the design and synthesis of conjugated polymers with ideal properties, such as low band gap to broaden the absorption range, and suitable donor-acceptor monomers. The particular donor monomers used in this study are introduced below along with the reasons for their selection (Doyle 2010).

The most common electron donors are thiophene and its derivatives: bithiophene, vinylene, and thienothiophene (Scheme 2). Extracted from petroleum or coal (Mishra 2011) thiophene groups belong to a class of heterocyclic compounds containing a five-membered ring made up of one sulphur as a heteroatom with the formula C_4H_4S. Considered to be among the best building blocks for the synthesis of D-A copolymers (Olivelli 2012), these groups have an enormous and attractive array of potential structural variations that allow electronic properties to be tuned over a wide range, which makes them high-potential candidates for organic electronics (Olivelli 2012). In addition to the stability of their chemical and physical proprieties in both conducting and semiconducting states, another reason that makes thiophenes optimal electron donors is the high degree of polarizability of their sulfur atoms, which leads to the stabilization of

the conjugated chain as well as offering highly beneficial charge transfer properties, an important crucial asset for OTFT applications (Olivelli 2012).

The electron donors selected for this research are based on thiophene groups because they offer the greatest mobility for organic semiconductor devices and because they are among the most ideal building blocks for transition metal-catalyzed cross-coupling reactions (Klauk 2006).

Scheme 2 shows the structure of thiophene, thieno[3,2-*b*]thiophene (TT), 2,2'-bithiophene (BT), and (*E*)-1,2-bis(thiophen-2-yl)ethene (BTV) electron donor building blocks.

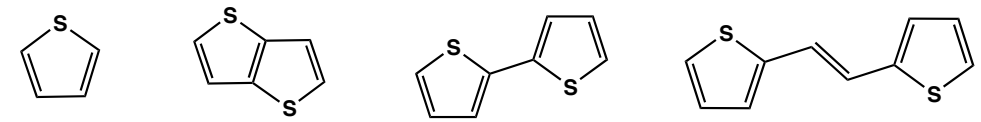

Thiophene **TT** **BT** **BTV**

Scheme 2: Structures of thiophene, thieno[3,2-*b*]thiophene (**TT**), 2,2'-bithiophene (**BT**), and (*E*)-1,2-bis(thiophen-2-yl)ethene (**BTV**) electron donor building blocks.

2.3 Electron Acceptors

An electron acceptor is an n-type organic semiconductor that enables the withdrawing of electrons. In this study, the thiazole group is employed as the primary functional group with respect to electron withdrawing moieties in conjugated polymers. These electron-accepting monomers contain an electron withdrawing azo group, which helps decrease the lowest unoccupied molecular orbital (LUMO) of the polymer, thus facilitating electron hopping within the polymer chain and increasing the intermolecular interaction between π-π polymer chains. The π-π distance in this type of polymer is known to be 4 Å (Zhao 2011). A low LUMO energy level of -4.0 eV is required for stable electron transport under ambient conditions, which is why using a group that can provide a strong electron acceptor function is important (Chen 2007). Scheme 3 illustrates two azo building blocks, **DTA-Me** and **DTAE**, used in this thesis, along with azobenzene, which was first discovered in the 19th century (Razus 2003).

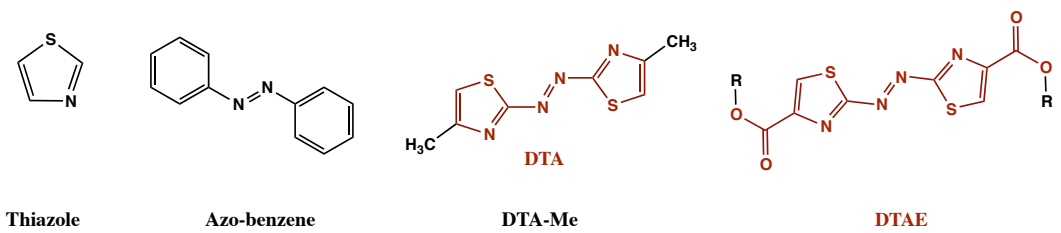

Scheme 3**:** Structures of thiazole, azobenzene, **DTA-Me**, and **DTAE** acceptor building blocks.

Making a π-conjugated polymer with azothiazole is both original and interesting. These monomers have exclusive proprieties that make them novel and easy to synthesize, as well as providing an opportunity for the *trans–cis–trans* photoisomerization of aromatic azo groups that can be induced by UV or visible light (Tanaka 2004).

In this research, **DTAE** has been developed (Scheme 3), in which an ester side chain was added to the **DTA** monomer, which was then copolymerized with an electron donor to form novel polymers with special characteristics. The synthesis of this monomer as well as the polymerization methods are explained in greater detail in Chapter 3, which also provides the characterizations of each polymer made and highlights the innovative nature of these types of π-conjugated copolymers.

2.4 Polymer Semiconductors

In the late 1980s, Nobel Prize winners Alan J. Heeger, Alan G. MacDiarmid, and Hideki Shirakawa discovered the electrical charge carrier transport in polymers (Chiang 1978), (Shirakawa 1977). The purpose of combining a donor with an acceptor is that these D-A copolymers help decrease the distance between polymer layers, thus facilitating charge hopping between polymers (Chiang 1978).

Because charge transfer and polymer chain building blocks are extremely important in obtaining high-mobility transformations, copolymerizing an electron donor with an electron acceptor helps provide an alternative building block that makes charge transfers much easier and supports decreased π-π distances, thus increasing intermolecular interaction. The synthesis of such a polymer is therefore one of the most promising strategies for achieving high-mobility conjugated polymers (Yan 2013).

Scheme 4 shows the structures of the related donor-acceptor copolymers that were used in this research and which were previously developed by Yan in 2013 (Yan 2013). However, because of the lack of pure monomers and the low molecular weight of the **DTA-BTV** polymer in the previous research, this polymer has been approached again in this study and remade with much greater purity of the acceptor monomer in order to obtain enhanced mobility as well as improved molecular weight. In a subsequent stage of this study, a new acceptor building block with an ester side chain was then designed, as shown in Scheme 5. The new polymer was created with the same donating monomers, thiophene and its derivatives, as a means of comparing it with the previously developed polymers.

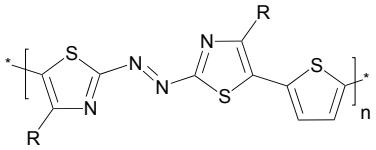

PDTAE-T

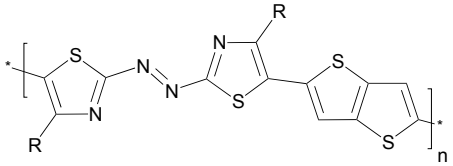

PDTAE-TT

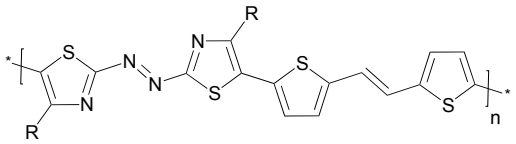

PDTAE-BTV

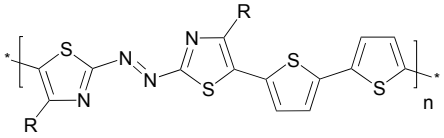

PDTA-BT

Scheme 4: Structures of the related D-A copolymers used in this thesis: P**DTA-T, PDTA-BT, PDTA-TT,** and **PDTA-BTV** (Yan 2013).

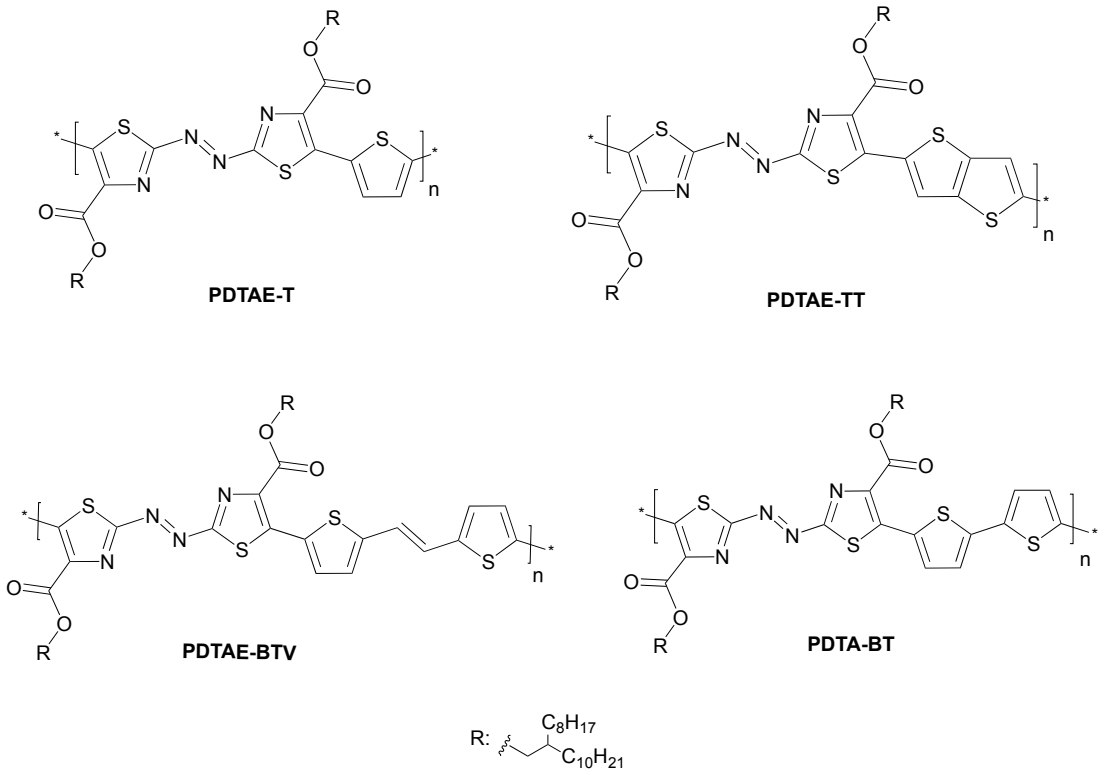

Scheme 5**:** Structure of **DTAE-**based donor-acceptor copolymers.

The copolymer developed for this thesis has much stronger electron acceptors because of the addition of an ester side chain, thus providing superior characterizations.

3. Polymerization Method Used in This Research

Numerous polymerization methods can be used for the synthesis of a D-A copolymer. However, the work presented in this thesis focused on two methods for synthesizing the π-conjugated copolymer: Stille Coupling Reactions and Direct Arylation Reactions.

3.1 Stille Coupling Reactions

The Stille coupling reaction is one of several traditional coupling methods used for the synthesis of π-conjugated polymers (Lee 2010), (Biniek 2009). Others include the Suzuki coupling reaction (Ohshita 2009), (Lee 2010); the Heck coupling reaction (Jana 2012), (Peng 2012); and the Sonogashira coupling reaction (Peyrard 2012), (Hebbar 2011). The Stille coupling

reaction has become established as one of the most general and most selective palladium-catalyzed cross-coupling reactions (Biniek 2009), (Tarkuc 2012).

John Kenneth Stille and David Milstein first introduced the Stille coupling reaction in 1977 (Lee 2010). Figure 3 illustrates the Stille coupling reaction of an organotin compound with an sp^2-hybridized organic halide catalyzed by palladium $Pd(^0)$ (Hebbar 2011), (Espinet 2004).

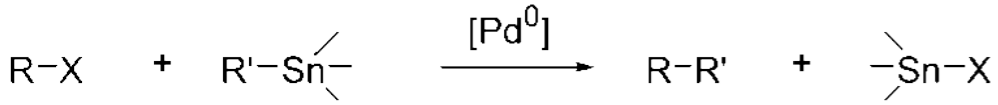

Figure 3: Stille coupling reaction (Espinet 2004).

A Stille reaction is one of the most extensively studied pathways for coupling reactions (Tarkuc 2012). One difference between the mechanism of the Suzuki method and that of the Stille coupling reaction is that the boronic acid has to be activated with a base. The activation of the boron atom facilitates transmetalation and improves the polarization of the organic ligand (Ohshita 2011). The Stille coupling reaction, on the other hand, does not require the use of a base, which makes it an effective method for synthesizing π-conjugated polymers, particularly the ones with base-sensitive functional groups (Lee 2010), (Biniek 2009).

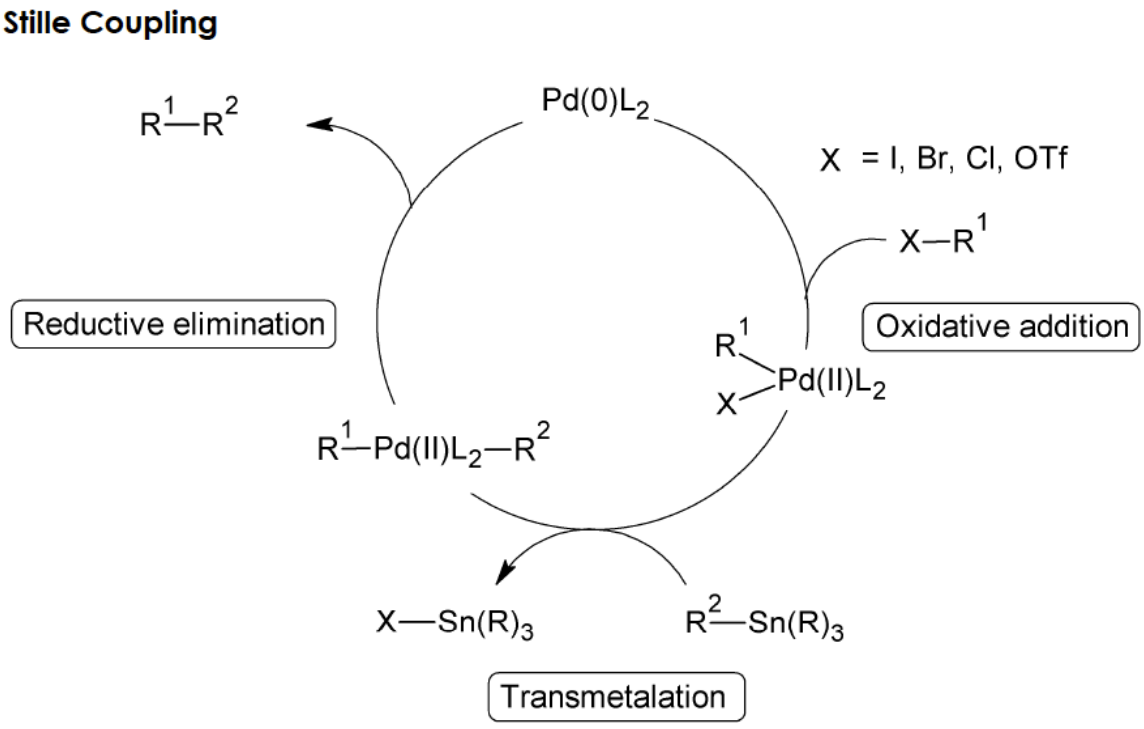

Figure 4: Mechanism of the Stille coupling reaction (Espinet 2004)

The mechanism of the Stille coupling reaction has been well studied and can be described as follows. Espinet in 2004 provided a simplified representation of the Pd-catalysed coupling of Sn with organic electrophiles, as shown in Figure 4 for the mechanism of the Stille coupling reaction. Three steps are involved: reductive-elimination, oxidative addition, and transmetalation. The transmetalation step is not entirely understandable as much as reductive elimination and oxidative addition do. (Stille 1986), (Espinet 2004). In the oxidative addition step, the palladium catalyst is reduced to the active Pd(^{0}) specie. The oxidative addition of the organohalide then provides a *cis* intermediate. This *cis* intermediate rapidly isomerized to the *trans* intermediate organostannane. Then the transmetalation with the organostannane forms intermediate, which produces the desired product and the active Pd(^{0}) species after reductive elimination. Finally, the reductive elimination and oxidative addition retain the stereochemical configuration of the respective reactants (Espinet 2004).

While the Stille coupling reaction, along with other traditional coupling methods, has been established for a long time, today's researchers have recently attempted to use other newer

methods for the synthesis of π-conjugated polymers. One of these new methods is direct arylation.

3.2 Direct Arylation

Direct Arylation Polymerization (DArP), and a catalytic C_{aryl}–C_{aryl} cross-coupling was first described by Corriu and Masse in early 1972 (Corriu 1972), when they investigated different nickel and cobalt compounds in the cross-coupling between alkenyl or aryl bromides and aryl Grignard reagents, using $Ni(acac)_2$ (Ackermann 2009).

Traditional coupling methods such as the Stille coupling reaction are not the only ones that can be used to synthesize π-conjugated polymers; an aryl-aryl coupling reaction though C-H bond activation can also be employed. Direct arylation, which could be defined as two activated arenes that can react selectively with the metal catalyst, is one of the methods increasingly being applied today for broad use in the synthesis of π-conjugated polymers (Campeau 2006). The difference between a traditional coupling reaction and direct arylation is that a direct arylation does not involve the tedious preparation of unstable toxic organometallic reagents. However, direct arylation is used primarily in the synthesis of small molecules and, until recently, has rarely been applied for the synthesis of polymers (Schipper 2011) (Campeau 2006).

Direct arylation occurs between carbon and carbon bonds (Vinyl arenes), carbon and nitrogen bonds (anilines), carbon and oxygen bonds (aryloxy), and/or carbon and hydrogen bonds (Ackermann 2009). In this research, the primary focus is the coupling reaction of an aryl halide with a simple arene for direct arylation in the presence of traditional metal catalysts and an inorganic base, such as K_2CO_3 or Cs_2CO_3. $Pd(OAc)_2$ is the one of the most common catalysts used for the synthesis of direct arylation polymers because of its strong electron-donation in the presence of N-Heterocyclic Carbene (NHC) ligands (Campeau 2006), (Schipper 2011). Figure 5 illustrates the direct arylation mechanism.

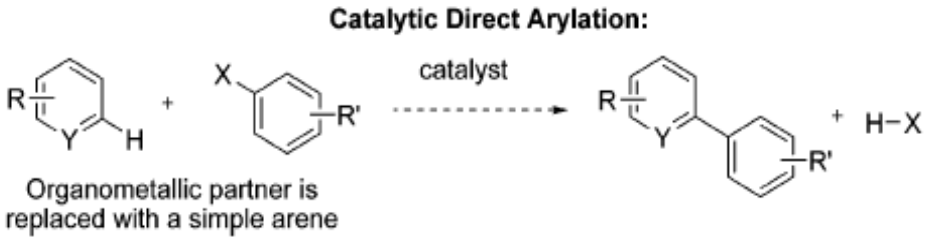

Figure 5: Mechanism of direct arylation (Campeau 2006)

However, it must be mentioned that since direct arylation is a relatively new method for the synthesis of a π-conjugated polymer, it is important to optimize reaction conditions, such as the selection of catalysts, ligands, solvents, and temperature, which could affect the final product with respect to the characteristics of the polymer products, such as yield, molecular weight (M_n), and the polydispersity index (PDI) (Schipper 2011).

Method

Two possible methodologies for direct arylation are direct arylation of simple arenes and direct arylation of hetrocyclic arenes. (Wang 2013), (Campeau 2006).

Direct arylation of simple arenes were first discovered by Ames and Bull (Ames 1982) when they observed an interesting side reaction while attempting a Heck reaction with bromocinnolines (Campeau 2006). Direct arylation of the pendant phenyl ring occurred when they were making a five-membered ring direct arylation product as shown in Figure 6

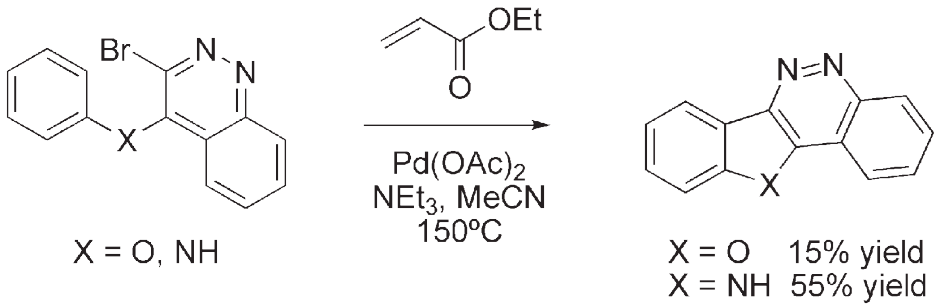

Figure 6: Ames' first examples with simple arenes (Campeau 2006)

Then in 1997, Rawal, Hennings, and coworkers (Hennings 1997) determined that the formation of six-membered ring benzopyrans is problematic. They used substrates bearing a phenol functionality that becomes deprotonated under the reaction conditions, which generates a more reactive coupling partner to avoid the lower nucleophilicity of simple arenes in these reactions (Campeau 2006). Figure 7 shows Rawal's anion-acceleration interamolecular direct arylation with reaction conditions.

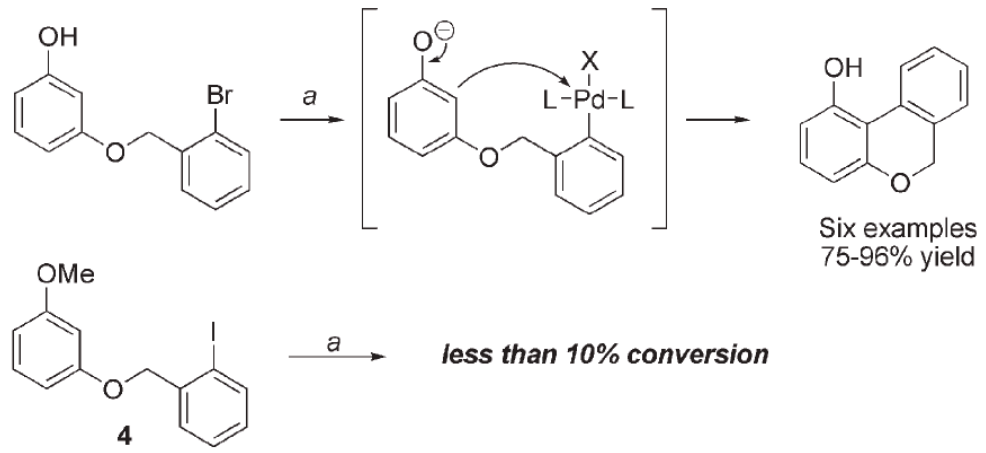

Figure 7: Rawal's anion-accelerated intramolecular direct arylation (Campeau 2006)

Reagents and conditions: (a) $Pd(OAc)_2$ 5 mol%, $(o\text{-tolyl})_3P$ 5 mol%, Cs_2CO_3 (3 equiv.) in DMA, 85–115 ^oC (Campeau 2006)

Direct arylation of hetrocyclic arenes was discovered by Aoyagi et al. (Aoyagi 1992), who confirmed that by using 2-chloro-3,6-dialkylpyrazines, N-substituted indoles could be arylated selectively at the 2-position (Campeau 2006), (Figure 8).

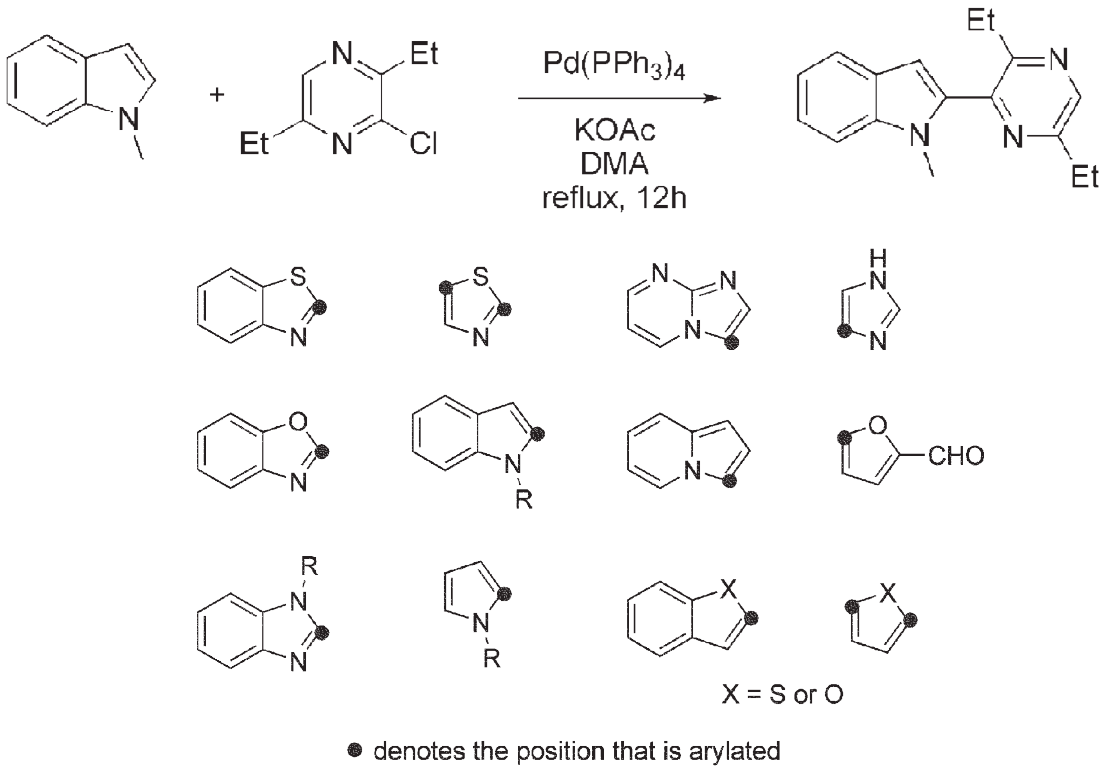

Figure 8: Examples of heteroaromatic compounds used in direct arylation (Campeau 2006)

Although simple arenes are much less reactive than the heteroaromatic counterparts in direct arylation reactions, which is attributable to the diminished nucleophilicity, significant advances in both intra- and intermolecular direct arylation reactions were made (Campeau 2006). The used of direct arylation polymerization (DArP) for the synthesis of D-A copolymers has been found in recent published papers such as the report by Rudenko and Wiley in 2013 (Rudenko 2013), who prepared a (P3HT) copolymer with a high yield of 60%, and a molecular weight of 20 kDa, polydispersity of 2.8. Mercier also used direct (hetero) arylation polymerization for the synthesis of three polymers (P3HT, PEDOT, and PProDOT) in 2012 (Mercier 2012), and Antonio Facchetti in 2012 also used a DArP method for the synthesis of a π-conjugated polymer based on the copolymerization of five-membered hetero-cycles such as poly(thiophene)s, and arylenes such as poly[naphthalenebis(dicarboxiimide)]s (Facchetti 2012).

Conjugated polymers made through these two methods, Stille coupling reaction and direct arylation reaction, are useful for channel electron transfer in sensors, batteries, switches, or displays. These conjugated polymers could be also used for a variety of electronic devices, such as organic light-emitting diodes (OLEDs) (Kulkarni 2006), (Chen 2004), organic photovoltaic devices (OPVs) (Blouin 2008), (Biniek 2009), and organic thin film transistors (OTFTs) (Kang 2010), (Ortiz 2010), for which they offer reduced costs and broad applicability. While OTFT device applications are the primary focus of this research, it is worth mentioning that the conjugated polymers developed during the work presented in this thesis can also be used for OPV applications because of their small band gap.

4. Organic Thin Film Transistors

The use of transistor technology has become significantly more widespread, partly because of substantial advances in materials such as organic thin film, which have facilitated the printing of electronic materials on flexible sheets such as plastic, metal, or even paper, enabling them to be bent, twisted, and folded (Li 2011). The type of transistors used in these applications is called organic thin film transistors (OTFTs). These developments have led to increased use of such materials and have also opened up significant opportunities for applications in products such as televisions and mobile phones, where they offer the advantage of lower costs than most

traditional methods (Liu 2010). Figure 9 shows examples of specific applications in which OTFTs are currently used.

Figure 9: Examples of commercial OTFT applications (Li. F. 2011)

An OTFT is an electronic valve or switch through which the current flows between the source and drain electrodes and is controlled by an electric field applied at the gate. The charge flow and semiconductor channel in the transistor can be dominated by holes (positive charges) in a p-type semiconductor, or electrons (negative charges) in an n-type semiconductor, or even holes and electrons together, which are defined as ambipolar semiconductors (Pu 2010), (Vachal 2004) (Yan 2013).

4.1 Structure

An OTFT consists of drain, source, dielectric, gate, and semiconductor layers. The operating mechanism of these devices starts with the application of one voltage between the source and the drain V_{sd}, as shown in Figure 10, and another voltage between the source and the gate V_{gs} (Olivelli 2012).

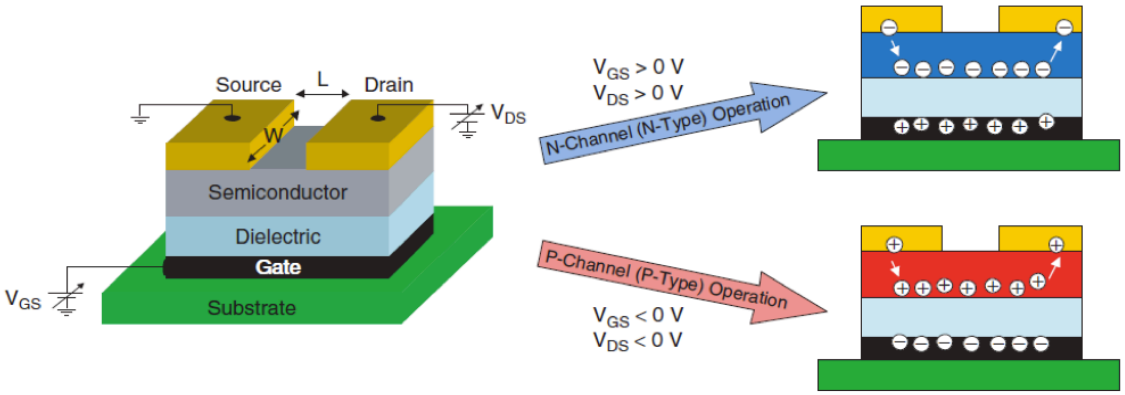

Figure 10: Schematic of a bottom-contact, bottom-gate OTFT with n and p types of semiconductors (Olivelli 2012)

The most common type of transistor is the thin film transistor (TFT). Thin film transistor is a three-terminal device composed of drain, source, gate electrodes, a dielectric (insulating) layer, and a semiconducting layer (Facchetti 2013) (Guo 2012), (Li 2012).

Two types of OTFT structures are standard used. One is called bottom-gate, bottom-contact (BGBC), and another is designated as bottom-gate, top-contact (BGTC) (Figure 11). The difference between these two devices is that in the top-contact organic thin film transistor (OTFT), the source and drain contacts are at the top of the organic semiconductor bottom-contact configuration (Figure 11 (a)), while in bottom-contact, the semiconductor layer is established on top of the source and drain contacts as showing in (Figure 11 (b)). However, the gate electrode is at the bottom of the dielectric insulating layer in both device configurations (Thompson 2008), (Li 2010), (Yan 2013).

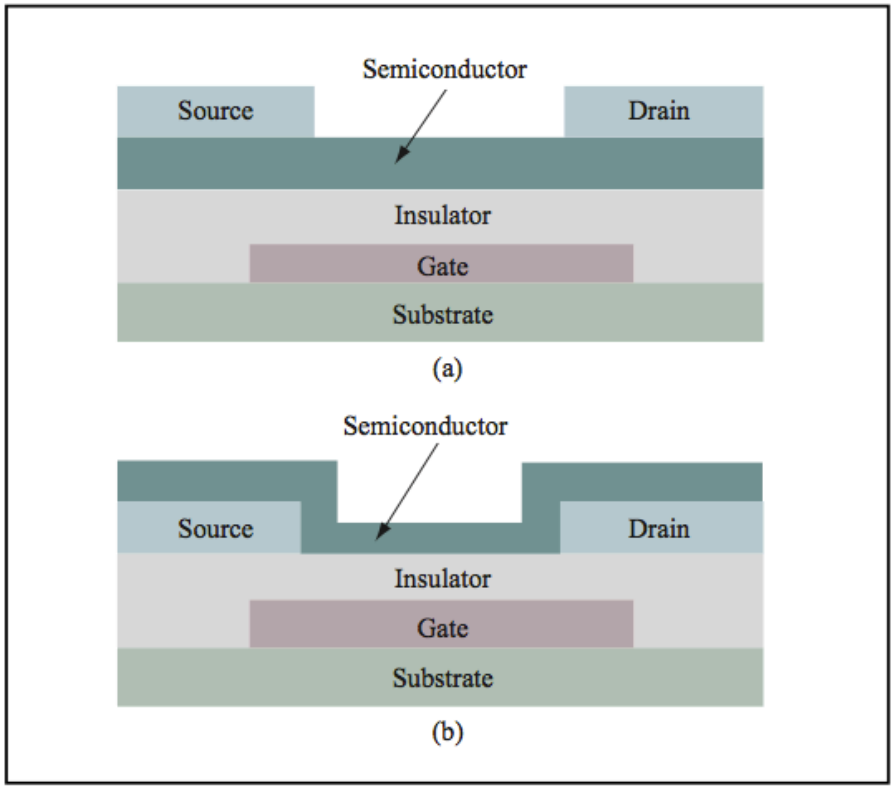

Figure 11: Thin film transistor (TFT) device configurations: a) Bottom-gate, top-contact (BGTC) device, with the organic semiconductor deposited on top of the dielectric and the pre-patterned source and drain electrodes; b) Bottom-gate, bottom-contact (BGBC) device, with the source and drain electrodes deposited on top of the organic semiconductor through a mask (Dimitrakopoulos 2001)

4.2 Performance

The ideal output and transfer curves for an OTFT can be explained as follows. When the performance of an OTFT device is evaluated, three main parameters are considered. The first is mobility (μ), which measured in m^2/Vs. Mobility (μ) describes how smoothly the charge carriers (electrons or holes) can move within a building block or material when subjected to an electric field. Mobility levels that are commonly produced are in the order of 10^{-1} m^2/Vs, which leads engineered researchers and companies producing mobility levels equal or close to 1 m^2/Vs (Dimitrakopoulos 2002). The second parameter is the on/off ratio (I_{on}/ I_{off}). This ratio measures the relative difference in the source-drain current at two fixed gate voltages, which are usually 0 V and 20 V. (Corporation 2012) (Li 2010), (Yan 2013). This ratio is usually 10^6 which is

preferable for most applications (Dimitrakopoulos 2002). The final parameter is the turn-on voltage (V_{on}). This parameter classifies which gate voltage the transistor switches on or off when the device requires a voltage bias. Turn-on voltage (V_{on}) is measured in volts and the ideal V_{on} is 0 V (Yan 2013), (Li 2011), (Li 2010).

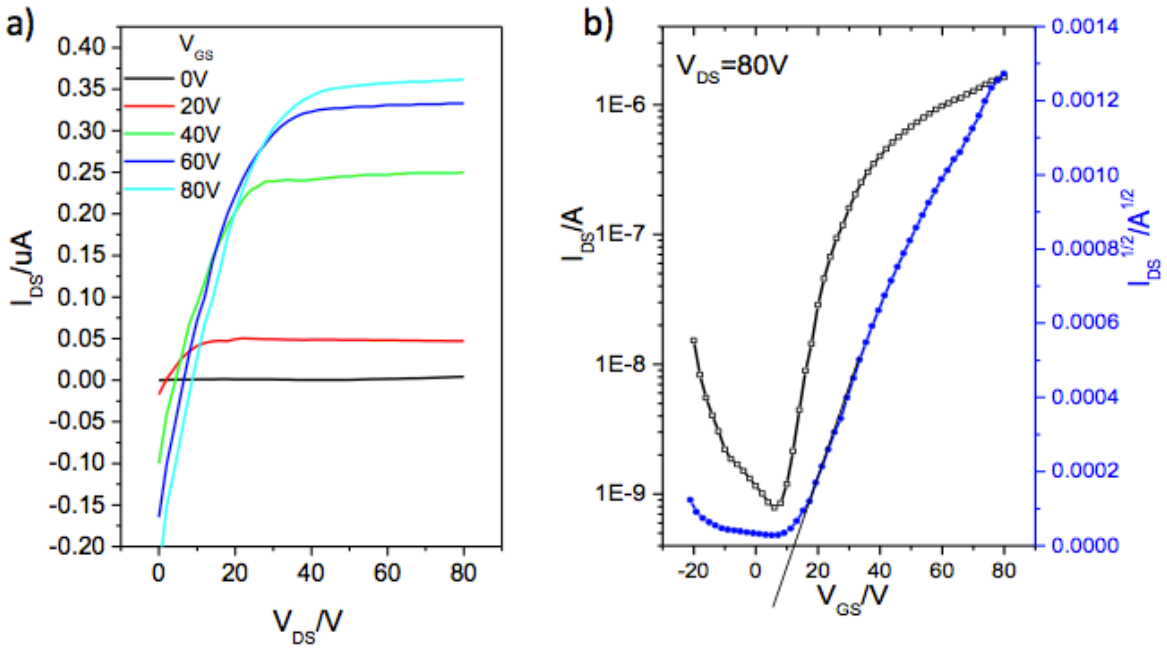

Figure 12: Characterization curves: (a) output characteristics (drain-source current, I_{DS}, vs. drain voltage, V_{DS}); (b) transfer characteristics (I_{DS} vs. gate voltage, V_{GS}) from a bottom-gate, bottom-contact (BGBC) PMMA-encapsulated OTFT device fabricated with an n-type thin film semiconductor. Device dimensions: channel length L = 30 μm; channel width W = 1000 μm (Yan 2013)

Figure 12 shows the ideal output characterization curve plots for the drain-source current, I_{DS} versus the drain voltage V_{DS} for a variety of gate voltages V_{GS}. When the V_{DS} is increased, the I_{DS} also increases and can be measured based on the following equations (Tecklenburg 1998), (Yan 2013):

$$I_{DS} = \frac{WCi\mu}{L}\left(V_{GS} - V_T - \frac{V_{DS}}{2}\right)V_{DS} \qquad (1)$$

$$I_{DSsat} = \frac{WCi\mu}{2L}(V_{GS} - V_T)^2 \qquad (2)$$

$$\sqrt{I_{DSsat}} = \sqrt{\frac{WCi\mu}{2L}} = (V_{GS} - V_T) \qquad (3)$$

where L is the channel length, W is the channel width, C_i is the capacitance per unit area of the dielectric, V_T is the threshold voltage, and μ is the mobility (Allard 2008) (Yan 2013). The drain-source current I_{DS} can then be calculated according to equation (**2**) (Tecklenburg 1998).

For the transfer characterization curve (Figure 12 (b)), however, the I_{DS} is plotted versus the V_{GS} at a constant V_{DS} within the saturated regime. If equation (2) is rewritten as equation (3), the mobility can thus be calculated from a determination of the slope of the straight line between V_{GS} and $\sqrt{I_{DSsat}}$. The threshold voltage in the other hand can be obtained from the extrapolation of the line to a zero current (Inganas 2010), (Scharber 2006), (Tecklenburg 1998), (Yan 2013).

5. Project Scope and Objectives

The goals of the research presented in this thesis were (i) to improve the mobility of previous developed polymers by increasing purity of the monomer, (ii) to increase the molecular weight of a polymer consisting of an azo-group accepting monomer and a thiazole donor, and (iii) to lower the LUMO energy level of a polymer semiconductor to facilitate electron injection. Achieving these goals required a strong electron-deficient acceptor; an ester group was therefore added to a polymer and an n-type polymer was observed. The final objective of this project was thus to develop novel electron acceptor building blocks for use in the construction of D-A copolymers with existing electron donors. The work was aimed not just at producing high-end products but rather at capturing the low-cost feature of organic materials and exploring new applications that have been inaccessible with traditional materials.

Chapter 2

DTA-Based Donor-Acceptor Copolymers for OTFTs and OPVs

1. Introduction

When it was first discovered, the azo group was used in dyes because a variety of colours can be obtained from suitable substitutions of the aromatic rings (Zollinger 1987), (Cojocariu 2004). The study of azo-group compounds has expanded in recent years. In 2012, Tseng et al used azobenzene and its derivatives as a hybrid double floating gate to induce electric bistability in pentacene thin-film transistors or in memories with enhanced response and retention, as well as memory windows (Tseng 2013). However, the use of azo groups as semiconductor polymers had not been previously reported until 2013, when Z. Yan, a student of Professor Li's group, tried to synthesize novel D-A copolymers using azo groups; however, her work was not totally finished, so herein came the initiative to complete it and there was a good deal investigation of enhanced results from the use of azo-group compounds as semiconductor channels in OTFT applications. The study of this novel monomer proved interesting and involved its copolymerization with other electronic donors to form new polymers for use in OTFTs at a lower cost and with improved benefits for industrial production.

This chapter presents this new monomer design, explains its use as an electron acceptor monomer in the synthesis of a D-A copolymer, provides characterizations of this polymer, and suggests possible applications.

2. Molecular Design

Building on the previous work, the electron acceptor monomer was recreated with much enhanced purity through the recrystallization of the monomer in methanol three times. The ^{1}H NMR data show a pure monomer, which proved advantageous for increasing the mobility of the polymer in subsequent phases of the research.

2.1 Computer Simulations

Producing the monomer began with computer simulations of the 1,2-bis(5-bromo-4-undecylthiazol-2-yl)diazene (**DTA**) accepting monomer in order to determine the highest

occupied molecular orbital (HOMO) and the lowest unoccupied molecular orbital (LUMO) energy levels of the azo-monomer as produced by computer simulation. The results showed -6.87 eV, and -3.62 eV, respectively, for these two energy levels (Figure 13) (Yan 2013).

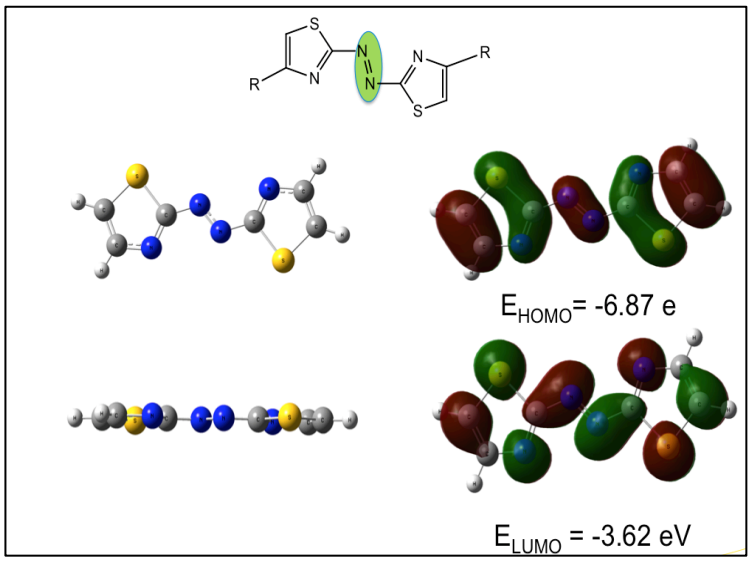

Figure 13: The structure of **DTA** and its HOMO/LUMO orbitals, and the HOMO/LUMO energy levels calculated with respect to vacuum (0 eV) (Yan 2013)

However, the computer simulation shows different energy levels for the **PDTA-BTV** polymer using the same acceptor monomer (**DTA**): -5.96 eV for the HOMO and -3.53 eV for the LUMO energy levels (Yan 2013) .

Also simulated was the polymer in this case, **PDTA-BTV,** which was the polymer focused on for resynthesis because it provided the most promising results in the previous work, in which it showed a mobility value of 1.5 x 10^{-3} cm^2 $V^{-1}s^{-1}$, higher than other polymers that were reported in the previous work: **PDTA-T**, **PDTA-TT**, and **PDAT-BT** (Yan 2013). The strectures of these polymers are showing in Scheme 4.

Figure 14 discloses the HOMO and LUMO energy levels of the polymer repeat unit by computer simulation.

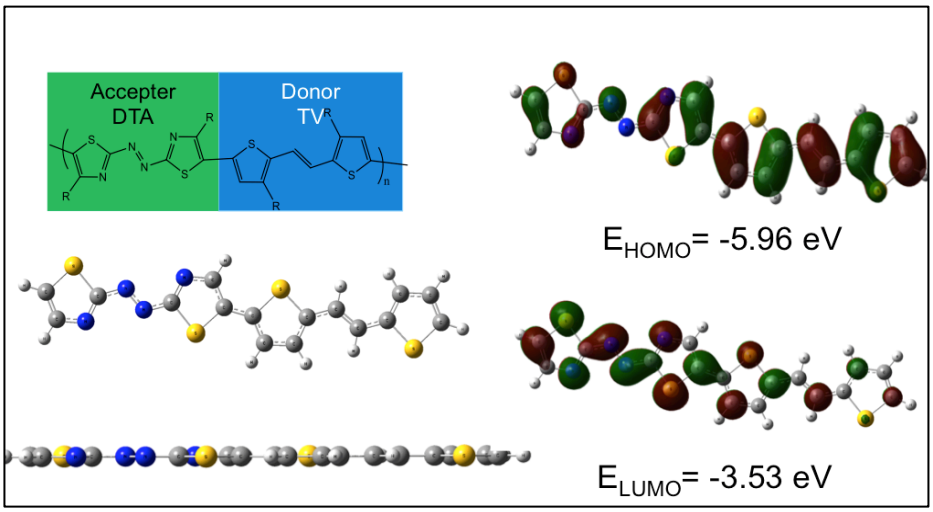

Figure 14: The structure of **P1-DPA-BTV** and the HOMO/LUMO orbitals, and the HOMO/LUMO energy levels of the polymer repeat unit calculated with respect to vacuum (0 eV) (Yan 2013)

For this thesis work, the objective of remaking this monomer was to improve the molecular weight and the mobility of the polymer, which was ultimately achieved by the end of the study. The following subsections explain the method used and demonstrate the success of the study by providing the data resulting from the device characterization.

3. Synthesis of the DTA Monomer

The synthesis of the **DTA** monomer was relatively straightforward because of its previous synthesis, and I followed the same procedure but with the addition of purification step and the use of a different solvent, where methanol was used instead of ethanol as explained in the following paragraph (Yan 2014).

Scheme 6 outlines the synthesis of the **DTA** (E)-1,2-di(thiazol-2-yl)diazene monomer prepared via the brominating of the corresponding methyl ketone. The brominating of tridecan-2-one gives a 78 % yield of white crystal boundary precipitation of 1-bromotridecan-2-one (**1**), which was first purified through column chromatography and then reacted with hydrazine-1,2-bis(carbothioamide) to save a 77 % yield of 1,2-bis(4-undecylthiazol-2-yl)hydrazine-2HBr (**2**) (Yan 2013). This reaction was followed by the oxidation of the monomer using sodium nitrite in

a water solution to obtain a 1,2-bis(4-undecylthiazol-2-yl)diazene compound (**3**). Compound (**3**) was brominated at 0 ^{o}C to minimize the brominating of the alkyl side chain and then purified through column chromatography to obtain a 38 % yield of the final orange solid product 1,2-bis(5-bromo-4-undecylthiazol-2-yl)diazene (**4**). Recrystallization of the final monomer, compound (**4**), in methanol three times was necessary in order to produce a pure product, which was the extra accomplishment beyond the work other researchers had previously reached. The importance of recrystallization in this phase is to ensure a high purity of the monomer because of the Stille coupling reaction requirement for a pure monomer to react with the donor derivative (Carsten 2011).

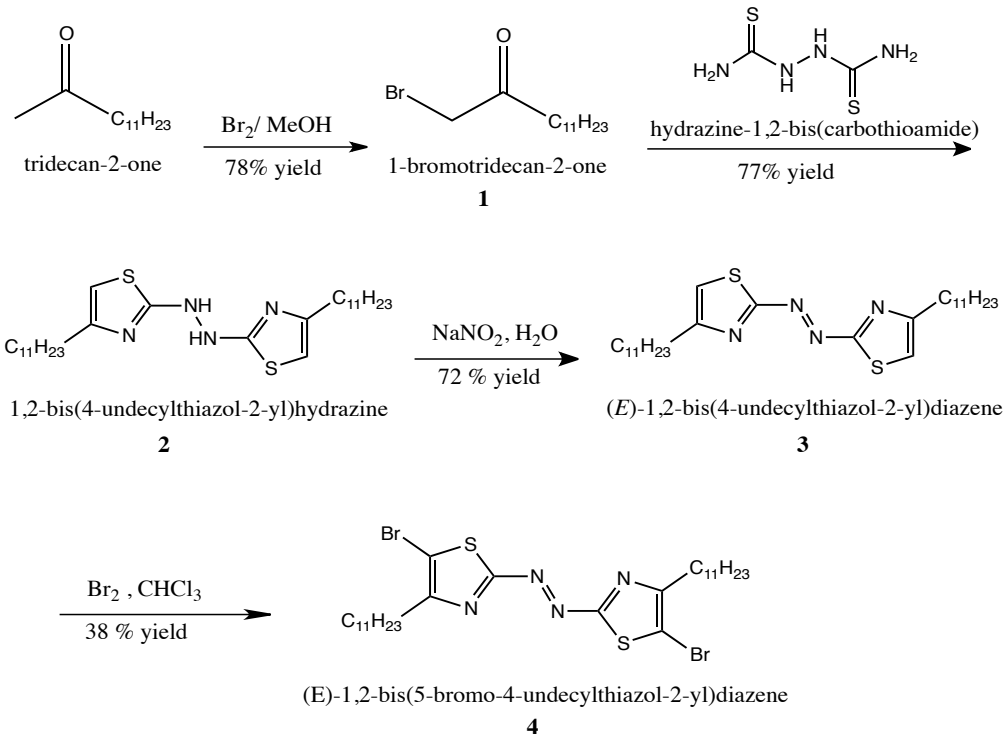

Scheme 6: Synthesis of the **DTA** monomer (Yan 2013).

4. Synthesis of the P1-DTA-BTV Polymer

Previous work has experimentally shown that the Stille coupling reaction is the best method for the synthesis of the **P1-PDA-BTV** polymer (Yan 2013). The strong intermolecular reaction between the donor BTV and the acceptor **DTA** helps decrease the π-π distance between

the D-A polymer, which facilitates the charge transport in the polymer. The compound (**4)** (**DTA**) electron-acceptor was copolymerized with an (*E*)-1,2-bis(3-dodecyl-5-(trimethylstannyl)thiophen-2-yl)ethane electron-donor in chlorobenzene catalyzed by $P(o\text{-tolyl})_3$ and $Pd_2(dba)_3$ to form the **P1-DTA-BTV** polymer via a Stille coupling reaction (Scheme 7).

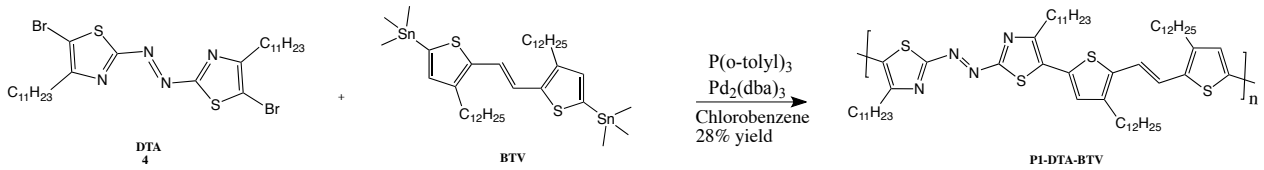

Scheme 7: Synthesis of **P1-DTA-BTV** via Stille coupling.

The polymer was purified though Soxhlet extraction using methanol, hexane, and chloroform. This polymer shows excellent solubility in chloroform with insignificant solubility in hexane. The difference between this polymer and the others made by Yan in 2013 (Yan 2013) is that this one shows substantial improvement with respect to yield and mobility. The yield was increased by ten times, and the mobility was significantly greater. The mobility of the previous polymer was about 1.5 x 10^{-3} cm^2 $V^{-1}s^{-1}$ and $I_{on/off}$= ~ 10^3 - 10^4 (Yan 2013), whereas the new polymer obtained a high mobility of 5.5 x 10^{-3} $cm^2V^{-1}s^{-1}$ ($I_{on/off}$= ~10^6).

P1-DTA-BTV was characterized by GPC, UV-Vis, CV, DSC, TGA, AFM, and XRD as well as through device performance.

5. Characterization

For all characterization methods, a brief introduction about the device is provided, along with an explanation of the measurement conditions or experimental setup and a report of the final results. It should be noted that UV-Vis is used for determining the band gap (the difference between the HOMO and LUMO energy levels) of this type of polymer whereas CV is used for studying the electrochemical behaviour (HOMO and LUMO energy levels). Both DSC and TGA are used for assessing the thermal stability of this type of polymer, XRD and AFM are used for examining its crystallinity, and an OTFT device is used for measuring the mobility, as explained below with supported references.

5.1 Gel Permeation Chromatography

5.1.1 Introduction

Gel Permeation Chromatography (GPC) is the most powerful technique for measuring molecular weight averages (M_W), as well as the full molecular weight distribution (*MWD*) or molecular number averages (M_n) of a polymer and poly dispersity index (PDI) (Dong 2006), (Houlgate 1999).

5.1.2 Measurement Conditions

GPC elution profile for the polymer created in this research were performed on a Malvern 350 HT-GPC system using 1,2,4-trichlorobenzene as an eluent and polystyrene as the standard at a column temperature of 140 ºC.

5.1.3 Results

The GPC measurement graph (Figure 15) shows a number average molecular weight (M_n) and a weight average molecular weight (M_w) for **P1-DTA-BTV** of 4.1 kDa and 8.4 kDa, respectively, and a PDI of 2.07.

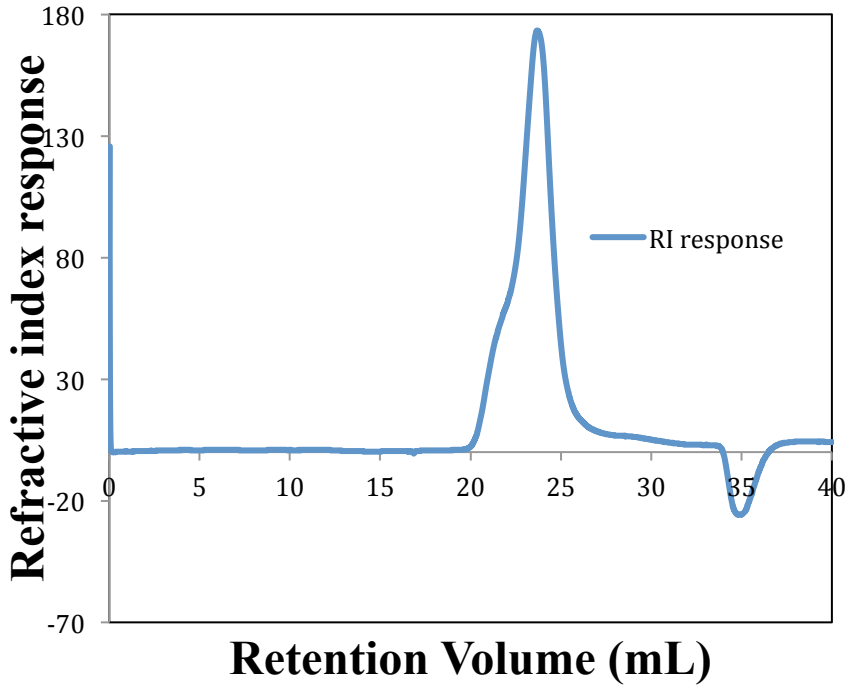

Figure 15: GPC measurements for **P1-DTA-BTV**

5.2 Ultraviolet-Visible Spectrometry

5.2.1 Introduction

UV-Vis spectroscopy was first discovered in the 1940s by Cary and Beckman (Prevatt 2004), (Qi 2010). The visible light range wavelength is known to be from 400 nm to 750 nm (Biesheuvel 2012). UV-Vis can be used to study molecules and their electronic transitions; the operating principle is dependent on the energy absorbed, which corresponds to the amount necessary to promote the movement of an electron from one orbital to another (Prevatt 2004).

The band gap is calculated using Planck's equation, as follows (Kakiuchi 1998):

$$\mathbf{E_g^{opt} = h\,\nu} \qquad (4)$$

where **h** is the Planck constant = 4.13×10^{-15} eV.s, and **ν** is the frequency defined as the number of wave cycles that travel past a fixed point per unit of time (second, or Hertz (Hz)), which has the following relationship with the wavelength (Li 2012):

$$\lambda = c / \nu \qquad (5)$$

The band gap equation then can be written as

$$\mathbf{E_g^{opt} = h}\, c / \lambda \qquad (6)$$

where c is the speed of light = 2.998×10^{8} m/s, and **λ** is the wavelength (onsite wavelength), which is found from a graph as the distance between adjacent peaks or troughs in the travelling electromagnetic wave and can be designated in meters, centimeters, or nanometers (10^{-9} meters) (Dietrich 1994), (Spectronic 2012), (Alupoaei 2005), (ElBatal 2011).

5.2.2 Measurement Conditions

UV-Vis spectra were recorded on a Thermo Scientific model GENESYSTM 10S VIS spectrophotometer.

5.2.3 Results

The UV-Vis-NIR spectra for **P1-DTA-BTV** were obtained for both a drop-cast film and a chloroform solution of the polymer (Figure 16). In the chloroform solution, **P1-DTA-BTV** exhibited maximum absorption (λ_{max}) at 778 nm. The **P1-DTA-BTV** thin film showed broader absorption with a blue shift in the λ_{max} but a red shift of ~350 nm in the onset wavelength. In solid state, **P1-DTA-BTV** showed maximum absorbance at 754 nm and onset absorption at

~1100 nm. The optical band gap of the polymer was then calculated to be 1.13 eV. This small band gap is due to the strong intramolecular and intermolecular D-A interactions as well as the extended π-conjugation along the polymer backbone. This ideal optical band gap is useful for OTFT and OPV applications as well as for facilitating effective light harvesting in organic solar cells (Yan. Z. 2013).

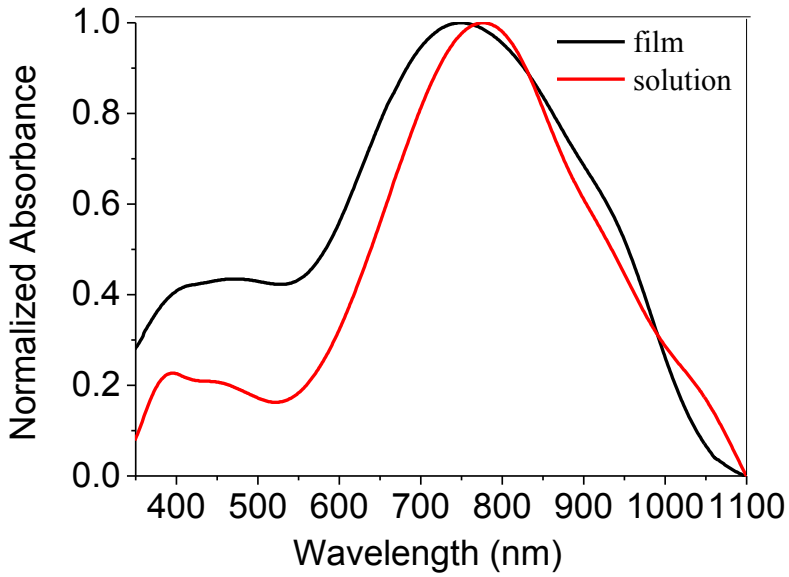

Figure 16: UV-Vis-NIR absorption spectra of **P1-DTA-BTV** in a solution of chloroform ($CHCl_3$) and in a thin film

5.3 Cyclic Voltammetry

5.3.1 Introduction

CV is a powerful technique for investigating the electrochemical properties of a polymer (the HOMO and the LUMO energy levels of the polymer) (Steckler 2009), (Li 2012), (Zhu 2006).

5.3.2 Measurement Conditions

Cyclic voltammograms were acquired with a Digi-Ivy model DY2111 Potentiostat using a platinum foil counter electrode, a platinum diskworking electrode, and an Ag/AgCl reference electrode (Yan. Z. 2013). The polymer film coating was applied on the working electrode by drop-casting a polymer solution (Lee 2011). CV measurements were collected in 0.1 M of tetrabutylammonium hexafluorophosphate in dry acetonitrile using a ferrocene/ferrocenium (Fc/Fc+) coupling as a standard at a scan rate of 50 mV s^{-1} (Zhu 2006), (Chen 2007), (Yan 2009).

The HOMO energy levels were calculated as follows:

$$\mathbf{E_{HOMO} = - (E_{ox} - E_{FC/FC+}) - 4.80\ eV} \qquad \mathbf{(7)}$$

where $\mathbf{E_{ox}}$ and $\mathbf{E_{FC/FC+}}$ are the onset oxidation potentials for the polymer sample and ferrocene versus the Ag/AgCl reference electrode, and -4.80 eV is the HOMO energy level of the ferroncene with respect to the vacuum level (0 eV) (Kumada 1968), (Shafiee 2011), (Bürgi 2008).

The LUMO energy level can be calculated using the same equation but from the perspective of $\mathbf{E_{red}}$ instead of $\mathbf{E_{ox}}$, as follows (Li 2012):

$$\mathbf{E_{LUMO} = - (E_{red} - E_{FC/FC+}) - 4.80\ eV} \qquad \mathbf{(8)}$$

The LUMO energy level can also be calculated using the HOMO energy level and band gap (Kakiuchi 1998), (Dandrade 2005):

$$\mathbf{E_{LUMO} = - E_{HOMO} + E_g^{opt}} \qquad \mathbf{(9)}$$

5.3.3 Results

The CV investigation of the electrochemistry of **P1-DTA-BTV** produced the following results (Figure 17). From the CV oxidation onset potential, the HOMO energy level of **P1-DTA-BTV** was determined to be -5.21 eV. Based on the optical band gap and the HOMO energy level, and the LUMO energy level was determined to be -4.08 eV. **P1-DTA-BTV** was predicted to be a hole-transporting (p-type) polymer semiconductor because a repeatable oxidation current with two oxidation peaks was observed and a weak reduction current was measured.

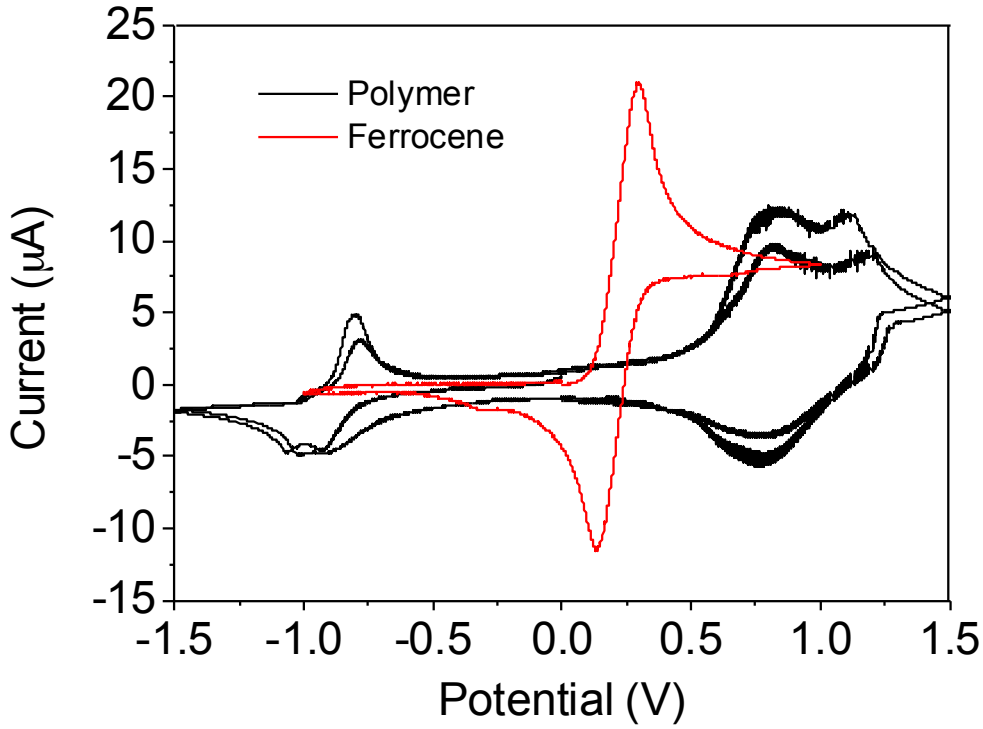

Figure 17: CV results (two cycles) for a **P1-DTA-BTV** thin film showing two oxidative and reductive cycles at a scan rate of 0.05 V s-1. The electrolyte was 0.1 M tetrabutylammonium hexafluorophosphate in anhydrous acetonitrile

The CV graph shows that $E_{FC/FC+}$ has a number of 0.01 and the E_{OX} = 0.51 eV. Calculations using equation (**7**) produce -5.21 eV for the HOMO. For the LUMO, the same number is calculated for $E_{FC/FC+,}$ but the E_{red} is 0.71 eV. Therefore, using equation (**8**) results in E_{LUMO} being equal to -4.08 eV. However, if the LUMO energy level is calculated from the band gap, the E_{LUMO} = -4.08 eV.

5.4 Differential Scanning Calorimetry

5.4.1 Introduction

To study the phase transition property of polymers, researchers use DSC analysis, which is a highly effective technique for analyzing thermal behaviour. DSC was developed in 1962, and then used in biochemistry in 1975 by P.L. Privalov *et al*; (Privalov 1975) it was also used to measure energy directory and heat capacity (Wunderlich 1990), (Dahimi 2014).

Differential Scanning Calorimetry (DSC) measures the heat flows and temperatures associated with transition in materials as a function of time and temperature in a controlled atmosphere, which provides information about endothermic or exothermic processes (Bhadeshia 2012), (Johnson 2010). Endothermic is the heat flow into the sample whereas exothermic is the heat flow out of the sample (Wunderlich 1990) (Dahimi 2014).

5.4.2 Measurement Conditions

The measurement of phase transition property of this polymer (**P1-DTA-BTV**) was performed with a heating rate of 10 °C/min under N_2. Bottom: DSC curves with a heating rate of 10 °C.min^{-1} under nitrogen.

5.4.3 Results

DSC analysis of **P1-DTA-BTV** revealed a small endothermic peak from 48 ^{o}C to 50 ^{o}C and a prominent exothermic pick from 190 ^{o}C to 220 ^{o}C in the first heating scan due to the degradation of **P1-DTA-BTV**. However, no exothermic peak resulted from the melting of the crystalline domains during the second heating scan (Figure 18).

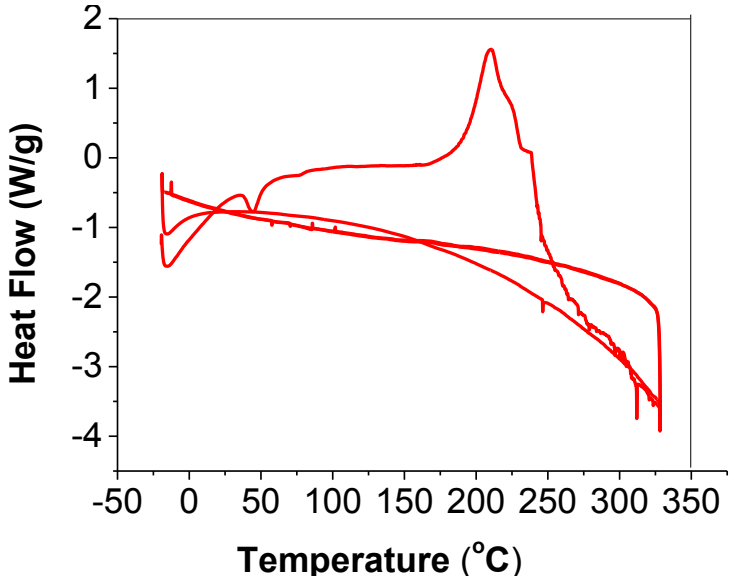

Figure 18: DSC profiles of **P1-DTA-BTV** obtained at a scanning rate of 10 °C.min^{-1} under N_2

5.5 Thermal Gravimetric Analysis

5.5.1 Introduction

TGA is a fundamental laboratory tool used for measuring mass and studying thermal behaviour when the weight of such materials increases or decreases and for selecting a temperature program in a specific atomizer. This tool has been manufactured for thermal analysis since 1960 (Mumpton 1960). Its measurements are based on the mass loss of the materials as a function of temperature (Skoog 1998).

5.5.2 Experimental Setup

TGA measurements for **P1-DTA-BTV** were obtained using a TGA Q500 (TA Instruments) at a heating rate of 10 °C/min under nitrogen.

5.5.3 Results

The graph of the TGA results shown in Figure 19 reveals a 5 % weight loss at 237 ^{o}C for the polymer **P1-DTA-BTV**, which means that this polymer is relatively stable with respect to thermal behaviour when a high temperature is applied.

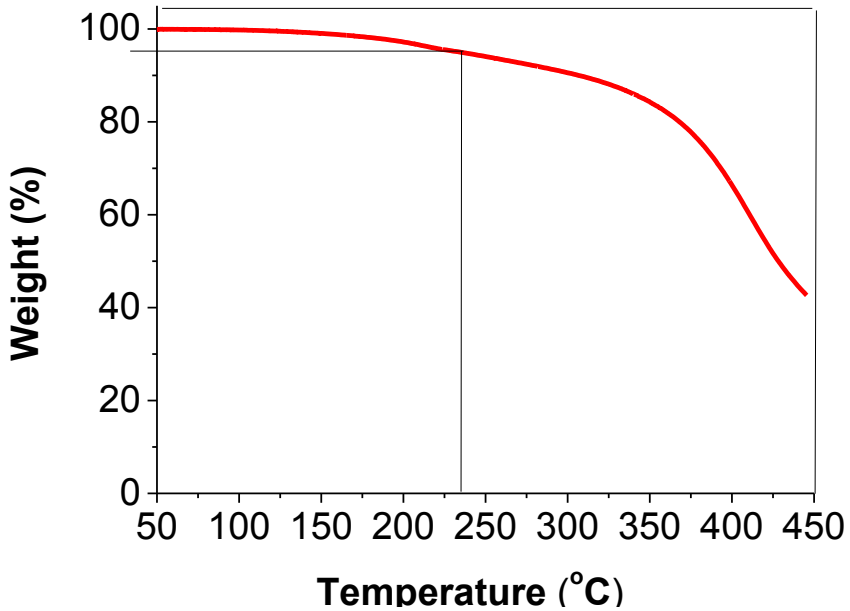

Figure 19: TGA curve for **P1-DTA-BTV** measured with a heating rate of 10 °C.min^{-1} under N_2

5.6 Atomic Force Microscopy

5.6.1 Introduction

Atomic Force Microscopy was first used as a tool in 1986 by Binnig, Quate and Gerber (Lang 2014), (Binnig 1986).

Atomic Force Microscopy (AFM) provides a 3D profile or image of the surface on a nanoscale, by measuring the forces between a sharp probe (<10 nm) and a surface at a very short distance (0.2-10 nm probe-sample separation). The probe is supported on a flexible cantilever, which is typically made from Si_3N_4, or Si (Robert 2007), (Binnig 1986).

5.6.2 Measurement Conditions

AFM, or scanning force microscopy (SFM), imaging was performed on polymer thin films on a DTS-modified SiO_2/Si substrate using a Dimension 3100 Scanning Probe Microscope.

5.6.3 Results

Figure 20 indicates that when the temperature is increased, the surface morphology of the polymer progressively crystalizes to form edges on the π-π laminar crystal layer at room temperatures up to 150 ^oC.

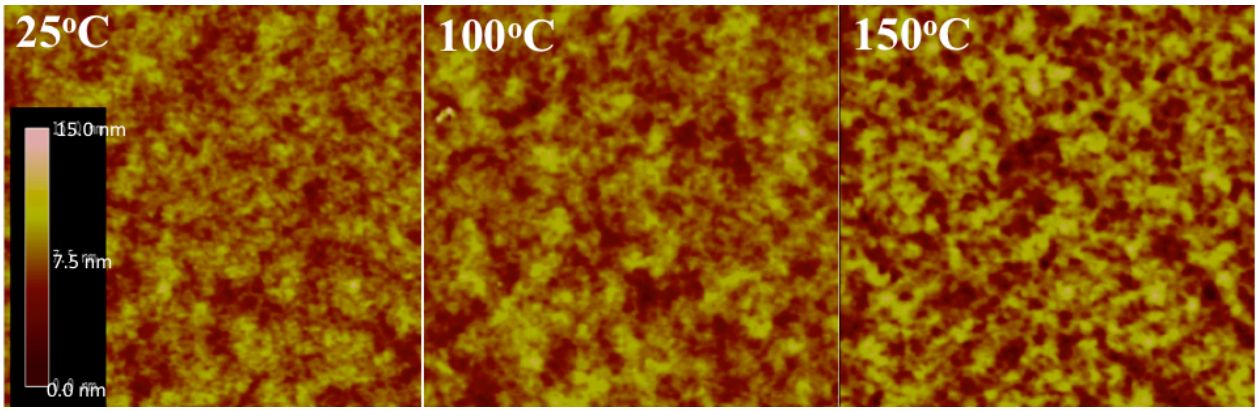

Figure 20: AFM height images (2 μm × 2 μm) of **P1-DTA-BTV** thin films (~35 nm) spin coated on DTS-modified SiO_2/Si substrates and annealed at a variety of temperatures for 15 min under N_2

5.7 X-Ray Diffraction

5.7.1 Introduction

In early 1913, W.H. Bragg and his son W.L. Bragg discovered an equation (equation **10**) to explain the reason behind the cleavage faces of crystals that appear to reflect X-ray beams at certain angles (theta, θ) of incident (Liljas 2013), (Paszkowicz 2006).

The ideal space between polymer layers is usually 14.9 Å, whereas the spacing between interlayers has been found to be 3.7 Å to 4 Å (Liljas 2013). Polymers layers can be found in different forms, such as edge-on, face-on, and tilted chain orientation (Paszkowicz 2006).

XRD analysis data can be processed using Bragg's law:

$$\mathbf{n\lambda = 2d\sin\theta} \qquad (10)$$

where **n** is an integer, **λ** is the wavelength of the incident X-ray beam, and **d** is the distance between the atomic layers in the crystals.

5.7.2 Experimental Conditions

The XRD measurements were carried out with a Bruker D8 Advance powder diffractmeter with Cu Kα radiation (λ = 1.5406 Å) using standard Bragg-Brentano geometry (Li 2012).

5.7.3 Results

a)

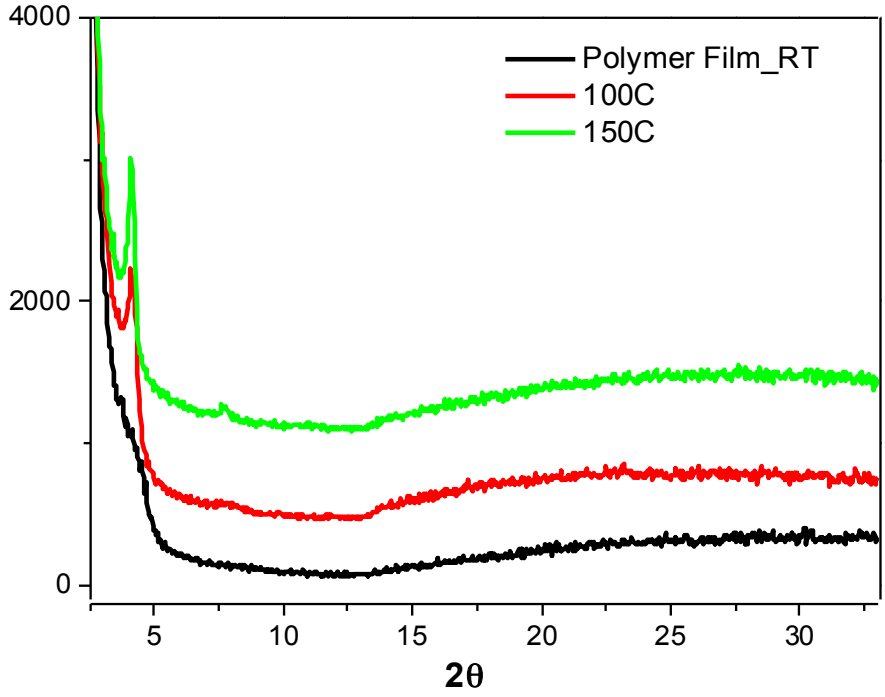

b)

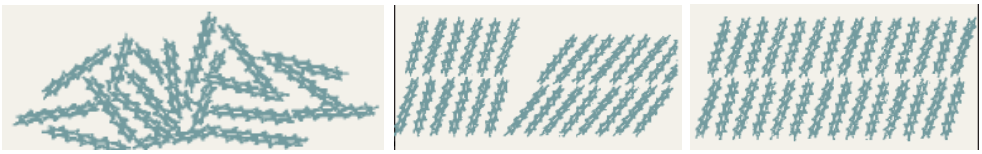

Figure 21: a) XRD data obtained from spin coated **P1-DTA-BTV** thin films on DTS-modified SiO_2/Si substrates annealed at a variety of temperatures, b) polymer layers orientation through the changing in temperature (Dimitrakopoulos 2001)

The XRD graph shown in Figure 21 illustrates the peak that was formed at 2θ = 4.115º, which means that the polymer layers form at the nano level between the interlayers in the polymer and crystallize in an edge-on form at 100 ^{o}C. However, when the temperature is increased to 150 ^{o}C, the polymer becomes more crystalline, which is in agreement with the AFM results in which increases in the surface morphology with increased temperatures could be observed. Based on Bragg's law from equation (**10**), it was found that the wavelength **λ** = 1.5406 Å, and θ is well known to be 2.058º. The calculations then resulted in a d-spacing distance between the atomic layers of 21.4 Å.

6. Device Performance of P1-DTA-BTV

P1-DTA-BTV was characterized and used as a channel semiconductor in organic thin film transistor devices with a bottom-gate, bottom-contact (BGBC) configuration. An n-doped silicon wafers were used as the gate electrode (300 nm SiO_2), and gold was used as the source and drain electrodes. The substrate was washed with acetone, IPA and DI water, and followed by DTS modification. The polymer thin film was then spin coated on top of the DTS-modified SiO_2/Si substrate using a 1 % chloroform solution of **P1-DTA-BTV.** Finally, the polymer film was optionally annealed at different temperatures (100 ^oC, 150 ^oC, and 200 ^oC) for 15 min in nitrogen. The device was then encapsulated in a layer of Poly(methyl methacrylate) PMMA with a thickness of 500 nm and dried at 80 ^oC for 30 min.

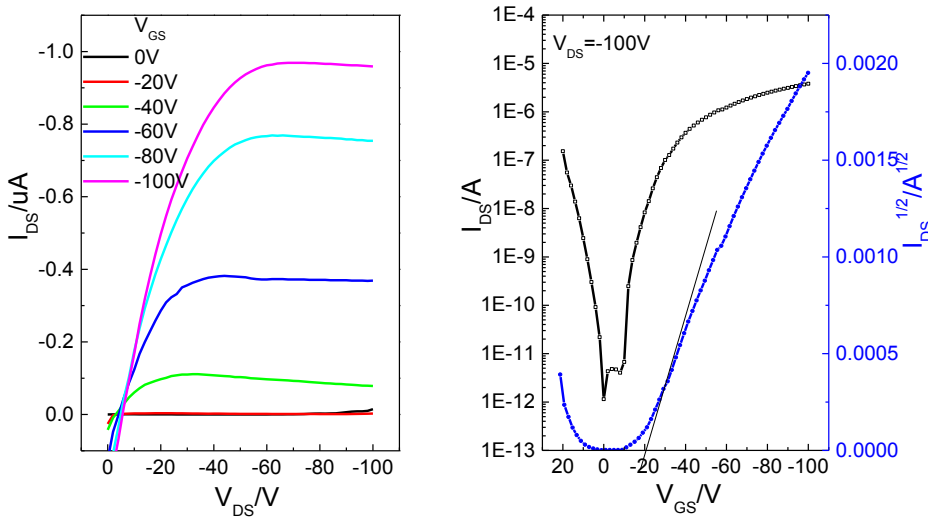

Figure 22: Illustration of the (a) output and (b) transfer curves in electron enhancement mode for a PMMA-encapsulated OTFT device fabricated with a **P1-DTA-BTV** thin film annealed at 100 ^oC for 15 min using an S770-2: L = 30 μm, W = 1mm

As anticipated, the device fabricated with a **P1-DTA-BTV** thin film showed an improving in the hole mobility exhibiting a p-type characteristics as showing in Figure 22. This OTFT device with non-annealed **P1-DTA-BTV** films displayed an average hole mobility of 5.5×10^{-3} $cm^2V^{-1}s^{-1}$ ($I_{on/off}$ = ~ 10^6) at 100 ^oC as provided in Table 1. However, the increasing the thermal annealing of the polymer thin film did not brought a significant improvement in the mobility. Figure 22 presents

the output (a), and transfer (b) curves for the OTFT giving the highest hole mobility at 100 ^{o}C with L= 30 μm, and W= 1 mm for the semiconductor channel in the device performance. An average hole mobility of 5.5 × 10^{-3} $cm^2V^{-1}s^{-1}$ (V_T = -21 V) in the saturation regime with a current on-to-off ratio (I_{on}/I_{off}) of 3.3x10^6 was obtained from OTFT device with **P1-DTA-BTV** thin films annealed at same temperature (100 ^{o}C). However, **P1-DTA-BTV** films annealed at 150 ^{o}C showed decreased mobility, while at 200 °C, no performance was observed. This is perhaps because of the instability of the polymer during the annealing process. **P1-DTA-BTV** exhibited improved mobility, and its excellent solubility and ultralow band gap also make this polymer a respectable potential candidate for OPV application because these application requisite an average mobility of ~10^{-3} (Braun 2009), (Chen 2012), (Yan 2009), which this polymer is provided. Table 1 summuraizes the OTFT device performance result for this polymer that used as a channel layer in the device.

Table 1: Summary of OTFT device performance using **P1-DTA-BTV** as the channel layers.[a]

Annealing temperature	**100 ^{o}C**		**150 ^{o}C**		**200 ^{o}C**
	Hole transport	Electron transport	Hole transport	Electron transport	
Mobility ($cm^2V^{-1}S^{-1}$)	5.4 × 10^{-3} **5.5 × 10^{-3}** 3.2 × 10^{-3}	5.98× 10^{-5}	6.5 × 10^{-4} 3.3 × 10^{-4} 6.3 × 10^{-4}	4.63× 10^{-5}	No performance
$I_{on/off}$	**3.3 × 10^6**		2.5 × 10^5		
V_{th}	-21 V		-31 V		

[a]The devices were annealed in a glove box on a hotplate at the selected temperature for 15 min under nitrogen. μ_h/μ_e are the hole/electron mobility values in the saturated regions in electron enhancement mode. Each set of data was obtained from three to five OTFT devices.

7. Conclusion

This chapter has focused on the development of an azothiazole polymer, which had already been synthesized by other members in the research group. However, it was tackled with a different approach in this research, and evidence of the fulfillment of several of the goals of the

work for this thesis has been presented, including the increase in the molecular weight and enhancement of the mobility of the polymer.

Table 2 shows the comparison between previous polymer (**PDTA-BTV**) and this polymer (**P1-DTA-BTV**) described in this chapter.

Table 2: Comparison of **P1-DTA-BTV** developed for this thesis and the previously created **PDTA-BTV** (Yan 2013).

	Band gap	HOMO	LUMO	Mobility	$I_{on/off}$	Yield
PDTA-BTV	1.18 eV	-5.32 eV	-4.14 eV	1.5×10^{-3}	$\sim 10^{3}$	7%
P1-DTA-BTV	1.13 eV	-5.20 eV	-4.07 eV	5.5×10^{-3}	3.3×10^{6}	28%

The following Experimental Section describes the methodology used to achieve the results and verify the device characterization findings.

8. Experimental Section

8.1. General

All chemicals were used as supplied by Sigma-Aldrich without further purification (Ramirez 1956), (Cooke 1973).

Geometry optimization of 1,2-bis(4-undecylthiazol-2-yl)hydrazine-2HBr, 1,2-bis(4-undecylthiazol-2-yl)diazene, 1,2-bis(5-bromo-4-undecylthiazol-2-yl)diazene, and (E)-1,2-bis(3-dodecyl-5-(trimethylstannyl)thiophen-2-yl)ethane was performed based on Density Functional Theory (DFT) calculations using the B3LYP hybrid functional with the 6-31G basis set (Frisch 2009), (Lee 1988), (Frisch 2009), (Frisch 2010), (Yan 2013).

8.2. Fabrication and Characterization of OTFT Devices

The **P1-DTA-BTV** thin film transistor was fabricated by employing a bottom-contact (Au electrode) structure on p-doped silicon wafers. A 300 nm SiO_2 layer on the p-silicon wafer was used as the gate insulator. The substrate was washed with acetone, isopropanol alcohol (IPA), and deionized (DI) water, and followed by dodecyltrichlorosilane DTS modification (10 mg/mL)

at 70 °C for 20 min in toluene. The polymer film was obtained by spin coating on substrate with a polymer solution. The devices were then annealed at 100 ^{o}C, 150 ^{o}C and 200 ^{o}C on a hotplate for 15 min in nitrogen atmosphere. The PMMA layer (~ 500 nm) was created by spin coating with 8 % (wt %) in butyl acetate (Sun 2012).

8.3. Synthesis procedures

Synthesis of 1-bromotridecan-2-one (1): This synthesis was referenced from a paper published by Xia Guo and others in 2012 (Guo 2012), who used the same reaction for the bromination of 2-octanone and 2-undecanone, and their reaction conditions were followed (Guo 2012). Compound (**1**) was made first by another master's student in Professor Li's group, but the synthesis was carefully completed in this thesis, beginning with this compound (**1**) and ending with the final pure **DTA** monomer used for the Stille coupling polymerization.

Synthesis of 1,2-bis(4-undecylthiazol-2-yl)hydrazine-2HBr (2): (2.77 g, 10.0 mmol, 2.0 equiv.) of 1-bromotridecan-2-one, compound (**1**) was added to a 50 ml round-bottom (RB) flask followed by (0.75 g, 5.0 mmol, 1.0 equivalent) of hydrazine-1,2- bis(carbothioamide). The reaction mixture was then heated in ethanol (15 mL) at 50 ^{o}C for 2.5 h under argon gas, and then cooled down to room temperature and allowed to sit overnight. The white solid was then collected by suction filtration, washed with ethanol and dried in a vacuum chamber for 1 h, to save 2.579 g (77 % yield) of 1,2-bis(4-undecylthiazol-2-yl)hydrazine-2HBr.

Synthesis of 1,2-bis(4-undecylthiazol-2-yl)diazene (3): An $NaNO_2$ (0.05 g, 0.75 mmol, 1.0 equiv.) solution in 2 mL of water was then added dropwise into 1,2-bis(4-undecylthiazol-2-yl)hydrazine-2HBr (0.5 g, 0.75 mmol, 1.0 equiv.) in 20 mL of water. The white dispersion immediately turned yellow and then changed to orange. The mixture was stirred for 30 min after the addition of the $NaNO_2$ solution. The orange solid was collected by suction filtration, washed briefly with ethanol and dried in a vacuum chamber to produce 0.3286 g of 1,2-bis(4-undecylthiazol-2-yl)diazene (72%) yield (Beyer 1952).

Synthesis of 1,2-bis(5-bromo-4-undecylthiazol-2-yl)diazene (DTA) (4): (1.14g, 2.26 mmol, 1.0 equiv.) of 1,2-bis(4-undecylthiazol-2-yl)diazene was added to a 100 ml round-bottom (RB) flask with a stir bar. 20 ml of chloroform was added and the solution was cooled in an ice-water bath. (0.72g) of Br_2 was then weighed into a vial, and 10 ml of chloroform was added. A Br_2 solvent was added dropwise with a pipette, and the solution was stirred in the dark for 1 h.

Extraction: The reaction mixture was poured into 50 ml of Dewater H_2O, and two layers were separated. The aqueous phase was extracted with 150 ml of dichloromethane (DCM). The organic was combined. The organic phase was washed with 50 ml of H_2O (Holt 1965). The organic was dried with $MgSO_4$, and the $MgSO_4$ was filtered off. The solution was then transferred into an RB flask. The solvent was evaporated off to save 0.5014 g of the product (38.42 % yield). Column chromatography was performed on the final result to ensure a pure product, and NMR was applied to make certain that a pure accepting monomer was obtained. Recrystallization of the monomer was also necessary for ascertaining the purification of the monomer, which was an additional step beyond those conducted in previous work. The monomer was recrystallized in methanol (Yan 2013).

^{1}H NMR (300 MHz, $CDCl_3$): 7.26, 2.85, 2.82, 1.76-1.1.76, 1.35, 1.26, 0.90, 0.88, 0.85, (Figure A-1). NMR data were referred to the ^{1}H NMR and ^{13}C NMR data schedules listed in reference (Fulmer 2010).

Synthesis of (E)-1,2-bis(3-dodecyl-5-(trimethylstannyl)thiophen-2-yl)ethane P1-DTA-BTV (5): (0.1716 g, 0.25 mmol, 1.0 equiv.) of **DTA** was added to a clean, dry two-necked 100 ml RB flask with a water condenser. (0.2213g, 0.259 mmol, 1.0 equiv) of (E)-1,2-bis(3-dodecyl-5-(trimethlstannyl)thiophen-2-yl)ethane was added to the same flask. (0.0063g, 0.0207mmol, 0.08 equiv.) of P(o-tolyl)$_3$ was then added to the same flask as well. Both necks of the flask were covered with rubber covers. (2ml) of chlorobenzene solvent was added to the mixture, with stirring under argon. Under argon gas, using an argon bag, (0.00474g, 0.00518mmol, 0.02equiv.) of $Pd_2(dba)_3$ was added to the mixture. 1 mL of solvent (chlorobenzene) was added to the reaction. The reaction mixture was heated to 90 ^{o}C under an oil bath and covered with aluminum foil to keep it safe and dark for 2 days and 10 hours (Yan 2013). The polymer was then collected by suction filtration and was purified using methanol, acetone, hexane, and chloroform successively. The final product was obtained by precipitation into methanol. The product was then dried under vacuum for 1 day to obtain 0.1139g (28.2 % yield). GPC results were as follows: M_n = 4.1 kDa, M_w = 8.4 kDa, PDI = 2.07.

Chapter 3

DTAE-Based Donor-Acceptor Copolymers for OTFTs

1. Introduction

As the main goals in Chapter 2 were reached, the focus was shifted in this chapter to achieving other goals. The main objective is to make this azothiazole electron accepting monomer stronger and to improve the molecular weight of its polymer. For that purpose, an ester side chain was added into the monomer. Among the other objectives, increasing the molecular weight, finding an n-type polymer, and obtaining better solubility are all equally targeted.

2. Molecular Design

The development of this monomer involved difficulties, but the author and the research group were resolute enough to fight their way through the challenges and were able, through strenuous search for more information and working extra hard in the laboratory, to accomplish the mission. Success was achieved after the third attempt to synthesize the monomer: (*E*)-bis(2-octyldodecyl) 2,2'-(diazene-1,2-diyl)bis(5-bromothiazole-4-carboxylate) (**DTAE-Br**).

The challenges arose from the fact that this monomer had never been made, which meant that very few references were available to support proposal. However, it is worth mentioning that the supervision and advice of Professor Li as well as experimental support from a PhD student, Jesse Quinn, in Professor Li's group were instrumental in the successful achievement of the results presented in this chapter.

The first step was to conduct a computer simulation of the polymer. Table 3 lists the data, and Figure 21 illustrates the results of the simulation as provided by Jesse Quinn.

Table 3: Summary of the computer simulation results for **P6-DTAE-TT.**

DTAE				
MO		**E (eV)**	**Symmetry**	**Eg (eV)**
231	L+1	-3.36	A	2.06
230	LUMO	-3.6	A	
229	HOMO	-5.66	A	
228	H-1	-6.02	A	

E_{HOMO} = -5.66 eV

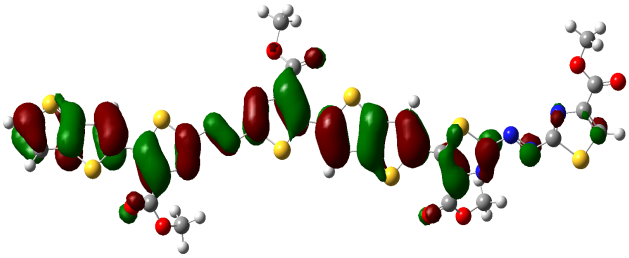

E_{LUMO} = -3.6 eV

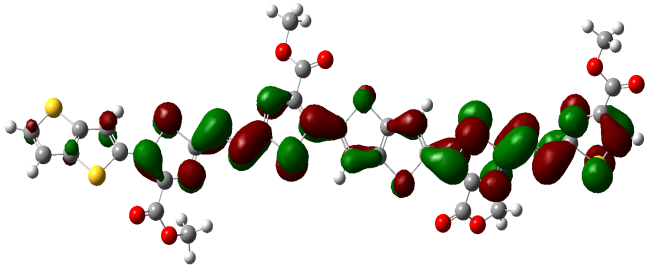

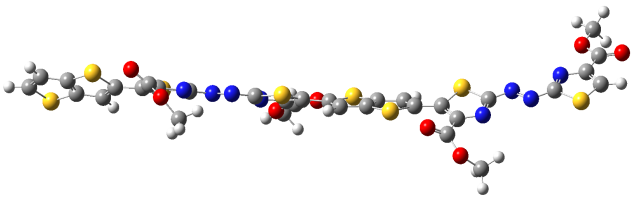

Figure 23: Computer simulation for the dimer for **P6-DTAE-TT** polymer and its HOMO and LUMO energy levels.

3. Synthesis of the DTAE Monomer

3.1 Methodology

Additional evidence of the importance of purity is revealed in the design of a novel ester side chain of an azo monomer ((*E*)-bis(2-octyldodecyl) 2,2'-(diazene-1,2-diyl)bis(5-bromothiazole-4-carboxylate): purity is important not just for the success of the synthesis of the monomer but also for improving the mobility of a polymer. Because this ester monomer (*E*)-bis(2-octyldodecyl) 2,2'-(diazene-1,2-diyl)bis(5-bromothiazole-4-carboxylate) (**DTAE-Br**) was novel and had never been made before, three methods were attempted in order to synthesize it so that a pure product could be derived. Because of impurities in the starting materials, the only successful method, and the one that resulted in the greatest purity, was the third method. The following subsections explain how this building block was developed and how the novel monomer was finally created.

3.1.1 First Method

The first method began with the esterification of a 2-oxopropanoic acid compound (**6**), which was successfully made. Then the bromination of compound (**6)** was performed at room temperature for one hour to obtain compound (**7**). Compound (**7**) was then reacted with 2,5-dithiobiurea for the achievement of the aromatic ring. ^{1}H NMR result for compound (**8**) shows that only one ester side chain formed, which was the reason for not obtaining the final **DTAE-Br** monomer, as shown in Scheme 8 (Kozłowski 1989).

All ^{1}H NMR results for compounds 6, 7 and 8 are shown in Figures A-4, A-5, A-6,7, respectively. (Appendix A-2)

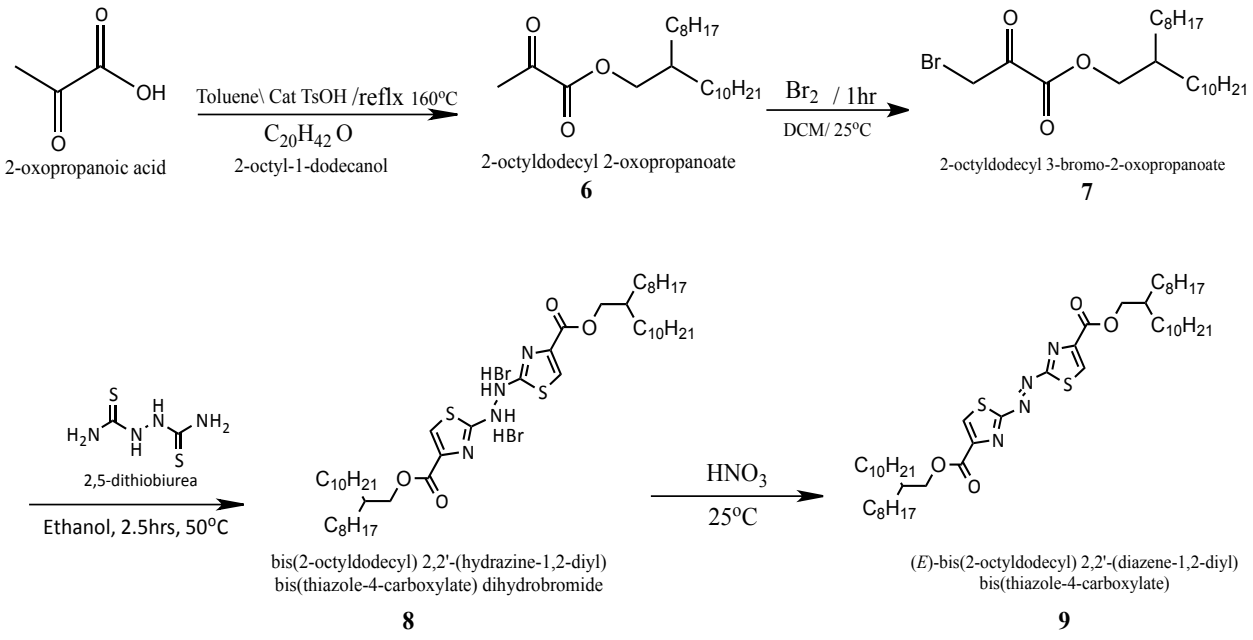

Scheme 8: Synthesis of **DTAE**, first method.

3.1.2 Second Method

The second method was initiated with bromo pyruvic acid reacting with 2,5-dithiobiurea, first to form the aromatic ring and then to form an ester side chain to produce the final monomer, which was the opposite of the first method. Although compound **11** was successfully synthesized, the expected results were not achieved because compound **12** also show ^{1}H NMR (Figure A-10) data with one carboxylic acid group but not on the other side and thus the final product (compound **13**) was not obtained. Scheme 9 illustrates this second method used to synthesize **DTAE**.

As a result, re-synthesis of **DTAE** was absolutely necessary, which led to the third method or the final method.

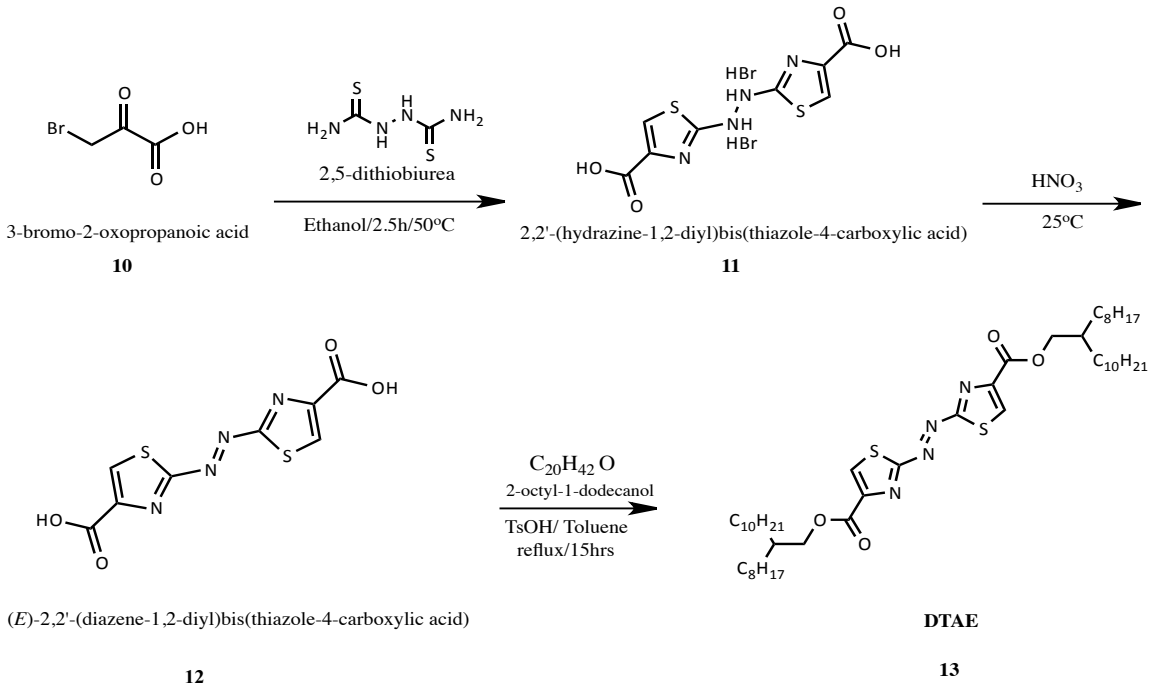

Scheme 9: Synthesis of **DTAE**, second method.

3.1.3 Final Method

This method was successful and bore impressive results, mainly because of the major changes that were applied to the starting materials. This synthesis involved different (3-bromo-2-oxopropanoic acid), which is commercially available from Sigma-Aldrich. This chemical was 97 % pure, which makes a substantial difference in the synthesis of (E)-bis(2-octyldodecyl) 2,2`-(diazene-1,2-diyl)bis(thiazole-4-carboxylate) (**DTAE**) because of its higher purity, which is further evidence of the importance of purity in the synthesis of an effective monomer. Scheme 10 illustrates the final method.

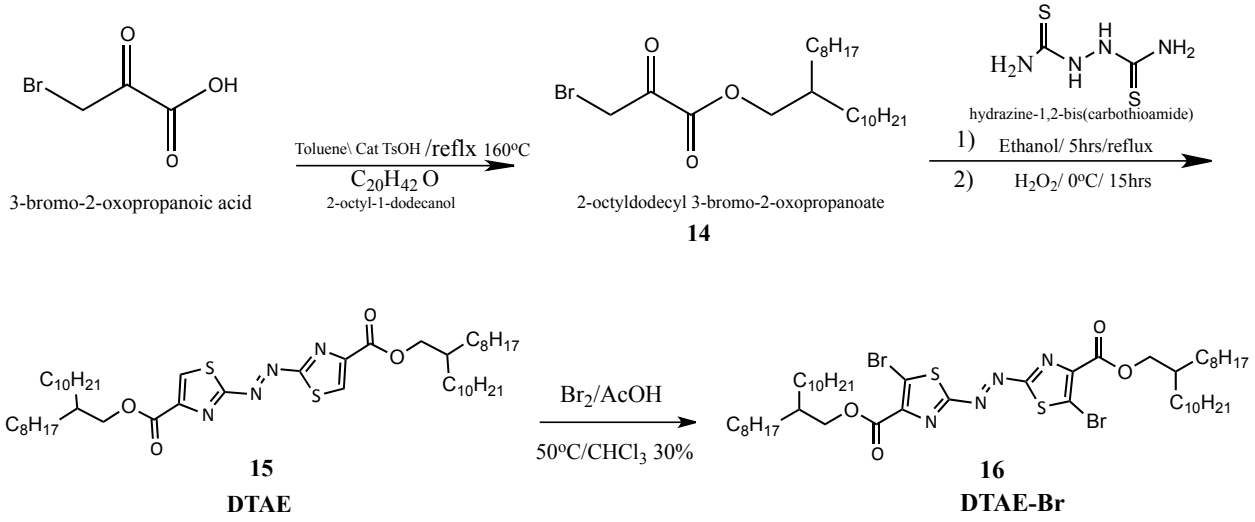

Scheme 10: Synthesis of **DTAE**, final method.

3-Bromo-2-oxopropanoic acid was esterified using 2-octyl-1-dodecanol in toluene. The reaction was heated to reflux for 12 h in the presence of p-TsOH as a catalyst to form compound (**14)**. Compound (**14)** was then reacted with hydrazine-1,2-bis(carbothioamide) using ethanol as a solvent and refluxing it for 5 h. Hydrogen peroxide was then immediately added to the mixture to form the **DTAE**, compound (**15)**. The final step was to purify the monomer through column chromatography in order to save a pure product of the monomer (compound (**15)**). Compound (**15**) was brominated to form compound (**16**), **DTAE-Br** which can be used for the Stille coupling reaction to prepare **P-DTAE-T** (Scheme 11). This step required heat and a catalyst; in this case, because of the long side chain and the low reactivity of the hydrogen in the thiazole ring, acetic acid was used as a catalyst and heated to 50 ^{o}C to obtain an ester monomer (**DTAE-Br**) compound (**16)** (Scheme 10). Column chromatography was essential at this stage for ensuring the purity of the monomer.

^{1}H NMR, and ^{13}C NMR for all of compounds 14, 15, and 16 are shown in Figure A-11, A-12, and A-13, respectively (Appendix A-2, final method).

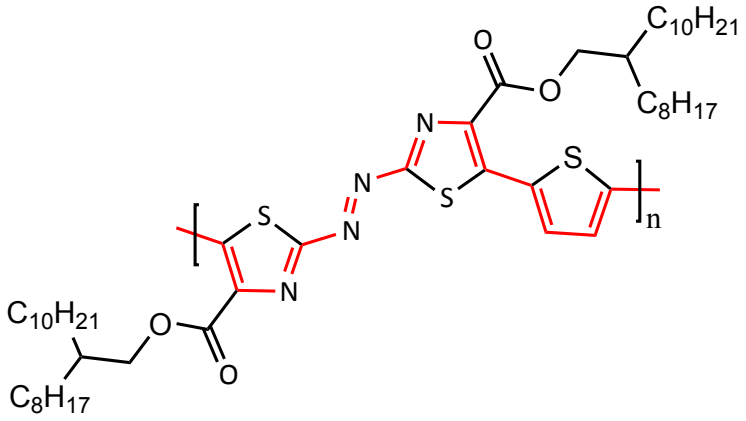

Scheme 11**:** Comparison of conjugation in **P-DTAE-T.**

4. Synthesis of P2-DTAE-BT

After the monomer had been made and its purity was verified through ^{1}H NMR and ^{13}C NMR, the results of which are shown in Figures A-12 (a) and A-12 (b), respectively. The monomer (**15**) was used for the first polymerization, with 5,5'-dibromo-2,2'-bithiophene **(BT-Br)** electron donating the monomer through a direct arylation mechanism (Scheme 12).

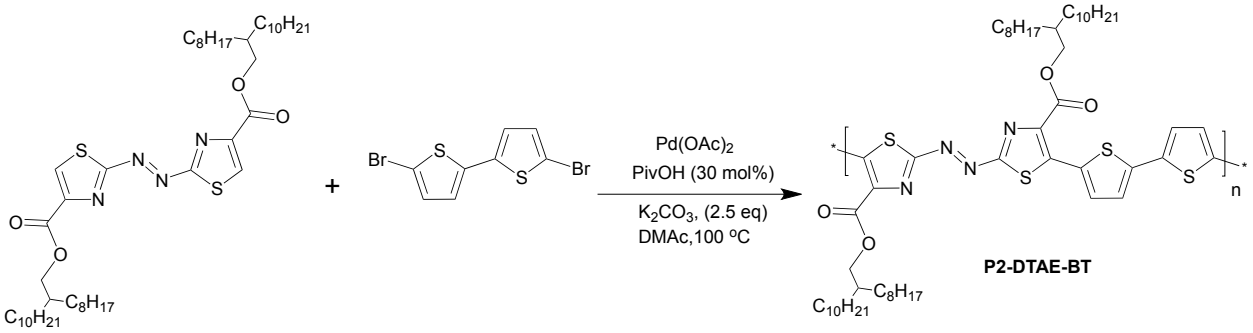

Scheme 12**:** Synthesis of **P2-DTAE-BT** through a direct arylation reaction.

The synthesis of the **P2-DTAE-BT** polymer was achieved through the reaction of compound (**15**) (**DTAE**) with 5,5'-dibromo-2,2'-bithiophene under the following conditions: temperature of 100 °C, *N,N*-Dimethylacetamide DMAc as a solvent, K_2CO_3 as a co-catalyst, $Pd(OAc)_2$ as a catalyst, and 30 mol % of PivOH. The polymerization was run for 24 h, after

which the solution was cooled down and precipitated dropwise from methanol to obtain a 31 % yield of the dark blue-greenish viscous polymer (Scheme 12). At room temperature, the polymer exhibits good solubility in common solvents such as hexane, acetone, and chloroform. The number average (M_n) and weight average molecular weights (M_w) were measured to be 1.15 kDa, and 1.80 kDa, respectively, using GPC at a column temperature of 40 ^oC with chloroform as an eluent and polystyrene as standards, with a flow rate of 1 mL/min. The PDI was measured to be 1.24. The synthesis was conducted under similar conditions in reference (Berrouard 2012).

4.1 Characterization of P2-DTAE-BT by UV-Vis, CV, TGA, and DSC

The polymer was characterized using both UV-visible light (UV-Vis) and cyclic voltammetry (CV). The UV-Vis spectrum shows a broad band gap of 1.5 eV, which was calculated from the onset wavelength of ~ 797 nm and a maximum absorbance (λ_{max}) of 597 nm (Figure 24). The HOMO and LUMO energy levels of the polymer were calculated from the CV graph, as shown in Figure 25. The oxidation and reduction onset potentials were found to be 0.710 eV and -0.303 eV, respectively. These measurements give a HOMO energy level of -5.5 eV and a LUMO energy level of -4.5 eV, which means that the addition of an ester group in the **DTAE** monomer side chain assists in decreasing the LUMO energy level, resulting in a low LUMO energy level being obtained, which could be beneficial with respect to electron injection and transport in OTFT applications.

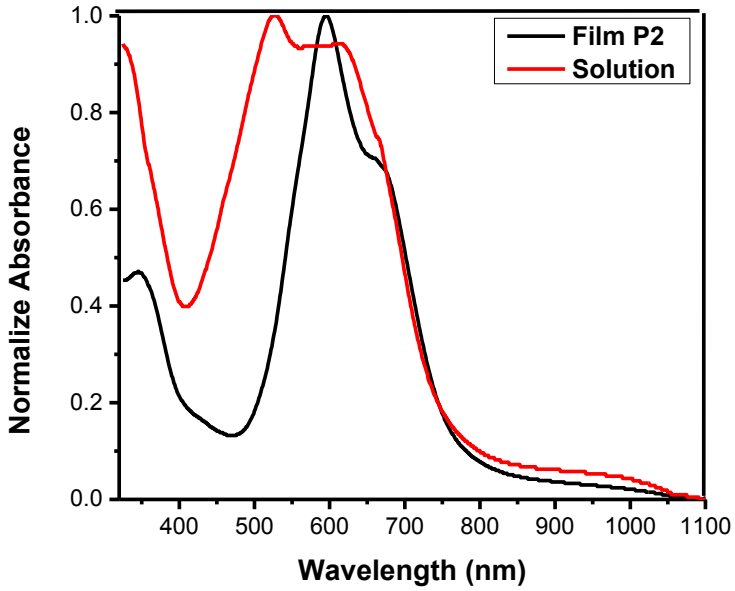

Figure 24: UV-Vis-NIR absorption spectra for **P2-DTAE-BT** in chloroform and in a thin film

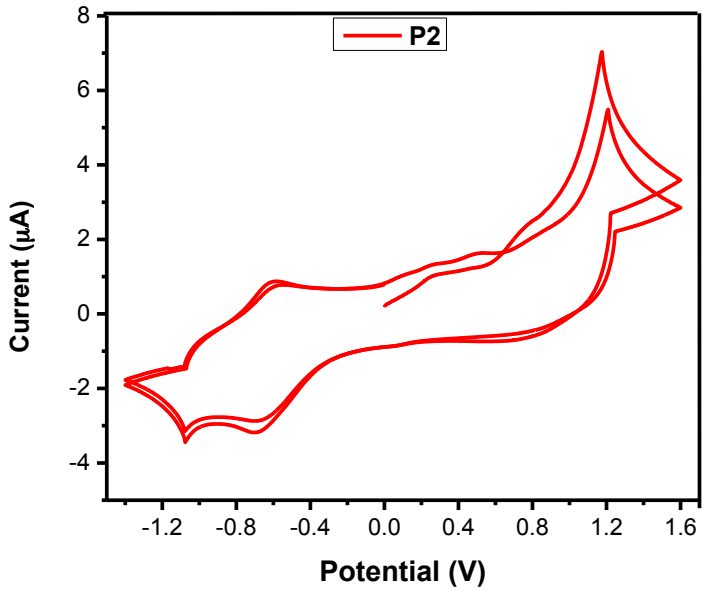

Figure 25: CV results (two cycles) for a **P2-DTAE-BT** thin film showing two oxidative and reductive cycles at a scan rate of 0.05 V s^{-1}. The electrolyte was 0.1 M tetrabutylammonium hexafluorophosphate in anhydrous acetonitrile.

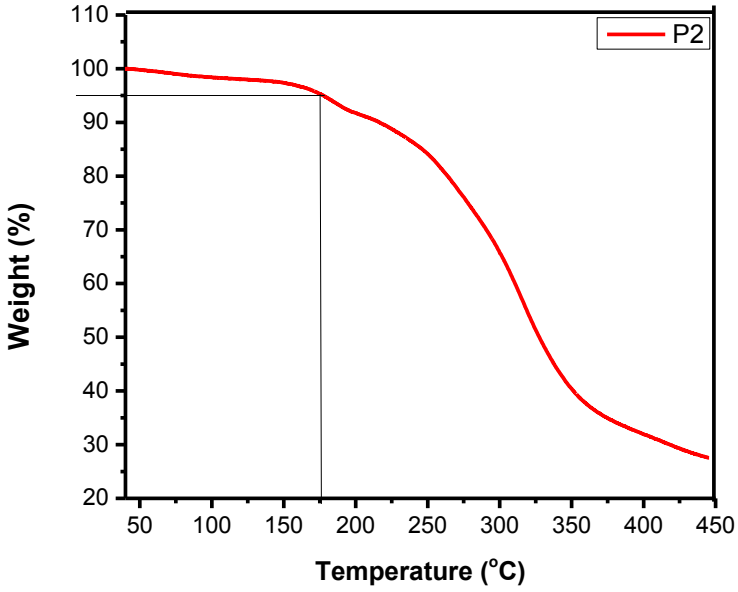

Figure 26: TGA curve for **P2-DTAE-BT** measured with a heating rate of 10 °C.min^{-1} under N_2

The polymer showed a 5 % weight loss at 176 ºC based on TGA (Figure 26). DSC graph shows noises around 150 °C (Figure 27), which coincides with the beginning of thermal

decomposition of this polymer as shown in the TGA graph.

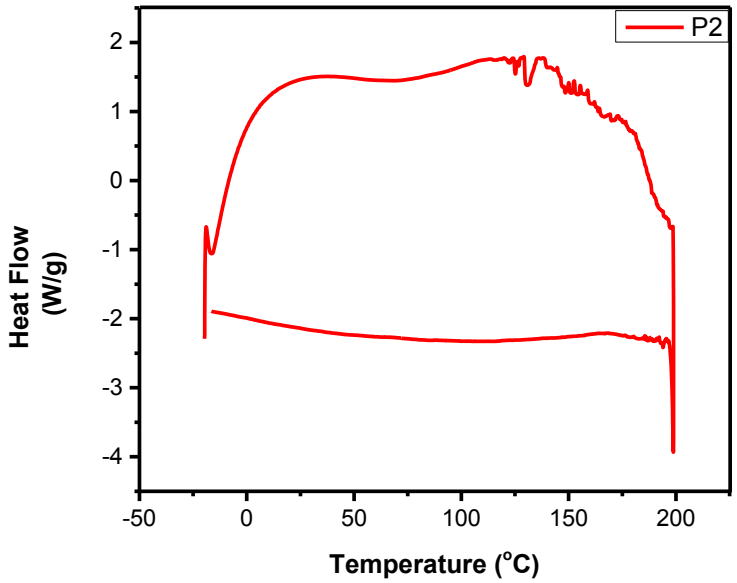

Figure 27: DSC profiles for **P2-DTAE-BT** obtained at a scanning rate of 10 °C.min^{-1} under N_2

5. Synthesis of P3-DTAE-B

Scheme 13 illustrates the synthesis of **P3-DTAE-B** reacting **DTAE** (compound **15**) monomer with 1,4-dibromobenzene (**B**) through direct arylation, (heterocyclic arenes direct arylation). The synthesis of **P3-DTAE-B** copolymer obtained average yield of 30% and exhibited dark blue-green viscous polymer. The polymerization was done under argon heated at 100 °C for 24 hours.

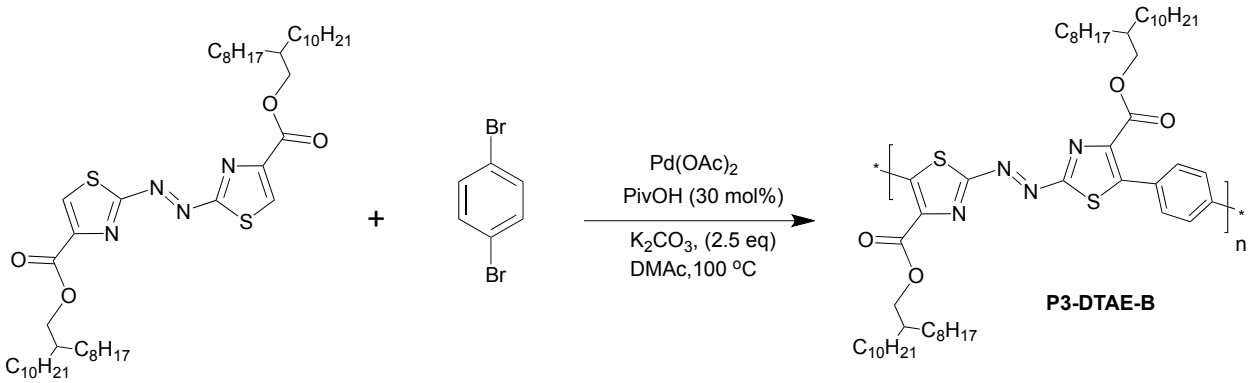

Scheme 13**:** Synthesis of **P3-DTAE-B** through a direct arylation reaction.

The 30 % yield was somewhat similar to that of **P2-DTAE-BT.** GPC measurement shows that M_n = 1.456, and M_w = 1.776, with a PDI of 1.22.

5.1 Characterization of P3-DTAE-B by UV-Vis, CV, TGA, and DSC:

UV-Vis spectrum indicates a band gap of 1.6 eV with two peaks showing in Figure 28 for **P3-DTAE-BT** film. The maximum wavelength (λ_{max}) value was found to be 602 nm and an onset wavelength of ~ 770 nm (Figure 28).

For the same measurement conditions, the CV curve of polymer **P3-DTAE-B** shows energy levels of -5.7 eV and -4.5 eV for the HOMO and LUMO energy levels, respectively, and a LUMO level of -4.1 eV if calculated based on band gap, as in equation **(9)** (Figure 29).

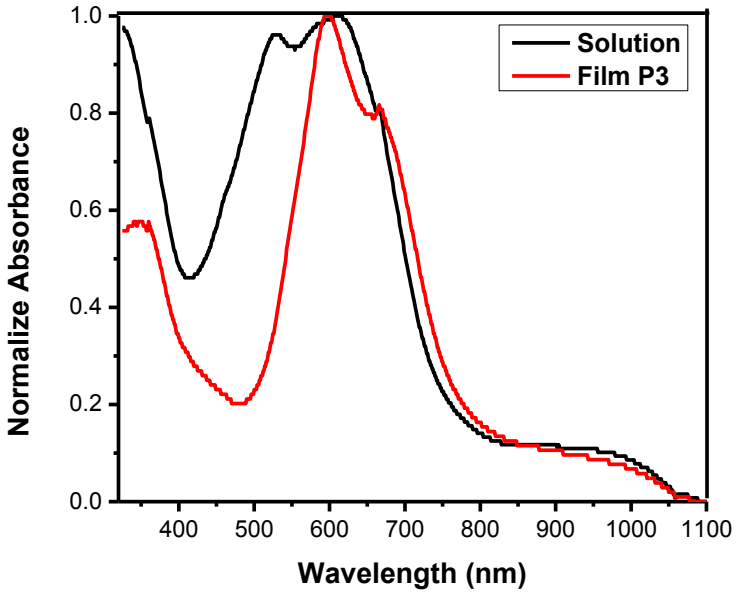

Figure 28: UV-Vis-NIR absorption spectra for **P3-DTAE-B** in chloroform and in a thin film

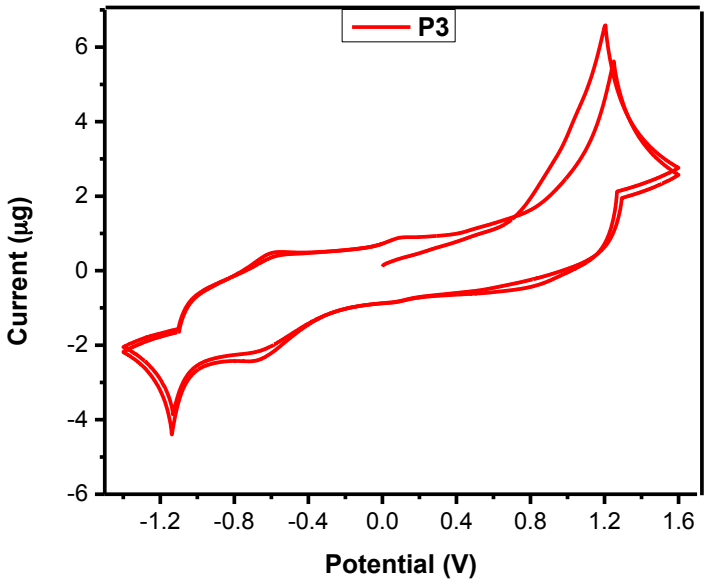

Figure 29: CV results (two cycles) for a **P3-DTAE-B** thin film showing two oxidative and reductive cycles at a scan rate of 0.05 V s^{-1}. The electrolyte was 0.1 M tetrabutylammonium hexafluorophosphate in anhydrous acetonitrile

The thermal behaviour of the polymer shows a slight improvement in thermal stability compared to the previous polymer: an absorbance of 214 ^{o}C with a 5 % weight loss (Figure 30). However, the DSC profile showed multiple peaks below 200 °C, which might be due to the presence of oligomers. The DSC profiles are shown in Figure 31.

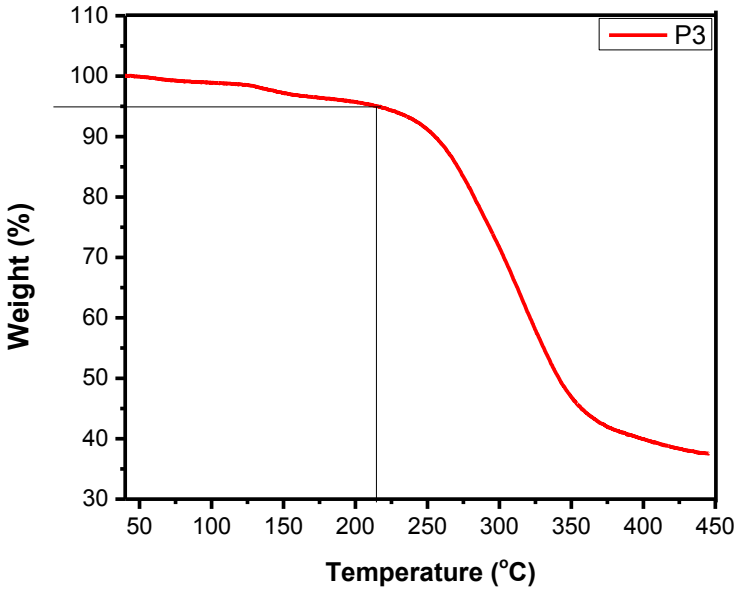

Figure 30: TGA curve for **P3-DTAE-B** measured at a heating rate of 10 °C.min^{-1} under N_2

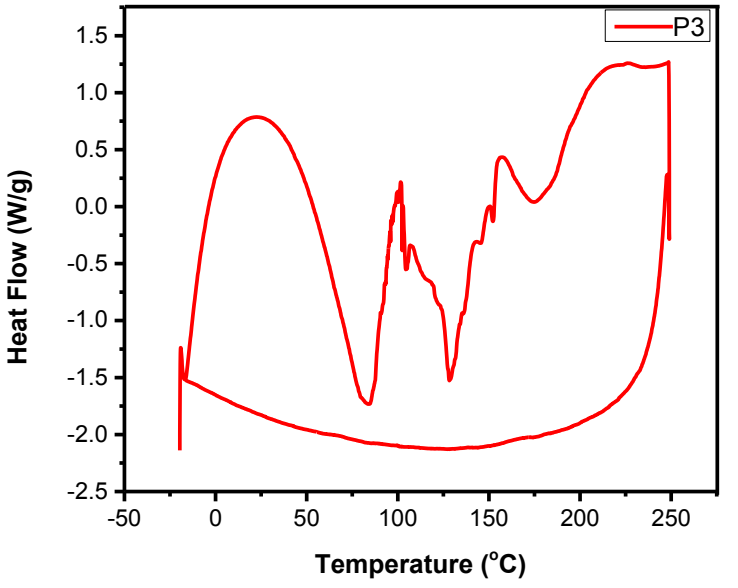

Figure 31: DSC profiles for **P3-DTAE-B** obtained at a scanning rate of 10°C.min^{-1} under N_2

6. Synthesis of P4-DTAE-B

Scheme 14 illustrates the synthesis of **P4-DTAE-B** via direct arylation reaction using **DTAE** monomer (compound **15**) that synthesized in CH_3CN solvent reacted with 1,4-dibromobenzene (**B**) in the presence of $Pd(OAc)_2$, PivOH catalysis, K_2CO_3 base, and DMAc solvent, heated at 100 ^oC for 24 hours. The monomer used in this polymerization is slightly different from the previous monomer. The difference between **P3** and **P4** is that the **DTAE** monomer used in the synthesis of **P4** is prepared using a CH_3CN solvent whereas the **P3** solvent is ethanol, as is the case for all other polymers. The reason for changing the solvent in this instance is as mentioned before: to determine the effects of both monomers on the polymerization at a (30 % yield).

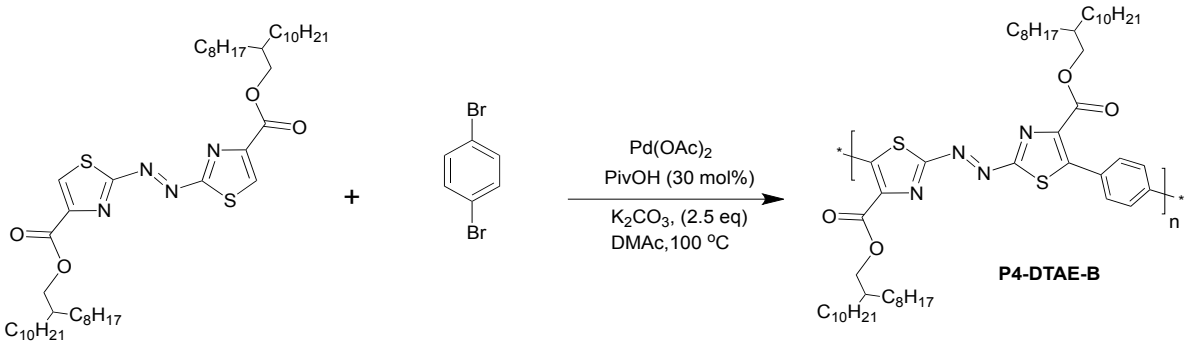

Scheme 14: Synthesis of **P4-DTAE-B** through a direct arylation reaction

6.1 Characterization of P4-DTAE-B by UV-Vis, CV, TGA, and DSC

The polymer exhibits a band gap of 1.59 eV, which is similar to those of other polymers, with a λ_{max} value of 325 nm and an onset wavelength of ~ 958 nm (Figure 32).

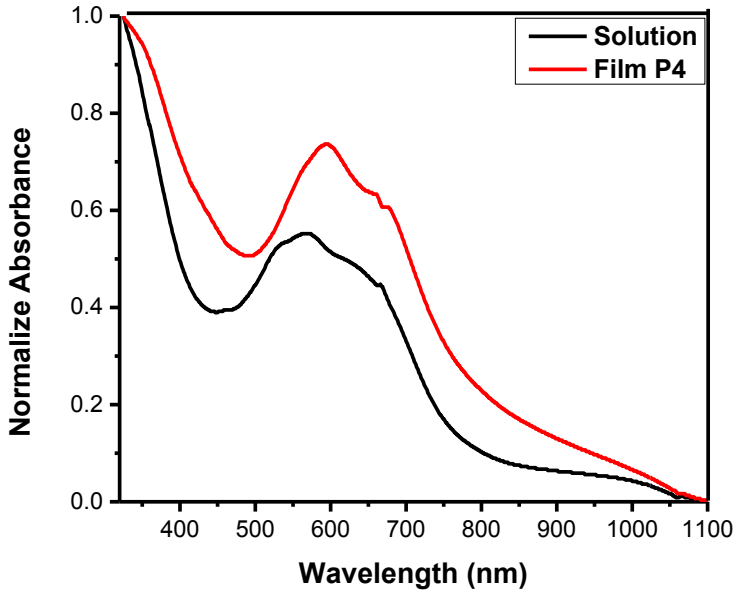

Figure 32: UV-Vis-NIR absorption spectra for **P4-DTAE-B** in chloroform and in a thin film

The GPC results show the number average (M_n) and weight average molecular weights (M_w) as 1.343 kDa, and 1.615 kDa, respectively, and a PDI of 1.20.

The CV graph for this polymer (**P4-DTAE-B)** indicates average HOMO and LUMO energy levels of -5.8 eV and -4.5 eV, respectively, and a LUMO level of -4.2 eV if calculated based on band gap, as in equation **(9).** The CV results are shown in Figure 33.

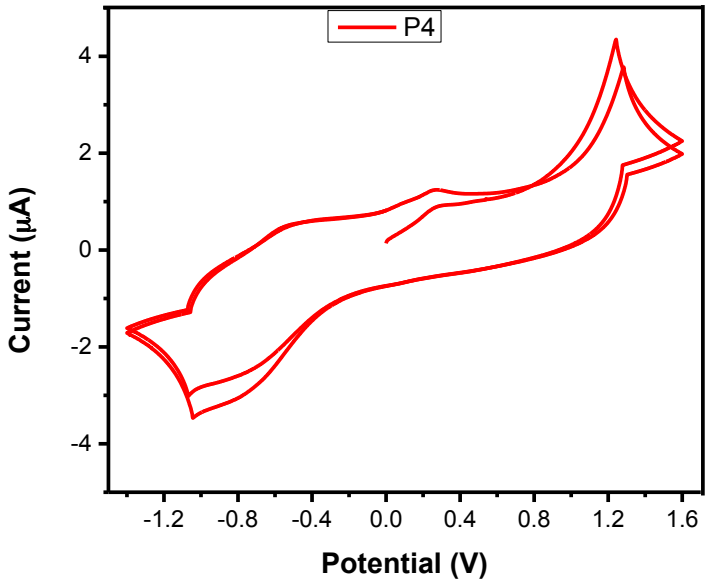

Figure 33: CV results (two cycles) for a **P4-DTAE-B** thin film showing two oxidative and reductive cycles at a scan rate of 0.05 V s^{-1}. The electrolyte was 0.1 M tetrabutylammonium hexafluorophosphate in anhydrous acetonitrile.

The polymer exhibits poor thermal stability, as can be seen in the TGA results shown in Figure 34: a 5 % weight loss was observed at 95 °C, which might be due to the very low molecular weight of this polymer. The DSC measurements also showed multiple peaks, which might also be due to the presence of oligomers (Figure 35).

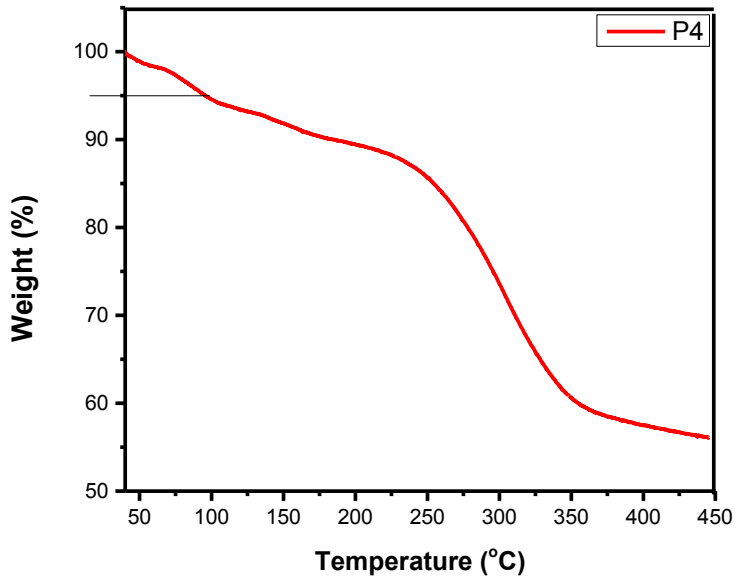

Figure 34: TGA curve for **P4-DTAE-B** measured at a heating rate of 10 °C.min^{-1} under N_2.

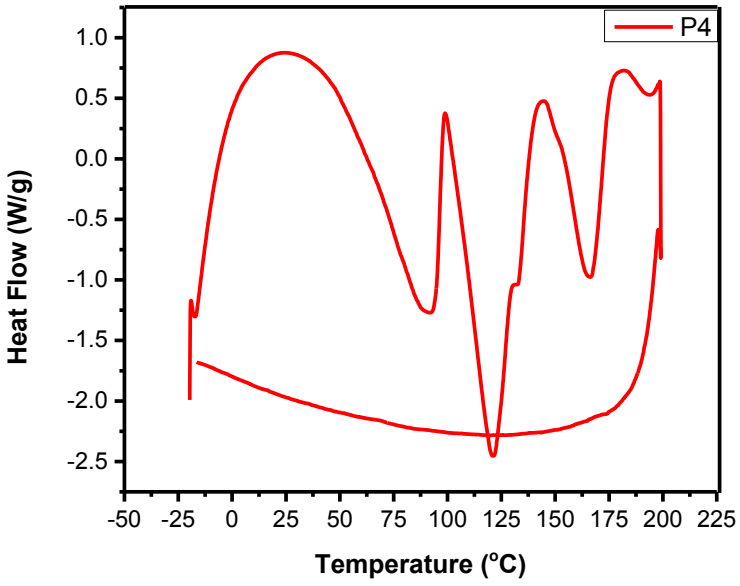

Figure 35: DSC profiles for **P4-DTAE-B** obtained at a scanning rate of 10°C.min^{-1} under N_2

Stille Coupling

The results from the direct arylation polymerization shown above were not satisfactory, so the polymerization synthesis was changed from direct arylation to Stille coupling reactions.

7 Synthesis of P5-DTAE-BT

The brominated monomer **DTAE-Br** (compound **16**) was first polymerized with 5,5'-bis(trimethylstannyl)-2,2'-bithiophene (**BT**) in the presence of $Pd_2(dba)_2$ and P(o-toly) catalysts in cholorobenzene. The polymerization was performed under argon for 2 days to obtain a viscous green solution, which was then precipitated from methanol to give a 20 % yield of the polymer (Scheme 15). This polymer was then purified through Soxhlet extraction using three different solvents: acetone, hexane, and chloroform. The polymerization was conducted according to the polymerization conditions reported for Song Park's Stille coupling polymerization for other D-A copolymers (Song 2011). This polymer was then characterized by GPC, UV-Vis, CV, DSC, TGA, and XRD, as explained below.

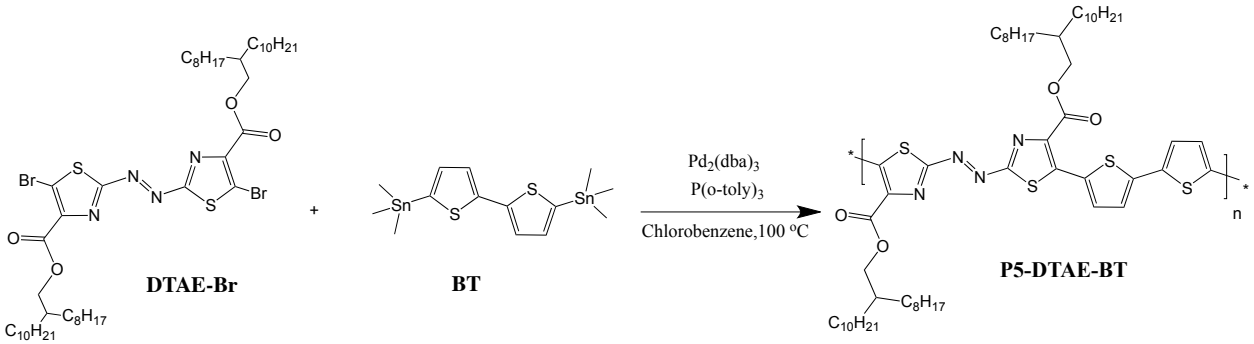

Scheme 15: Synthesis of **P5-DTAE-BT** through Stille coupling.

The GPC results demonstrate a substantial improvement in molecular weight. The polymer exhibits a number molecular weight of 6.1 kDa, which is six times higher than that of all other previous polymers made by direct arylation polymerization. A weight average molecular weight of 37.116 kDa and a PDI of 6.11 were obtained. This is a significant improvement in the molecular weight of the polymer, which shows that using the Stille coupling reaction for the polymerization is more effective.

7.1 Characterization of P5-DTAE-BT

7.1.1 Ultraviolet-Visible Spectrometry

The graph showing the UV-Vis results is distinguished by two peaks for the solid thin film version of the **P5-DTAE-BT** polymer, located at 445 nm and 687 nm (Figure 36). The second peak is slightly red shifted from solution to the film. The optical band gap was calculated from the onset of the absorption of the polymer thin film to be ~1.29 eV.

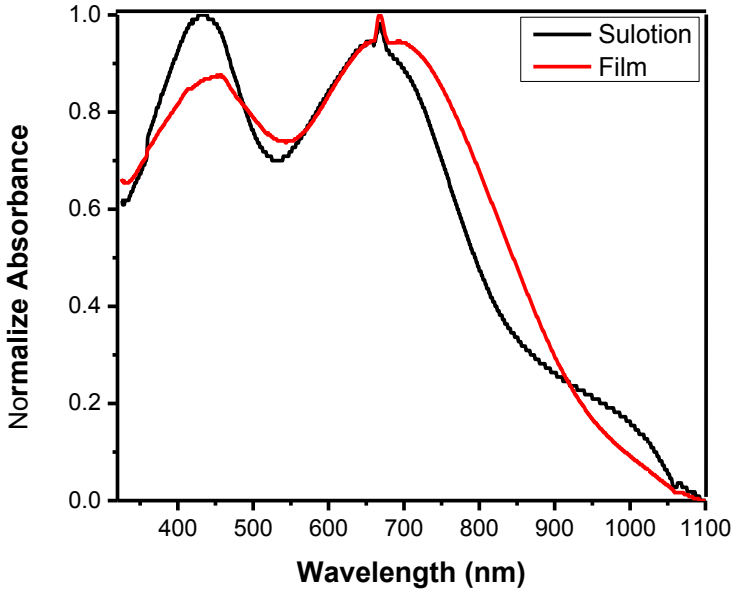

Figure 36: UV-Vis-NIR absorption spectra for **P5-DTAE-BT** in chloroform and in a thin film

7.1.2 Cyclic Voltammetry

As shown in Figure 37, a pronounced oxidation result was evident from the CV measurements as well as a reduction in absorption, based on the calculation of the HOMO and LUMO energy levels: E_{HOMO} = -5.43 eV, and E_{LUMO} = -4.40 eV, or -4.14 eV if calculated based on the band gap.

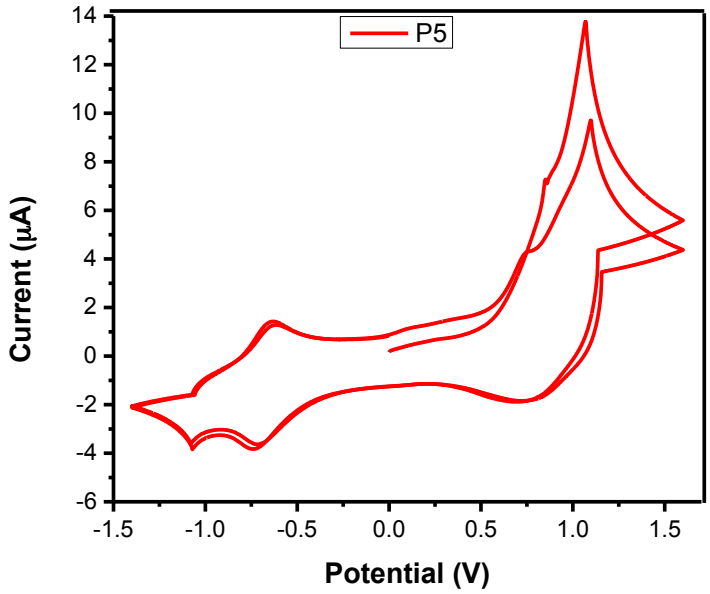

Figure 37: CV results (two cycles) for a **P5-DTAE-BT** thin film showing two oxidative and reductive cycles at a scan rate of 0.05 V s^{-1}. The electrolyte was 0.1 M tetrabutylammonium hexafluorophosphate in anhydrous acetonitrile

7.1.3 Differential Scanning Calorimetry and Thermal Gravimetric Analysis

DSC and TGA were used for studying the thermal behaviour of the polymer, and the resulting curves indicate that **P5-DTAE-BT** has much greater thermal stability than other polymers previously produced: a 5 % weight loss was observed at 212 ºC (Figure 38). With respect to the DSC curve (Figure 39), neither exothermic nor endothermic processes were observed for the polymer thin film.

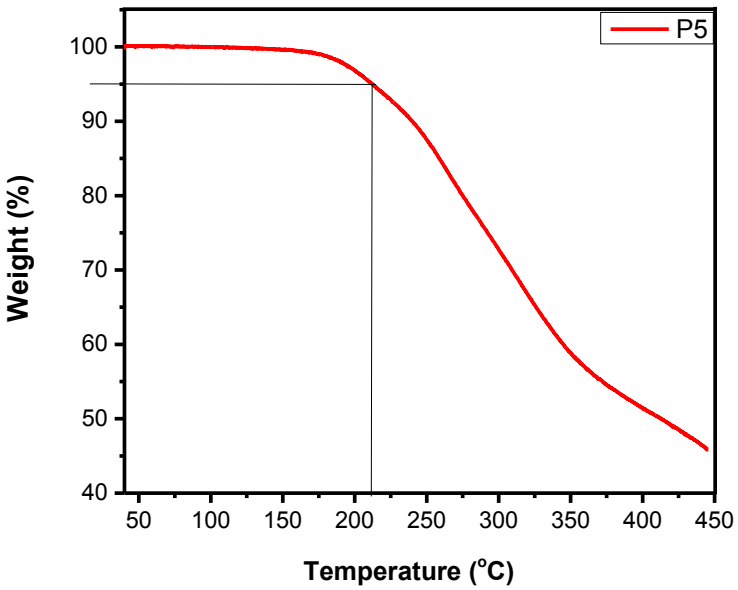

Figure 38: TGA curve for **P5-DTAE-BT** measured with a heating rate of 10 °C.min^{-1} under N_2

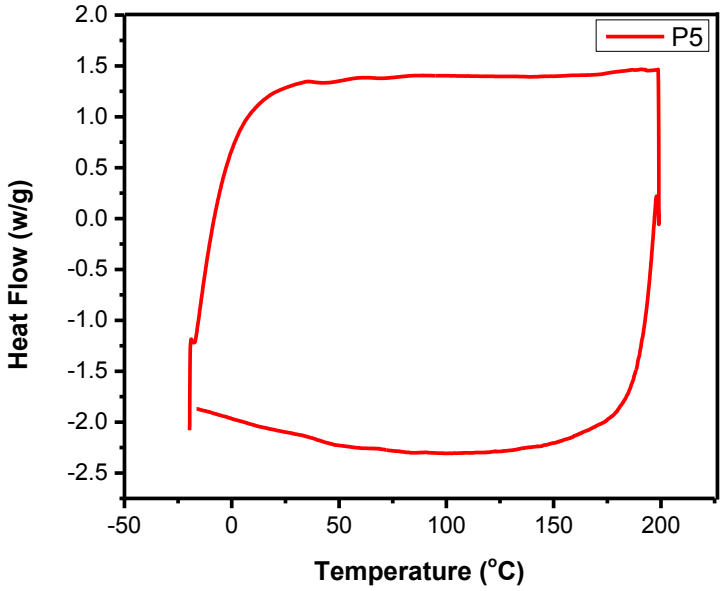

Figure 39: DSC profiles for **P5-DTAE-BT** obtained at a scanning rate of 10 °C.min^{-1} under N_2

7.1.4 X-Ray Diffraction

The XRD results show that only the film annealed at 150 °C exhibited a small peak at 2θ = 3.1°, which means that this polymer has very poor crystallinity (Figure 40) The 200 °C-annealed showed reflection peaks, indicating this polymer was decomposed at this temperature in agreement with the TGA results (Figure 35).

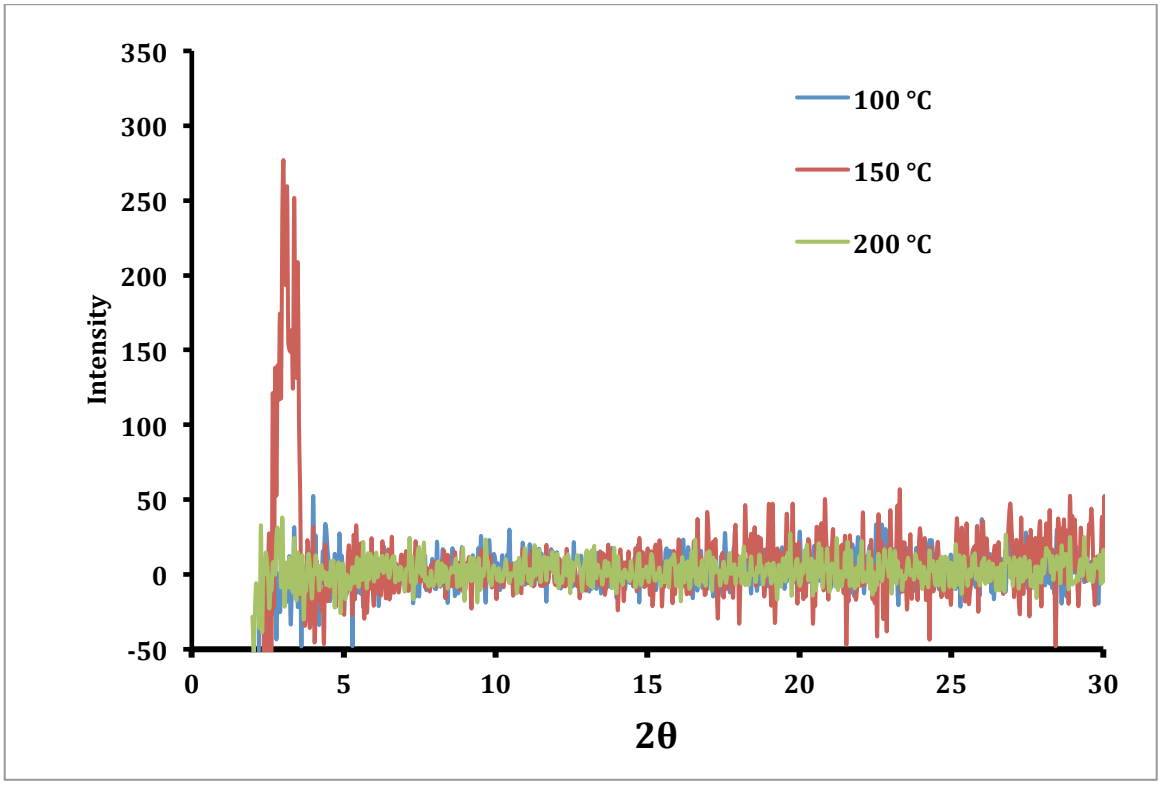

Figure 40: XRD diagram obtained for the spin coated **P6-DTAE-TT** thin film on dodecyltrichlorosilane (DTS)-modified SiO_2/Si substrates annealed at different temperatures in nitrogen.

8 Synthesis of P6-DTAE-TT

The synthesis of **P6-DTAE-TT** was achieved using the Stille coupling reaction with the **DTAE-Br (16)** with 2,5-bis(trimethylstannyl)thieno[3,2-*b*]thiophene (**TT**) in chlorobenzene at 100 °C via a palladium catalyst coupling reaction, as illustrated in Scheme 16. The polymer gives a blue-coloured solid product precipitated in methanol, which was then purified via Soxhlet extraction. Acetone and hexane were used in the Soxhlet extraction to remove impurities and oligomers from the polymer, and chloroform was employed for dissolving the polymer and extracting the final pure polymer used for the characterization and devices. The polymer

exhibited good solubility in chloroform with a high yield of 41 %, which was the highest yield reported for the **DTAE-Br** monomer compared to copolymerization with the other donor monomers used in this thesis. This polymer was characterized using GPC, UV-Vis, CV, TGA, DSC, XRD, and AFM as well as with an OTFT device. The synthesis was conducted under similar conditions in reference (Carsten 2011).

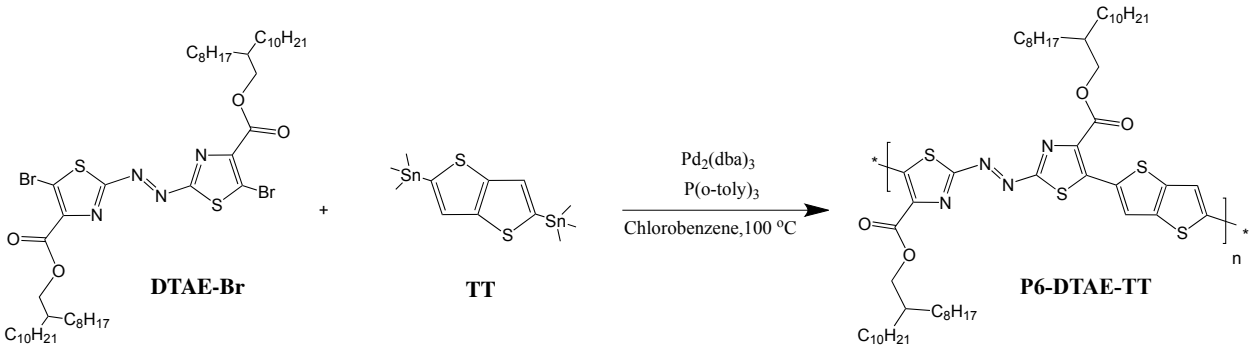

Scheme 16: Synthesis of **P6-DTAE-TT** through Stille coupling.

8.1 Characterization of P6-DTAE-TT

8.1.1 Gel permeation chromatography

The number average (M_n) and weight average molecular weights (M_w) were determined to be 11.8 kDa and 33.7 kDa, respectively, using GPC at a column temperature of 40 ^oC with chloroform as the eluent and polystyrene as the standard. The number average molecular weight (M_n) and weight average molecule weight (M_w) of **P5-DTAE-BT** polymer were higher than those of the previous polymers (**P2-DTAE-BT**, **P3-DTAE-B,** and **P4-DTAE-B**), this polymer (**P6-DTAE-TT**) shows the highest number average molecular weight (M_n) and weight average molecular weight (M_w), and its PDI was measured at 2.85.

8.1.2 Thermal gravimetric analysis

The TGA measurements for the **P6-DTAE-TT** polymer revealed the highest and most stable thermal behaviour results, as shown in Figure 41: observations of 233 ^oC with a 5 % weight loss.

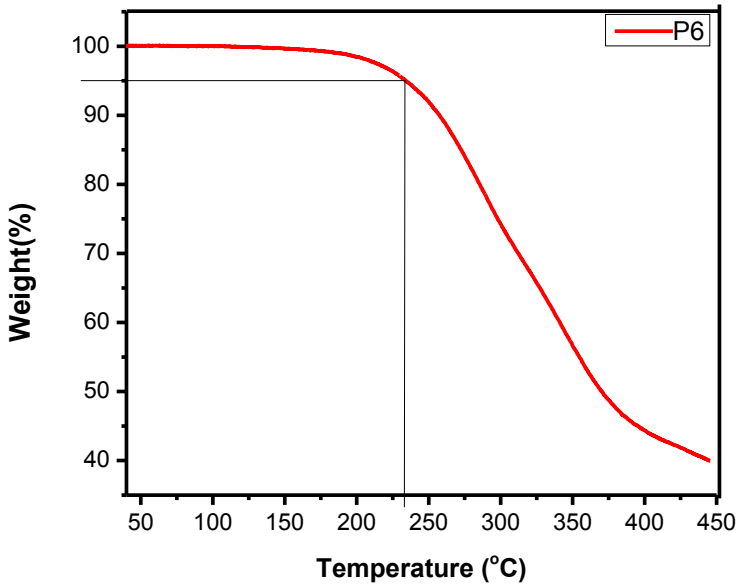

Figure 41: TGA curve for **P6-DTAE-TT** measured at a heating rate of 10 °C.min^{-1} under N_2

8.1.3 Differential Scanning Calorimetry

As shown in Figure 42, the DSC curves for **P6-DTAE-TT** show results similar to those for **P5-DTAE-BT:** no exothermic or endothermic peaks. The DSC and TGA results indicate that this polymer has much more stability than **P5-DTAE-BT** or other direct arylation polymers.

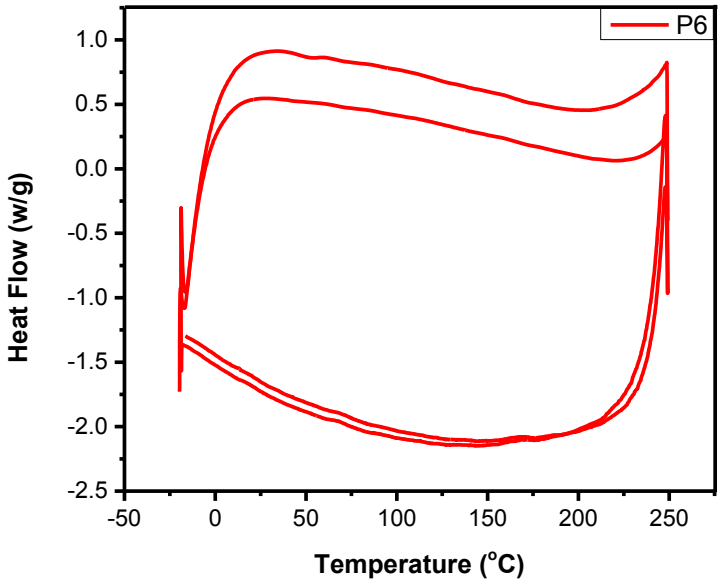

Figure 42: DSC profiles for **P6-DTAE-TT** obtained at a scanning rate of 10°C.min^{-1} under N_2

8.1.4 Ultraviolet-Visible Spectrometry and Cyclic Voltammetry

The electrochemical characterization of the **P6-DTAE-TT** copolymer was tested through UV-Vis and CV measurements. The results show a band gap of 1.32 eV for calculations using the onset wavelength, which equates to 937 nm (Figure 43). This band gap is also in the range of a narrow band gap, which means that there is an extended π-conjugation along the polymer backbone and strong intramolecular and/or intermolecular D-A interactions in the polymer backbone (Yan 2013). The CV curve (Figure 44) shows striking E_{HOMO} and E_{LUMO} results for the **P6-DTAE-TT** thin film. The oxidation and reduction effects are clear in the graph: -5.38 eV and -4.38 eV for the HOMO and LUMO energy levels, respectively, or -4.06 eV for the LUMO if the calculations are based on the band gap.

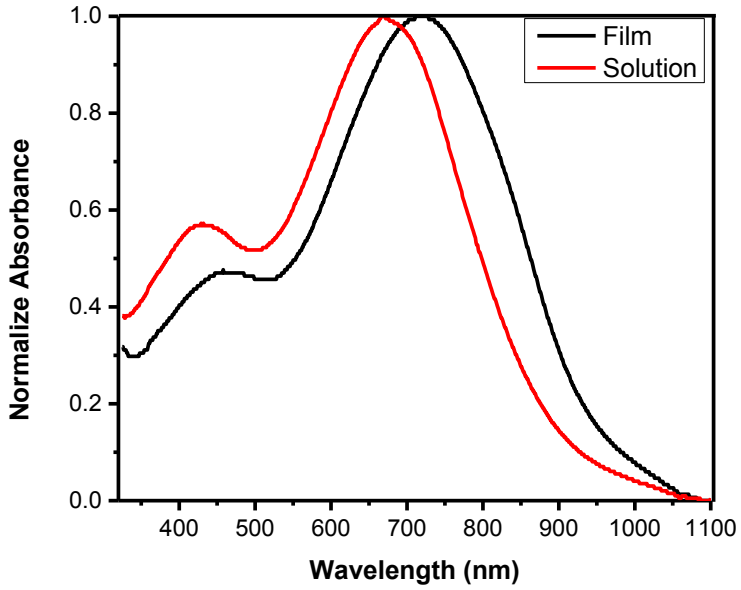

Figure 43: UV-Vis-NIR absorption spectra for **P6-DTAE-TT** in chloroform and in a thin film

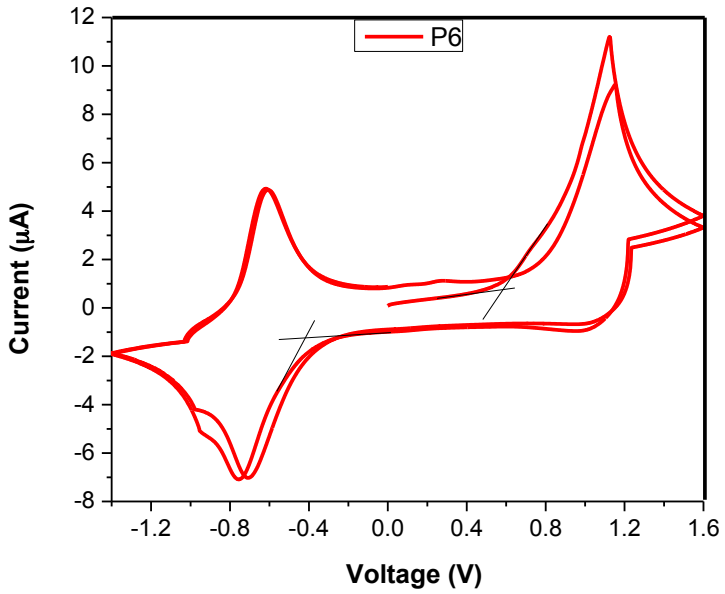

Figure 44: CV results (two cycles) for a **P6-DTAE-TT** thin film showing two oxidative and reductive cycles at a scan rate of 0.05 V s^{-1}. The electrolyte was 0.1 M tetrabutylammonium hexafluorophosphate in anhydrous acetonitrile

8.1.5 Atomic Force Microscopy

The AFM images show the surface morphology of the **P6-DTAE-TT** thin film spin coated on dodecyltrichlorosilane (DTS) (Figure 35). There are some pinholes in the polymer thin films.

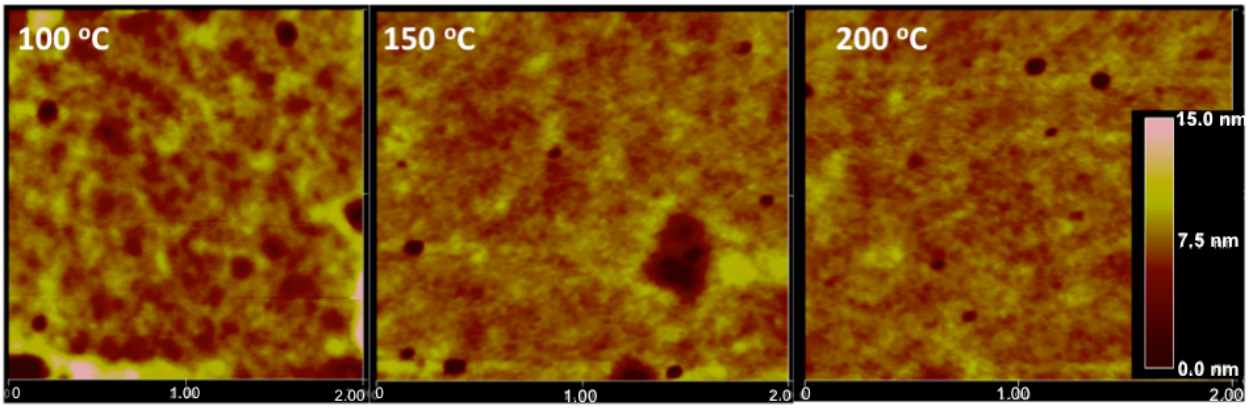

Figure 45: AFM height images (2 μm × 2 μm) of **P6-DTAE-TT** thin films (~35 nm) spin coated on DTS-modified SiO_2/Si substrates and annealed at a variety of temperatures for 15 min under N_2.

8.1.6 X-Ray Diffraction

Figure 46 discribes the crystanility strecture for polymer **P6-DTAE-TT**. **P6-DTAE-TT** shows an improvement in the crystallinity compared to **P5-DTAE-BT**. **P6-DTAE-TT** showed a small peak at 100 ^{o}C and this peak is increased when the annealing temperature is increased to 150 °C. A high crystanility was observe at 150 ^{o}C in the **P6-DTAE-TT** film annealed at 2θ = 3.5^{o}.

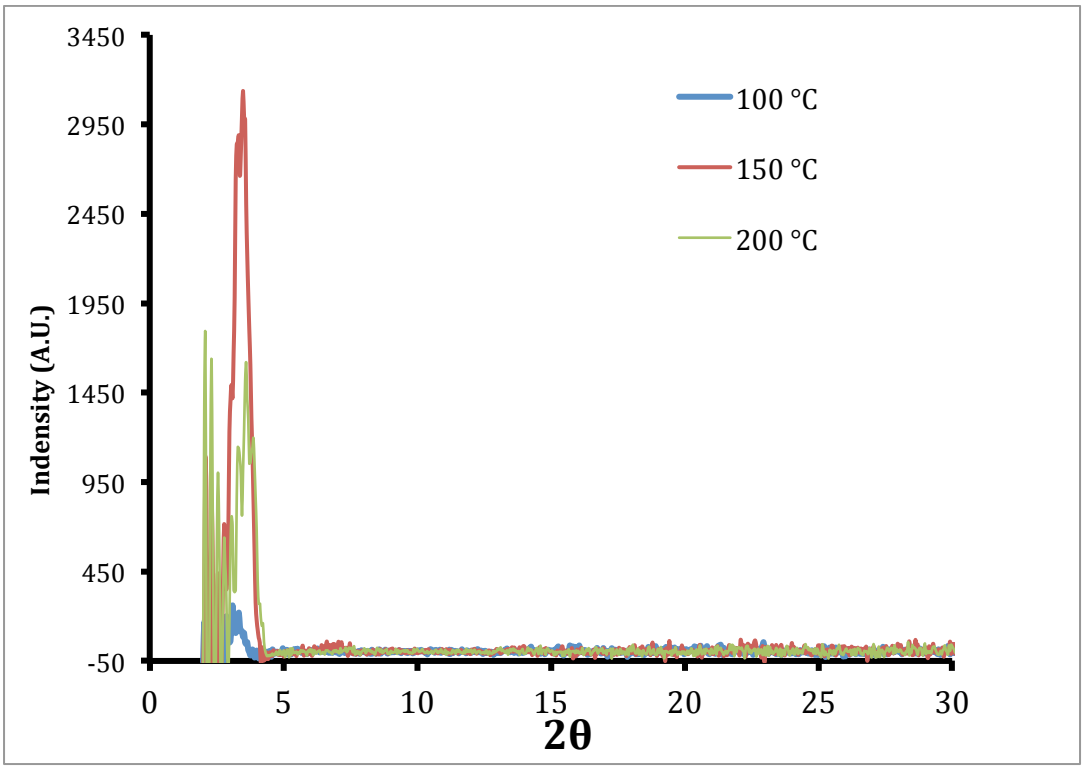

Figure 46: X-RD diagram obtained from the spin-coated **P6-DTAE-TT** thin film on dodecyltrichlorosilane (DTS)-modified SiO_2/Si substrates annealed at 150 ^{o}C in nitrogen

9 Device Performance of P6-DTAE-TT

P6-DTAE-TT was evaluated as a channel semiconductor for OTFT devices with a bottom-gate, bottom-contact configuration as well. Gold (Au) was used as source and drain electrodes, however, an n-silicon wafer was used as a gate electrode. Polymer thin film from a 1 % chloroform solution of **P6-DTAE-TT** was spin coated on top of the DTS-modified SiO_2/Si substrate**.** The polymer film was optionally annealed at the selected temperature for 20 min under

nitrogen air. The results of the device performance are shown in Table 4.

Table 4: Summary of the OTFT device performance using **P6-DTAE-TT** as the **n-type** semiconductor channel layers. [a]

Annealing temperature	**Electron mobility ($cm^2V^{-1}s^{-1}$)**	V_T **(V)**	V_D
150 °C	4.0×10^{-4}	78.4 V	100
	3.1×10^{-4}	78.2	
	7.5×10^{-5}	71.8	
	5.7×10^{-4}	**85.5**	
	2.8×10^{-4}	85.3	
200 °C	5.0×10^{-4}	59.4	
	4.0×10^{-4}	51.7	
	3.8×10^{-5}	50.6	
	1.7×10^{-4}	73.7	
	4.6×10^{-4}	78.7	

[a] The devices were annealed in a glove box on a hotplate at the selected temperature for 10 min under nitrogen. μ_{e-} is the electron mobility in the saturated regions in electron enhancement mode. Each set of the data was obtained from 3-5 OTFT devices.

The results show that **P6-DTAE-TT** thin film is an n-type semiconductor that exhibits the highest mobility of 5.7×10^{-4} cm^2 V^{-1} s^{-1} at 150 °C (V_T = 85.5 V). Increased thermal annealing of the polymer thin film does not seem to offer increased mobility. The output and transfer curves for the device performances are presented in Figure 47. The excellent solubility of the **P6-DTAE-TT** copolymer demonstrated by the above results as well as its stable thermal behaviour and low band gap, with low levels of LUMO energy, makes it well suited as a semiconductor channel for OTFT, OPV and other applications.

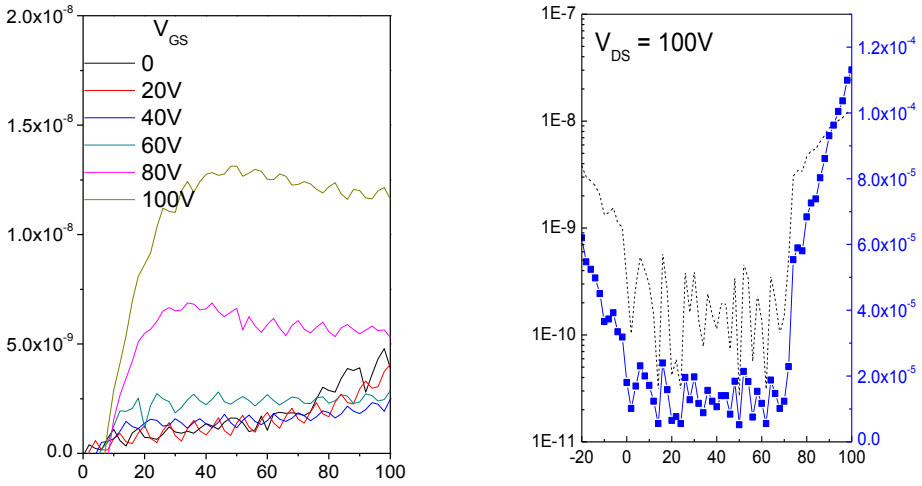

Figure 47: Output (left) and transfer (right) characteristics of **P6-DTAE-TT** based on OTFT device measurements, showing the best performance. A **P6-DTAE-TT** thin film annealed at 100 ^{o}C was used as the channel layer. The electron mobility is calculated at 5.7×10^{-4} $cm^2V^{-1}s^{-1}$ at V_{DS} = -80 V. Device dimensions: channel length (L) = 30 µm; channel width (W) = 1 mm

Among all the results shown above, **P6-DTAE-TT** shows the most promising result in terms of narrow band gap, lower LUMO energy level, thermal stability, better crystallization in its layers, as well as a higher mobility of 5.7 x 10^{-4} cm^2 V^{-1} s^{-1} which makes this polymer suitable for OPVs and OTFT application for a novel π-conjugated polymer.

10 Conclusion

The following conclusions can be drawn from these experimental results:

- First, using the ethanol solvent for the monomer purification produces results that are significantly superior to those obtained with CH_3CN, as could be seen from **P3** and **P4**.
- Second, with respect to the polymers, a Stille coupling reaction is a more effective method for the synthesis of an azo compound than is direct arylation.

In conclusion, this chapter has presented experimental results that show that the **DTAE** electron acceptor can be used as a building block for making polymer semiconductors.

As described, the new polymers exhibited improvements in the molecular weight. The research also resulted in the discovery of an easy method of synthesizing the monomer and obtaining an n-type polymer that could be used for a variety of applications such as OTFTs and OPVs.

As demonstrated, not only was the molecular weight of this type of polymer improved, but an n-type polymer for the same functional group was also obtained with simple replacing the alkyl side chains with ester side chains.

11 Experimental Section

11.1 General

All chemicals were purchased from Sigma-Aldrich and were used without further purification.

The geometry optimization of 2-octyldodecyl 3-bromo-2-oxopropanoate, (E)-bis(2-octyldodecyl) 2,2'-(diazene-1,2-diyl)bis(thiazole-4-carboxylate), (E)-bis(2-octyldodecyl) 2,2'-(diazene-1,2-diyl)bis(5-bromothiazole-4-carboxylate) **DTAE,** (*E*)-2-octyldodecyl 5-([2,2'-bithiophen]-5-yl)-2-((4-(((2-octyldodecyl)oxy)carbonyl)thiazol-2-yl)diazenyl)thiazole-4-carboxylate (**DTAE-BT**), (*E*)-2-octyldodecyl 2-((4-(((2-octyldodecyl)oxy)carbonyl)thiazol-2-yl)diazenyl)-5-phenylthiazole-4-carboxylate (**DTAE-B**), and (*E*)-2-octyldodecyl 2-((4-(((2-octyldodecyl)oxy)carbonyl)thiazol-2-yl)diazenyl)-5-(thieno[3,2-*b*]thiophen-2-yl)thiazole-4-carboxylate (**DTAE-TT**) was performed based on density functional theory (DFT) calculations using the B3LYP hybrid functional with the 6-31G basis set (Frisch 2009), (Lee 1988), (Frisch 2009), (Frisch 2010).

^{1}H NMR and ^{13}C NMR results were collected on Bruker DPX spectrometer at 300 MHz and 75 MHz, respectively.

UV-Vis, CV, TGA, DSC, AFM, and XRD measurement conditions were the same as the ones presented in Chapter 2, with the UV-Vis data recorded on a Thermo Scientific model GENSYS^{TM} 10S VIS spectrophotometer and the CV measurements obtained with a Digi-Ivy model DY2111 Potentiostat using an Ag/AgCl reference electrode, a platinum foil counter electrode, and a platinum disk working electrode. TGA was conducted using a TGA Q500 (TA

Instruments) at a heating rate of 10 °C.min^{-1} under nitrogen, and DSC data were calculated using a heating rate of 10 °C.min^{-1} under N_2. AFM images were scanned for polymer thin films on a DTS-modified SiO2/Si substrate using a Dimension 3100 Scanning Probe Microscope, and XRD measurements were taken with a Bruker D8 Advance powder diffractometer with Cu Ka radiation (λ = 1.5406 Å) using standard Bragg-Brentano geometry. However, the GPC measurement conditions were slightly different for the work described in this chapter: all polymer results were obtained using a Malvern GPC system with chloroform as an eluent and polystyrene as a standard at a low column temperature of 40 ^{o}C (Li 2012).

11.2 Fabrication and Characterization of OTFT Devices

The fabrication of the **P6-DTAE-TT** polymer was quite similar to that of **P1-DTA-BTV** with respect to the layer used as the gate dielectric in the glove box as well as the temperature used. A bottom-gate, bottom-contact OTFT structure was employed for the evaluation of **P6-DTAE-TT** with a heavily n-doped Si/SiO_2 wafer as the substrate. However, this substrate was first cleaned with an ultrasonic deionized water (DI) bath and then rinsed with acetone and isopropanol solvents. The gold source and drain electrode pairs in the bottom-gate, bottom-contact device were deposited using conventional photolithography to obtain the defined device dimensions with a channel length (L) of 30 μm and a channel width (W) of 1000 μm (Guo 2014). The film was around 30 nm to 50 nm thick and was deposited on the substrate by spin coating a polymer solution in chloroform (5 mg mL^{-1}) at 3000 rpm for 40 second and subsequently annealing it at 150 ^{o}C, and 200 ^{o}C for 20 minutes for each temperature. A Si layer (~300 nm) was then spin coated as the gate, and SiO_2 layer fraction as a dielectric in a glove box under nitrogen, dried at 100 ^{o}C . Then the devices were preformed in air in the absence of light using an Agilent B2900A Semiconductor Analyzer. The carrier mobility was determined in the saturation regime according to the following equation, as explained in the introductory chapter. This device characterization was done with the assistance of Chang Guo, a PhD student in Prof. Li's group using the same measurement conditions in (Guo 2014):

$$I_{DSsat} = \frac{WCi\mu}{2L}(V_{GS} - V_T)^2$$

11.3 Synthesis procedures

11.3.1 Procedure for the First Method

Synthesis of 2-octyldodecyl 2-oxopropanoate (6): (2.0g – 1.0 equivalent) of 2-oxopropanoic acid was added to a 100 ml RB flask. Then, (6.78 g, 1.0 equivalent) of 2-octyl-1-dodecanol was also added to the same flask. 80 ml of toluene was added to the mixture, which was heated at 80 ^{o}C with a stir bar and refluxed. (0.136 g) of toluenesulfonic acid (TsOH) was added to the reaction, which was then left for 72 h to react. After the 72 h, the reaction changed colour from white to clear yellow. The reaction was cooled down to room temperature, extracted, and tested using thin layer chromatography (TLC). Three spots were shown by the TLC, the second of which is the major spot, which is the product. The product was then purified by column chromatography, tested using ^{1}H NMR to save 8.21 g (95% yield) of pure product (ester, compound (**6**). The synthesis was conducted under similar conditions in reference (Kozłowski 1989).

^{1}H NMR (300 MHz, $CDCl_3$): 7.27, 4.18. 2.4, 1.5, 1.3, 1.2, 0.89, 0.01 (Figure A-4).

^{1}H NMR data were compared with ^{1}H NMR data schedule listed in references (Gottlieb 1997).

Synthesis of 2-octyldodecyl 3-bromo-2-oxopropanoate (7): To brominate the ester**,** (2-octyldodecyl-2-oxopropanoate) (2 g, 5.32 mmol, 1.0 equivalent) was added to a clean, dry 50 ml RB flask at room temperature. A bromine (0.867 mL, 5.42 mmol, 1 equivalent) solution in dichloromethane DCM (7 mL) was added dropwise to the same flask. The mixture was then stirred for 1 h at room temperature in the dark. The reaction mixture was poured into 100 mL of 0.1 M $Na_2S_2O_3$ solution, and the two layers were separated. The aqueous layer was extracted with methylene chloride (50 mL), and the combined organics were washed with water (50 mL), dried over $MgSO_4$, and filtered. The solvent was evaporated under reduced pressure to save approximately 1.730 g of liquid (75 % yield). Reaction conditions is similar to that in (Kozłowski 1989).

^{1}H NMR (300 MHz, $CDCl_3$): 7.27, 4.31, 4.24, 2.48, 1.79, 1.7, 1.5, 1.28, 0.89, 0.01 (Figure A-5)

Synthesis of bis(2-octyldodecyl) 2,2'-(hydrazine-1,2-diyl)bis(thiazole-4-carboxylate) dihydrobromide (8): 2-octyldodecyl-3-bromo-2-oxopropanoate (1.019 g, 1.474 mmol, 2.0 equivalent) and 2,5-dithiobiurea (0.1105 g, 0.732 mmol, 1.0 equivalent) were heated in ethanol (5 mL) at 50 ^{o}C for 2.5 h under argon. The mixture was then cooled to room temperature and tested by H NMR using both $CDCL_3$ and DMSO. 30 ml of ethanol was then added to the mixture reaction and refluxed for 5 h under argon. The reaction was then collected by evaporating the solvent to save 1.0739 g (95 % yield)

^{1}H NMR (300 MHz, DMSO): 7.70, 4.08, 2.50, 1.23, 0.84 (Figure A-6)

^{1}H NMR (300 MHz, $CDCl_3$): 7.28, 4.23, 3.64, 1.76, 1.28, 0.90, 0.023 (Figure A-7)

Synthesis of DTAE (9): 8 ml of HNO_3 was added dropwise to (0.997 g, 0.087 mmol, 1.0 equivalent) bis(2-octyldodecyl) 2,2'-(hydrazine-1,2-diyl)bis(thiazole-4-carboxylate) dihydrobromide. The white dispersion turned yellow immediately and then became orange. The mixture was stirred for 30 min after the addition of the HNO_3 solution. The extraction was made so that the reaction mixture separated into two layers, and a base was added until the PH = 7, in order to eliminate the acid in the solution. The orange solid was collected by suction filtration, washed briefly with EtOH, and dried in a vacuum chamber to produce 1.5286 g (weight of wet solid). This reaction was not successful.

^{1}HNMR (300 MHz, $CDCl_3$): 7.26, 1.54, 1.25, 0.88 (Figure A-8).

11.3.2 Procedure for the Second Method

Synthesis of 3-bromo-2-oxopropanoic acid (10): 2-oxopropanoic acid (2.990 g, 33.95 mmol, 1.0 equivalent) was added to a clean, dry 50 ml RB flask at room temperature. A bromine (1.75 mL, 34.06 mmol, 1 equivalent) solution was added dropwise. The mixture was stirred overnight at room temperature in the dark. After the mixture was stirred over the weekend at room temperature, brown particles precipitated from the reaction mixture. The particles were collected by suction filtration and broken with a spatula. The crystals were then washed with water until an orange colour was observed. The solid was then dried in a vacuum chamber at 50 ^{o}C for 1 h and then at room temperature for 3 h to save 5.31 g (93 % yield).

Synthesis of 2,2'-(hydrazine-1,2-diyl)bis(thiazole-4-carboxylic acid) (11): 3-bromo-2-oxopropanoic acid (2.027 g, 12.410 mmol, 2.0 equivalent) and 2,5-dithiobiurea (0.8488 g, 12.10 mmol, 1.0 equivalent) were heated in ethanol (5 mL) at 50 ^{o}C for 2.5 h under argon. The mixture was then cooled to room temperature and tested by H NMR using both $CDCL_3$ and DMSO. 30 ml of ethanol was then added to the mixture, and the reaction was refluxed for 5 h under argon. The reaction was then collected by evaporating the solvent to save 2.96 g (95 % yield).

^{1}H NMR (300 MHz, DMSO): 7.55, 3.22, 2.37, 1.95, 1.10, 0.92 (Figure A-9).

Synthesis of (*E*)-2,2'-(diazene-1,2-diyl)bis(thiazole-4-carboxylic acid) (12): 16 ml of HNO_3 was added dropwise to (2.96 g, 6.605 mmol, 1.0 equivalent) 2,2'-(hydrazine-1,2-diyl)bis(thiazole-

4-carboxylic acid) dihydrobromide. The white dispersion turned yellow immediately and then became orange. The mixture was stirred for 30 min after the addition of an HNO_3 solution. Extraction caused the reaction mixture to separate into two layers, and a base was added until the PH = 7 to eliminate the acid in the solution. The orange solid was collected by suction filtration, washed briefly with EtOH, and dried in a vacuum chamber to produce 0.93 g (weight of wet solid).

^{1}H NMR (300 MHz, DMSO): 8.66, 4.23, 3.22, 2.36, 1.94, 1.21 (Figure A-10).

Synthesis of (*E*)-bis(2-octyldodecyl) 2,2'-(diazene-1,2-diyl)bis(thiazole-4-carboxylate) DTAE (13): (0.4097g – 1.0 equivalent) of (*E*)-2,2'-(diazene-1,2-diyl)bis(thiazole-4-carboxylic acid) was added to a 150 ml RB flask. (0.860 g, 2.0 equiv.) of $C_{20}H_{42}O$ 2-octyl-1-dodecano was added to the same flask. 100 ml of toluene was added to the mixture. Heating began at 160 ^oC with a stir bar and refluxing. (0.140 g) of TsOH was added to the reaction, which was left to react overnight. After 12 h, the reaction did not change colour. This reaction was not successful.

11.3.3 Procedure for the Third Method

Synthesis of 2-octyldodecyl 3-bromo-2-oxopropanoate (14): (3.74 g, 22.40 mmol, 1.0 equivalent) of 3-bromo-2-oxopropanoic acid was added to a 250 ml RB flask. (6.84 g, 22.91 mmol, 1.0 equivalent) of $C_{20}H_{42}O$ 2-octyl-1-dodecano was added to the same flask. 200 ml of toluene was added to the mixture. Heating began at 160 ^oC with a stir bar and refluxing. (0.34 g) of TsOH was added to the reaction, which was left to react overnight. After 12 h, the reaction changed colour from cloudy white to yellow. The ester was then extracted and the reaction was suction vacuumed to save 9.98 g (95 % yield).

^{1}HNMR (300 MHz, $CDCl_3$): 7.26, 7.17, 4.29, 4.22, 4.21, 2.35, 1.75, 1.73, 1.30, 1.26, 0.40 (Figure A-11(a)).

^{13}C NMR (75 MHz, $CDCl_3$): 184.67, 159.70, 129.14, 128.33, 77.58, 77.16, 76.74, 69.94, 32.04, 32.01, 31.16, 30.79, 29.99, 29.75, 29.69, 29.65, 29.47, 29.71, 26.74, 22.81, 14.22 (Figure A-11(b)).

Synthesis of (E)-bis(2-octyldodecyl) 2,2'-(diazene-1,2-diyl)bis(thiazole-4-carboxylate) DTAE (15): (4.0336 g, 9.013mmol, 2.0 equivalent) of 2-octyldodecyl 3-bromo-2-oxopropanoate was added to a 150 ml RB flask, which had been dried and filled with argon gas. (0.678 g, 9.013 mmol, 1.0 equivalent) of Hydrazine-1.2-bis(carbothioamide) was then added to the same flask.

80 ml of ethanol was added to the mixture. The reaction was refluxed at 110 ^{o}C under argon for 5 h, after which, the colour turned to a clear yellow. The reaction was then cooled down to room temperature and left over the weekend (50 h) (**15**). After 50 h, 5 ml of H_2O_2 was added dropwise to the reaction at 0 ^{o}C using an ice bath. The colour of the reaction became dark yellow and then orange. The reaction was left to react for 15 h under argon, after which the reaction was suction filtered and then dried in a vacuum for 2 h to save 2.3562 g of dry orange powder. Column chromatography was then performed for the 2.3562 g of product (toluene: ethyl acetate) (9.5: 0.5). The first spot was collected, evaporated, and then dried in the vacuum to save 1.51 g of pure product. (First spot only), orange powder (**15**) (62% yield).

^{1}HNMR (300 MHz, $CDCl_3$): 8.35, 7.26, 4.33, 4.31, 1.84, 1.66, 1.37, 1.25, 1.07, 0.88, 0.86, 0.84 (Figure A-12 (a)).

^{13}C NMR (75 MHz, $CDCl_3$): 173.99, 160.84, 148.95, 131.14, 77.58, 77.36, 77.16, 76.74, 69.05, 37.52, 32.04, 31.37, 30.08, 29.77, 29.71, 29.79, 29.69, 29.47, 26.43, 22.82, 14.24 (Figure A-12(b)).

Synthesis of (E)-bis(2-octyldodecyl) 2,2'-(diazene-1,2-diyl)bis(5-bromothiazole-4-carboxylate) DTAE-Br (16): (0.2075 g, 0.245mmol, 1 equivalent) of (E)-bis(2-octyldodecyl) 2,2'-(diazene-1,2-diyl)bis(thiazole-4-carboxylate) (**15**) was added to a 100 ml clean, dry RB flask. (3.96 mmol/40 mL) of a chloroform solution and (7.92 mmol/10 mL) of a chloroform bromine solution were then added to the reaction. (0.62 mL) of (0.792M) was used for bromine in chloroform. (2.5 mL) of chloroform was used for (**15**). The mixture was then heated to 50 ^{o}C under argon. (0.273 g) of the product was observed.

Column chromatography was then done for the final product in DCM. First spot was collected. (0.200 g) of pure monomer was obtain after column chromatography, red powder. (74% yield).

^{1}HNMR (300 MHz, $CDCl_3$): 7.26, 4.35, 4.33, 2.04, 1.85, 1.59, 1.35, 1.26, 1.07, 0.87, 0.07 (Figure A-13 (a))

^{13}C NMR (75 MHz, $CDCl_3$): 171.74, 160.51, 145.90, 124.22, 77.58, 77.18, 76.75, 69.35, 37.44, 32.06, 32.09, 31.30, 30.08, 29.79, 29.75, 29.71, 29.50, 29.45, 26.79, 22.83, 22.82, 14.27 (Figure A-13 (b)).

11.3.4 Polymerization

12.3.4.1 Direct Arylation

Synthesis of P2-DTAE-BT: The synthesis was conducted under similar conditions in reference (Berrouard 2012). (0.304 g, 0.359 mmol, 1.0 equivalent) of (E)-bis(2-octyldodecyl) 2,2'-(diazene-1,2-diyl)bis(thiazole-4-carboxylate) (**15**), and (0.117 g, 0.359 mmol, 1.0 equivalent) of 5,5'-dibromo-2,2'-bithiophene were added to a clean, dry two-necked 25 ml RB flask with a coater condenser. (0.0016 g, 0.00718 mmol, 0.02 equivalent) of palladium acetate (Pd $(OAc)_2$) and (0.011 g, 0.1077 mmol, 0.30 equivalent) of pivalic acid (PivOH) were then added to the same flask. 3 ml of DMAc *N,N*-Dimethylacetamide was injected using a long needle under argon. The reaction was heated at 100 ^oC and refluxed under argon for 24 h. After 1 day, the reaction mixture was then cooled down to room temperature and precipitated out in 100 ml of ethanol. The solvent was then filtered out to collect 0.0853 g of the polymer (31 % yield).

Synthesis of P3-DTAE-B: The synthesis was conducted under similar conditions in references (Berrouard 2012), and (Okamoto 2013). (0.2005 g, 0.237 mmol, 1.0 equivalent) of (E)-bis(2-octyldodecyl) 2,2'-(diazene-1,2-diyl)bis(thiazole-4-carboxylate) (**15**) and (0.0559 g, 0.237 mmol, 1.0 equivalent) of 1,4-dibromobenzene were added to a clean, dry two-necked 25 ml RB flask with a coater condenser. (0.0010 g, 0.00474 mmol, 0.02 equivalent) of palladium acetate (Pd $(OAc)_2$), and (0.0272 g, 0.0711 mmol, 0.30 equivalent) of pivalic acid (PivOH) were then added to the same flask. 2 ml of DMAc (*N,N*-Dimethylacetamide) was injected using a long needle under argon. The reaction was heated at 100 ^oC and refluxed under argon for 24 h. After 1 day, the reaction mixture was cooled down to room temperature and precipitated out in 100 ml of ethanol. The solvent was then filtered out to collect 0.069 g of the polymer (30 % yield).

Synthesis of P4-DTAE-B: (0.100 g, 0.1182 mmol, 1.0 equivalent) of (E)-bis(2-octyldodecyl) 2,2'-(diazene-1,2-diyl)bis(thiazole-4-carboxylate) (**15**) that was made from the CH_3CN solvent reaction, and (0.0279 g, 0.1182 mmol, 1.0 equivalent) of 1,4-dibromobenzene were added to a clean, dry two-necked 25 ml RB flask with a coater condenser. (0.00053 g, 0.0023 mmol, 0.02 equivalent) of palladium acetate (Pd $(OAc)_2$) and (0.035 g, 0.0036 mmol, 0.30 equivalent) of (PivOH) were then added to the same flask. 1 ml of DMAc *N,N*-Dimethylacetamide was injected using a long needle under argon. The reaction was heated at 60 ^oC under argon for 24 h. The colour of the reaction changed immediately to brown and then green. The color stayed green, and some solid remained on the wall of the RB flask. After 1 day, the reaction mixture was cooled

down to room temperature, a small amount was removed and added dropwise into 50 ml of methanol, and the polymer was fully dissolved in the methanol, with no clear precipitation showing. The polymer was then heated up to 80 ^{o}C and left overnight to react. (0.035 g) of the polymer was collected the next day through suction filtration (30 % yield).

11.3.4.2 Stille Coupling Polymerization

Synthesis of P5-DTAE-BT: The synthesis was conducted under similar conditions in reference (Yan. Z. 2013). **(**0.1630 g) of (*E*)-bis(2-octyldodecyl) 2,2'-(diazene-1,2-diyl)bis(5-bromothiazole-4-carboxylate) (**DTAE-Br**, compound **16)** was weighed and placed into a clean, dry two-necked 50 ml RB flask with a stir bar and water condenser. It was then dried with a heat gun. The solvent was pumped out three times, and the flask was filled with argon three times as well. Both necks were covered with rubber covers. (0.0799 g) of **BT** was weighed and added to the same flask. (0.0039 g) of P(o-tolyl)$_3$ was weighed and added to the same flask. Both necks of the flask were covered with rubber covers. Under argon gas, using an argon bag, the bag was filled with argon three times, and (0.0029 g) of $Pd_2(dba)_3$ were weighed. (0.7 mL) of solvent was added to the $Pd_2(dba)_3$ catalyst, which was injected into the reaction using a 3 ml needle. The reaction was heated up to 100 ^{o}C in an oil bath under argon and was covered to keep it uncontaminated and dark. The reaction was left to react for 2 days (48 h). The mixture was added dropwise to 150 ml of methanol and filtered out. It was then washed with methanol, dried, and further purified through Soxhlet extraction using acetone, hexane, and chloroform to remove oligomers and other impurities. The remaining polymer was dissolved in chlorobenzene. A black film was obtained upon removal of the solvent. (0.02 g) of pure polymer was collected through chloroform extraction (20 % yield). This polymer was then dried in the vacuum for 2 h. Some of the polymer was dissolved in chloroform, and the colour of the polymer solution was blue-dark green.

Synthesis of P6-DTAE-TT: (0.160 g, 0.159 mmol, 1.0 equivalent) of brominated polymer (**8**) was added to a clean, dry 25ml RB flask. (0.0743 g, 0.159 mmol, 1.0 equivalent) of (dimethyl (5-(trimethylstannyl)thieno[3,2-b]thiophen-2-yl)stannyl)methylium was then added to the same flask with a small stir bar. (0.00388 g, 0.002 mmol, 2 % equivalent) of tris(dibenzylideneacetone)dipalladium was also added to the same flask. (0.0031 g, 0.0018 mmol, 80 % equivalent) of tri(o-tolyl)phosphine was added to the same reaction flask under argon. 1 ml of chloroform was added to the reaction, which was heated up to 100 ºC and stirred in the dark

for 3 days. The polymer was then precipitated in methanol dropwise using a pipette and then filtered with suction filtration to obtain the final impure polymer, which was then purified through Soxhlet extraction with an acetone, hexane, and chloroform solvent. The polymer was purified with acetone for 4 h, and a yellow solution was observed when the polymer was filtered. The second purification used hexane, refluxed for 17 h. (0.035 g) of polymer was collected from suction filtration in hexane, with a clear solution showing after filtration using methanol. The final step in the Soxhlet extraction was to dissolve the polymer in chloroform to obtain the pure polymer. This final process took about 3 h of refluxing, and (0.065 g) of polymer was collected with a clear methanol solution during filtration to save the pure polymer (41 % yield). The polymer was then dried in the vacuum for 2 h. Reaction conditions: (Carsten 2011).

Chapter 4

Summary and Future Work

1 Conclusion and Future Work

The first part of my thesis focused on the development of an azo thiazole (**DTA**) polymer, which had already been synthesized by other members in the research group. However, it was tackled with a different approach in this research, and evidence of the fulfillment of several of the goals of the work for this thesis has been presented, including the increase in the molecular weight and enhancement of the mobility of the polymer.

The second part of my thesis has devoted to the development of a new azo thiazole electron acceptor building block with ester side chains, **DTAE**, in order to lower the LUMO energy level of the resulting polymers to achieve n-type semiconductor performance. Two different polymerization techniques were utilized: direct arylation and Stille coupling. It was found that the direct arylation polymerization was not suitable for making **DTAE** polymers, resulting in only low molecular weight polymers with low yields. On the other hand, the Stille coupling polymerization method could produce **DTAE** polymers with much improved yields and molecular weight. On of the **DTAE** polymers, **P6-DTAE-TT**, made by Stille coupling reaction was evaluated in OTFT devices. This polymer showed n-type semiconductor performance due to the decreased LUMO energy level of P6 compared to the **DTAE** polymer counterpart with alkyl chain substitution prepared previously in our laboratory. This indicates that the incorporation of ester side chains has a significant effect to lower the LUMO energy level of the **DTAE** polymers, facilitating the electron transport.

Based on my successful preliminary results, the future direction for this project would be to further optimize the side chains to improve the crystallinity of the resulting polymers, since it is well known that a high molecular packing order is critical for efficient charge transport. Another improvement needs to be made is to further increase the molecular weight of the polymers. Although the molecular weight of the polymers made using the Stille coupling reaction was higher than that of the polymers made using the direct arylation, the molecular weight is still

unsatisfactory for optimum device performance. It is reported that a sufficiently high molecular weight is extremely important to achieve high charge carrier mobility. The molecular weight of the polymers for OTFTs needs to be at least M_n = 20-30 kD, while the Mn of our **P6-DTAE-TT** is only about 12 kD.

I also synthesized another **DTAE** polymer, **P7-DTAE-T** as shown in Scheme 17. Characterization of this new polymer and the device evaluation of **P5-DTAE-BT** are needed to further understand the rstructure-performance relationship of this new type of polymers.

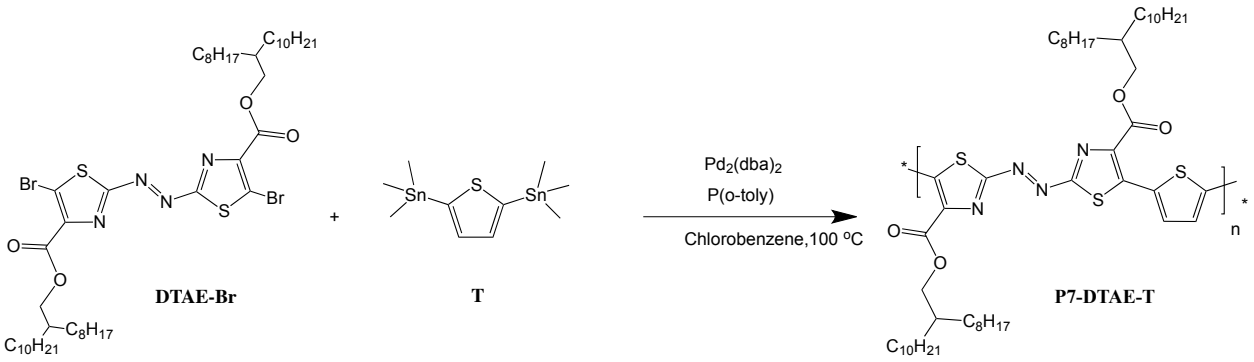

Scheme 17: Synthesis of **P7-DTAE-T** through Stille coupling.

The synthesis of this polymer shows in the Appendix A-3 section with ^{1}H NMR result for the polymer in $CDCl_3$.

Another future polymer could be made with different promising reaction conditions such as reaction condition showing in Scheme 18:

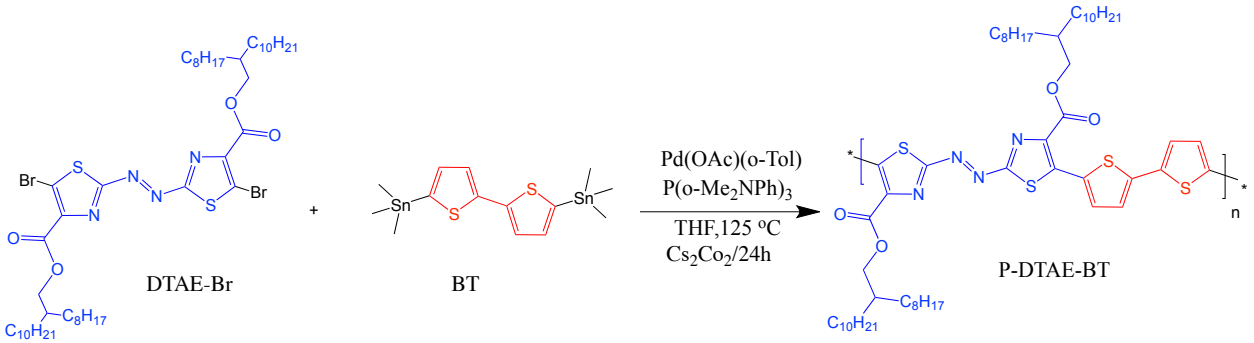

Scheme 18: Synthesis of **P-DTAE-BT** polymer with different reaction condition through direct arylation.

Appendix A

Additional Data

Appendix A-1 Chapter 2, NMR result:

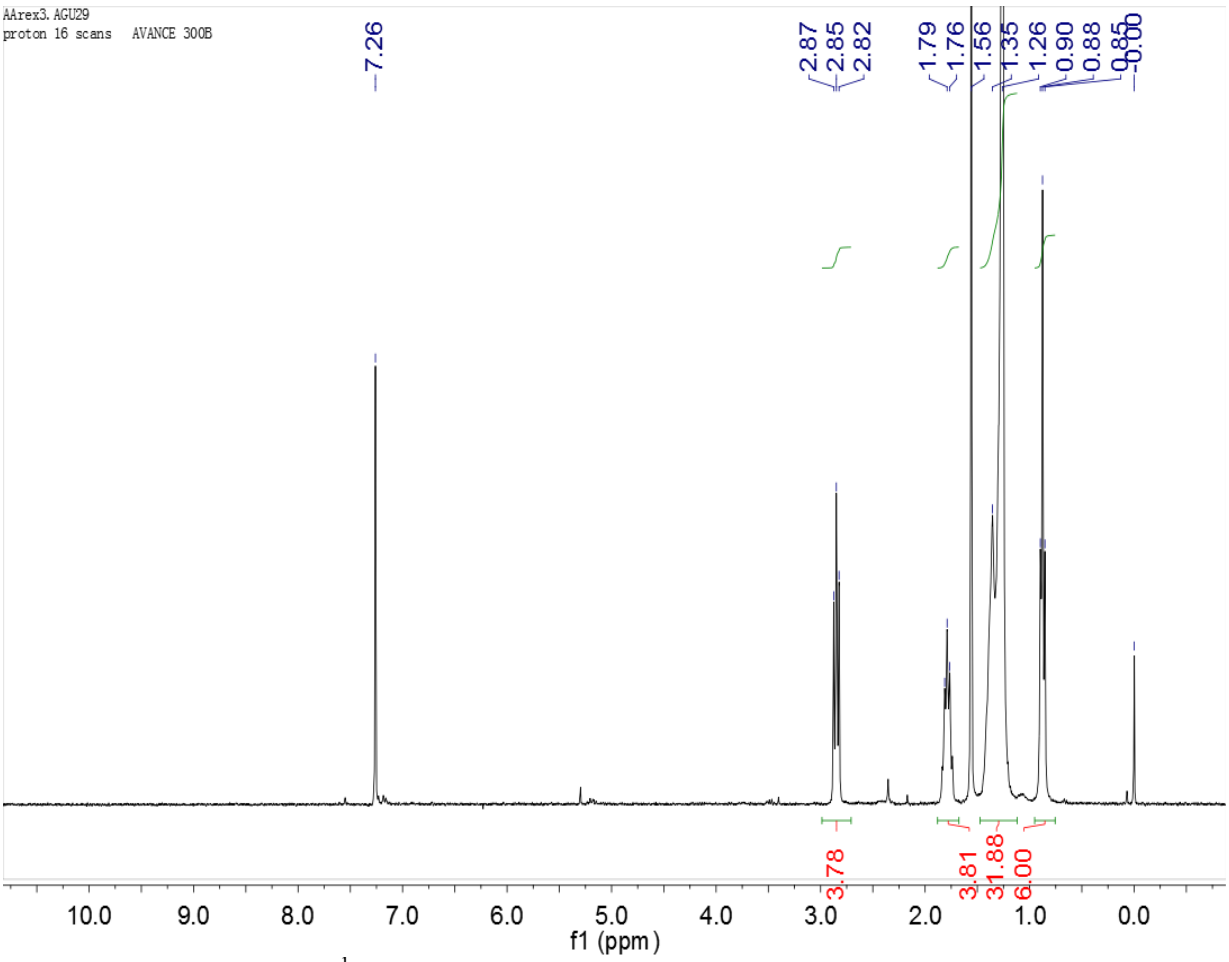

Figure A- 1: 300 MHz ^{1}H NMR spectrums for (E)-1,2-di(thiazol-2-yl)diazene (**DTA**) (**4**) in $CDCl_3$

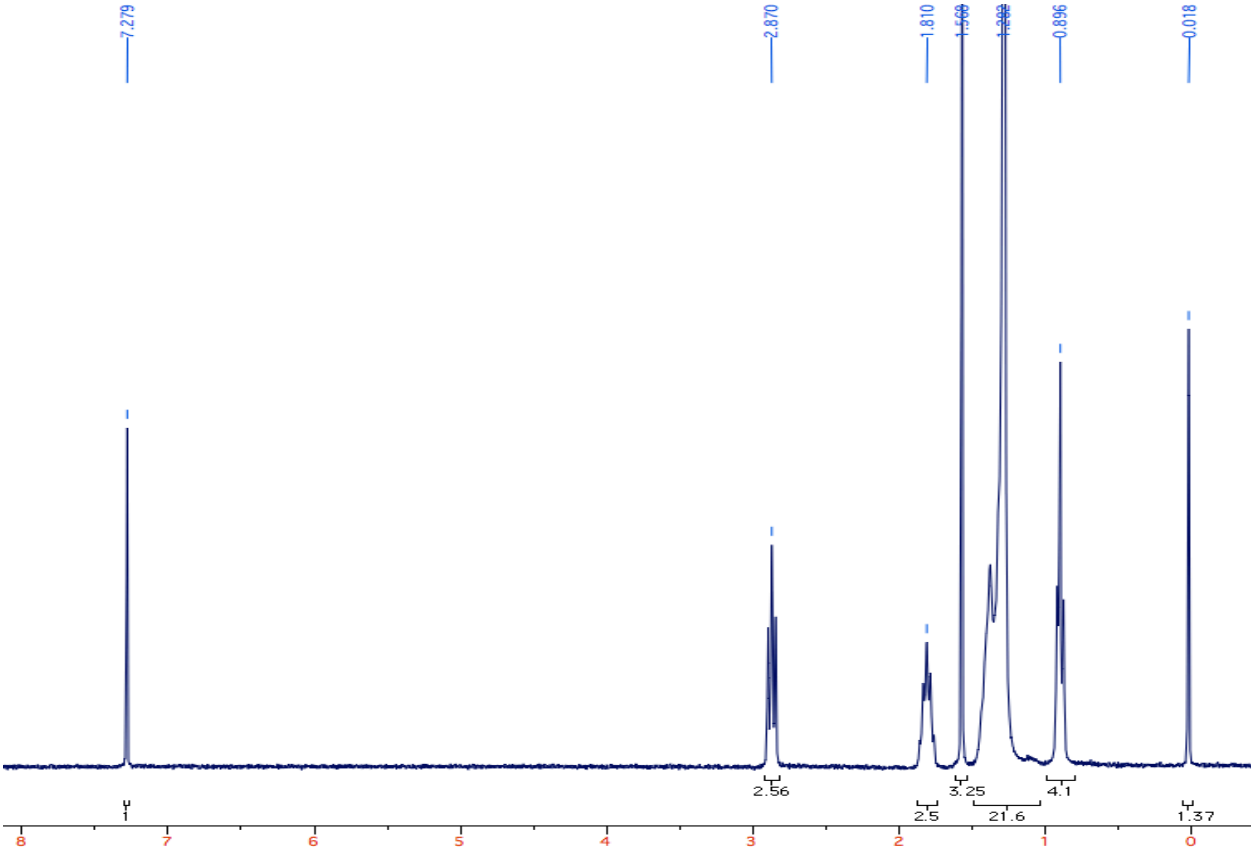

Figure A- 2: 300 MHz ^{1}H NMR spectrums for (E)-1,2-di(thiazol-2-yl)diazene (**DTA**) (**4**) in $CDCl_3$ after recrystallization.

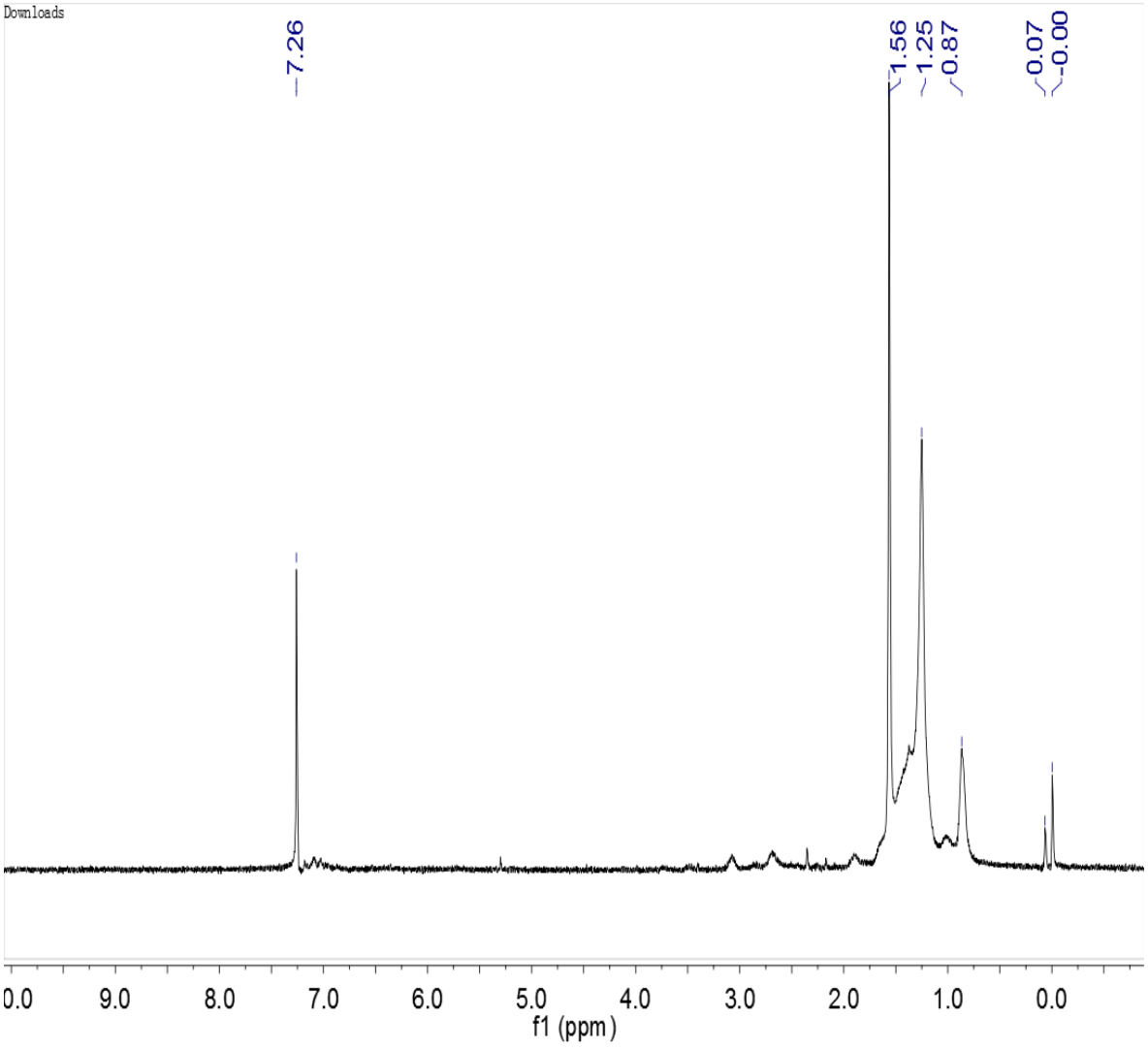

Figure A- 3: 300 MHz ^{1}H NMR spectrums for **P1-DTA-BTV** in $CHCl_3$

Appendix A-2 Chapter 3, NMR result:

First method:

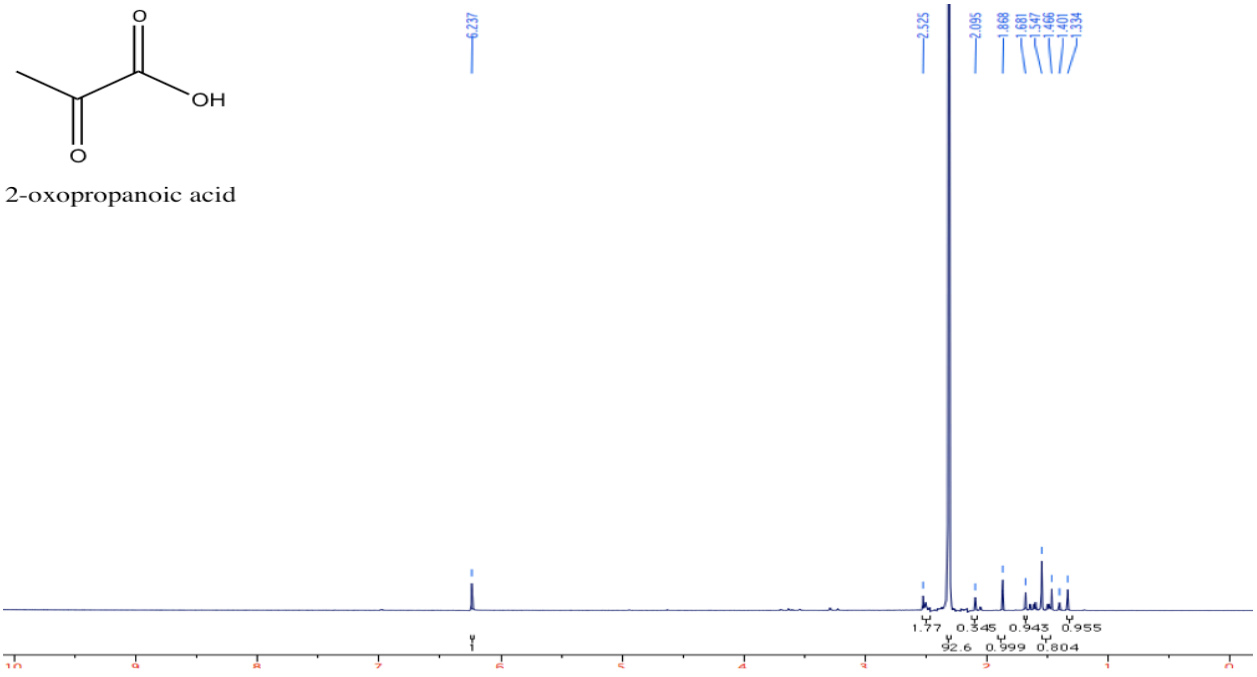

Figure A- 4: Starting materials for the first method.

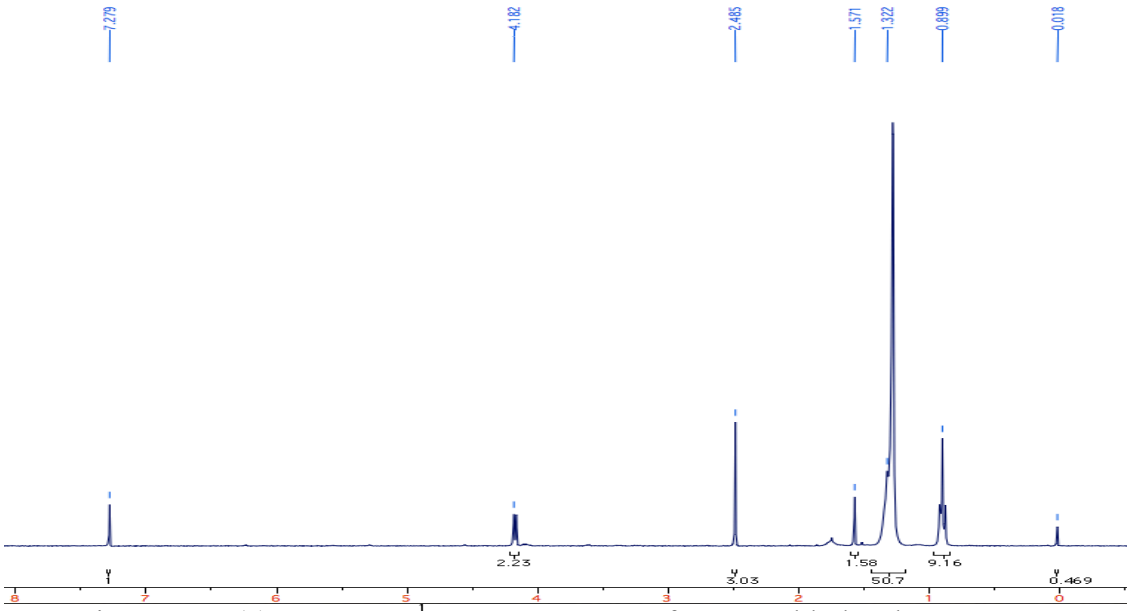

Figure A- 5 (a): 300 MHz ^{1}H NMR spectrum for 2-octyldodecyl 2-oxopropanoate (compound **6**) in $CDCl_3$.

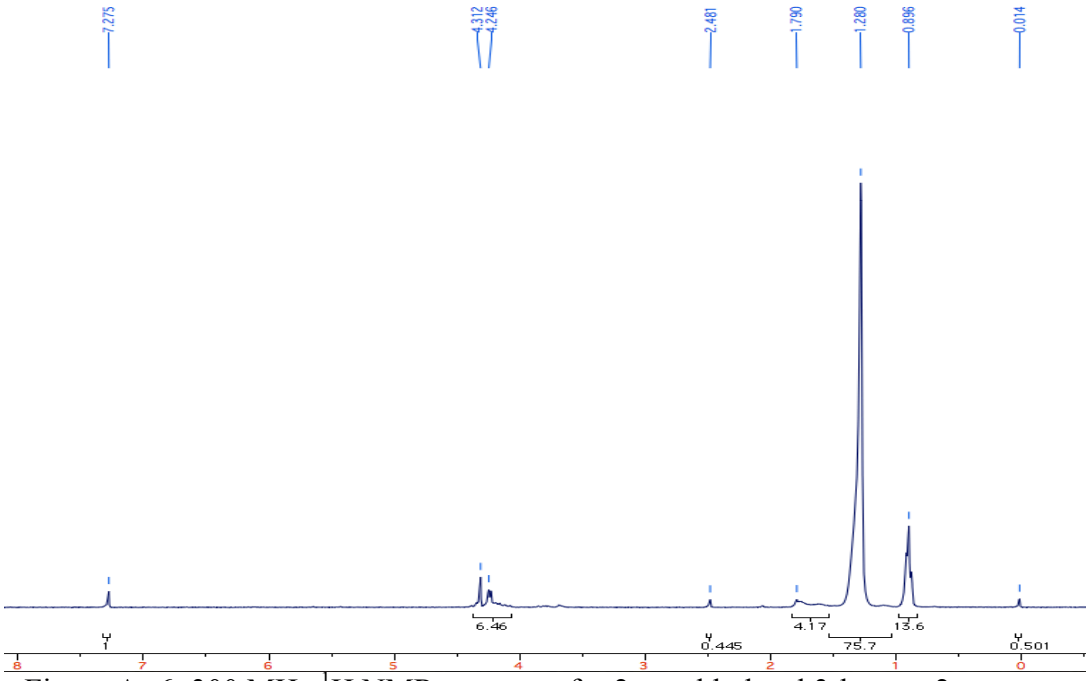

Figure A- 6: 300 MHz ^{1}H NMR spectrum for 2-octyldodecyl 3-bromo-2-oxopropanoate (compound **7**) in $CDCl_3$.

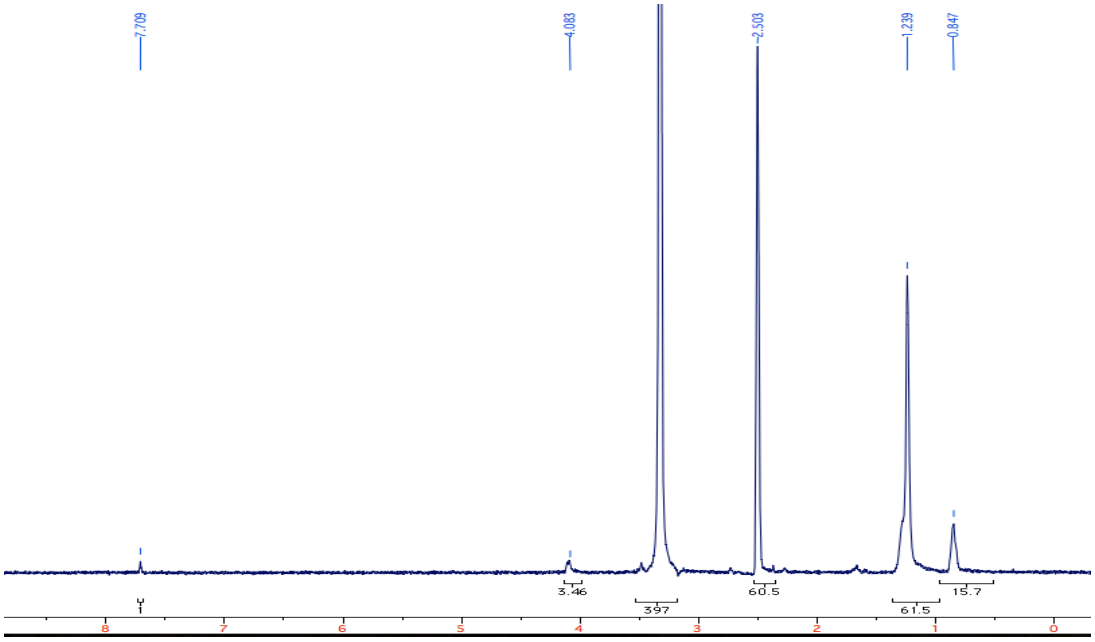

Figure A- 7: 300 MHz ^{1}H NMR spectrum for bis(2-octyldodecyl) 2,2'-(hydrazine-1,2-diyl)bis(thiazole-4-carboxylate) dihydrobromide (**8**) in DMSO.

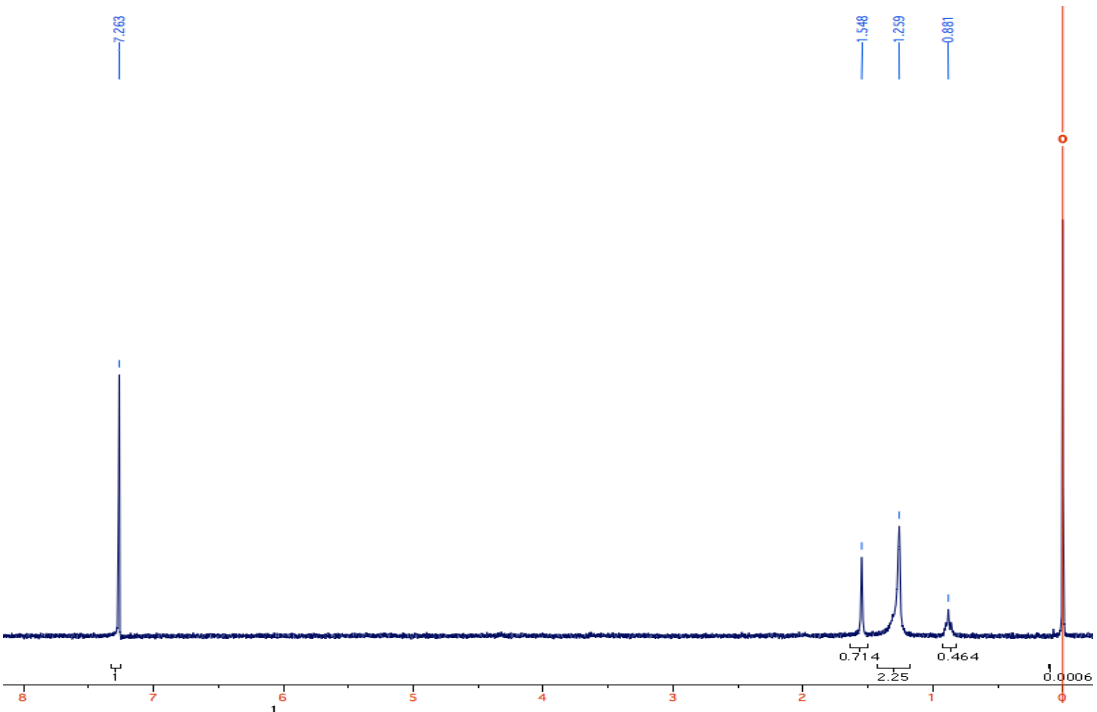

Figure A- 8: 300 MHz ^{1}H NMR spectrum for bis(2-octyldodecyl) 2,2'-(hydrazine-1,2-diyl)bis(thiazole-4-carboxylate) dihydrobromide in (**8**) $CDCl_3$.

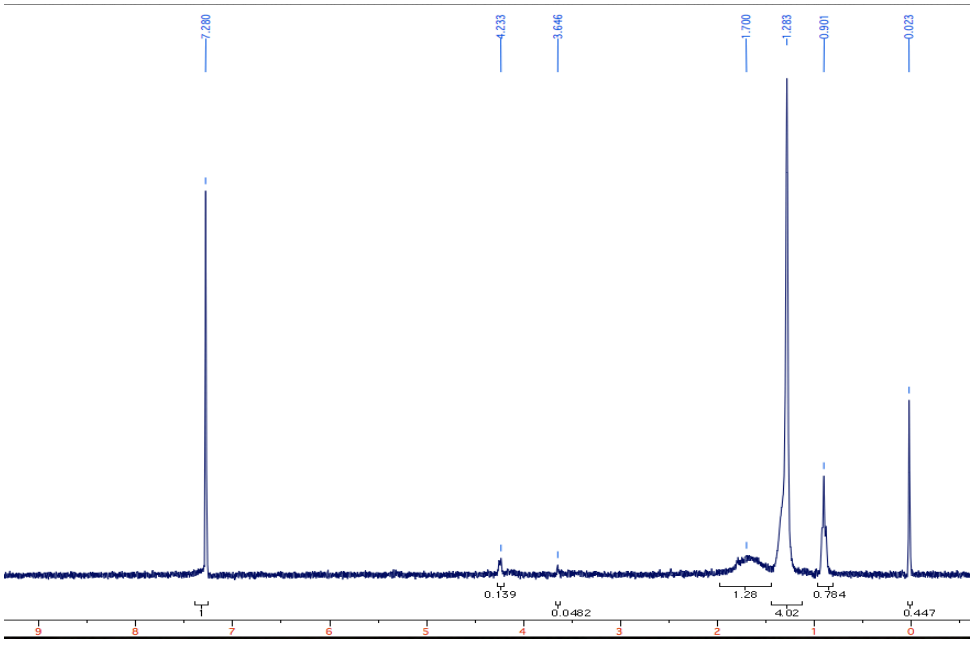

Figure A- 9: 300 MHz ^{1}H NMR spectrum for compound (**9**) in $CDCl_3$

Second method NMR results:

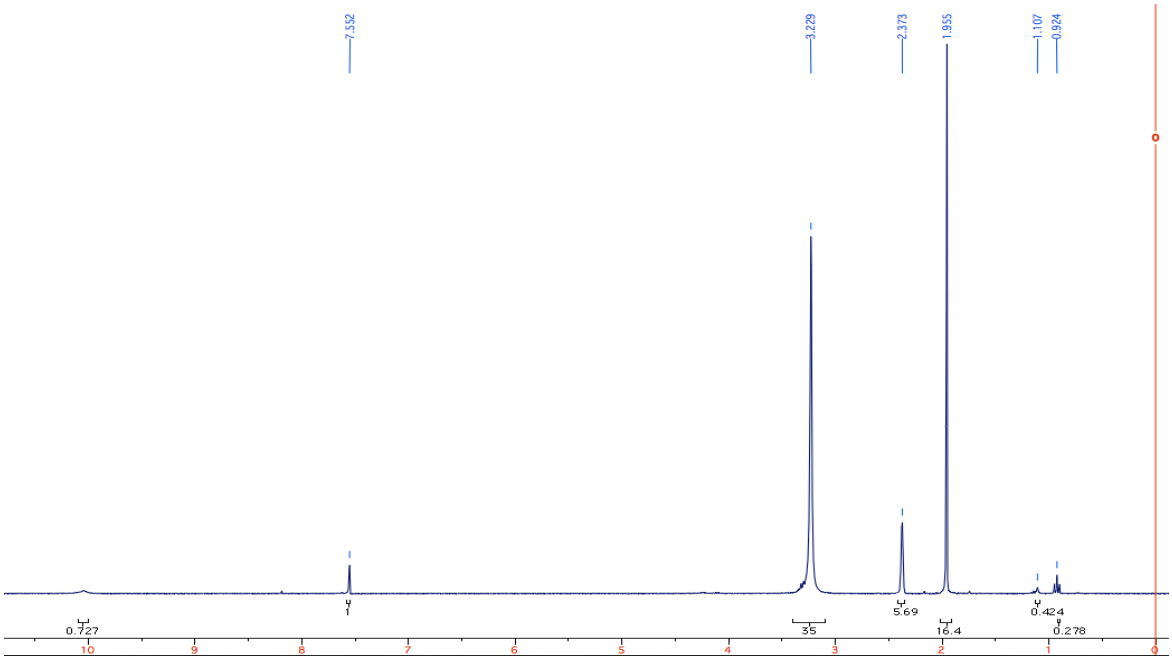

Figure A- 10: 300 MHz ^{1}H NMR spectrum for 2,2'-(hydrazine-1,2-diyl)bis(thiazole-4-carboxylic acid) (compound **11**) in DMSO

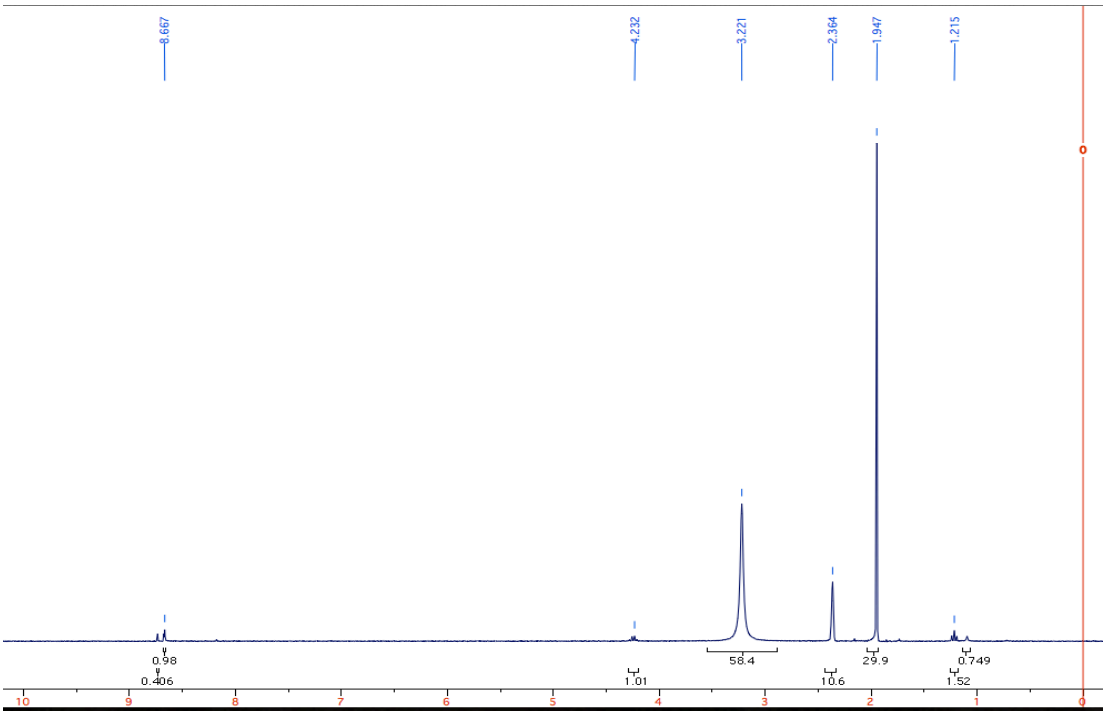

Figure A- 11: 300 MHz ^{1}H NMR spectrum for (*E*)-2,2'-(diazene-1,2-diyl)bis(thiazole-4-carboxylic acid) (compound **12**) in DMSO

Final method NMR results:

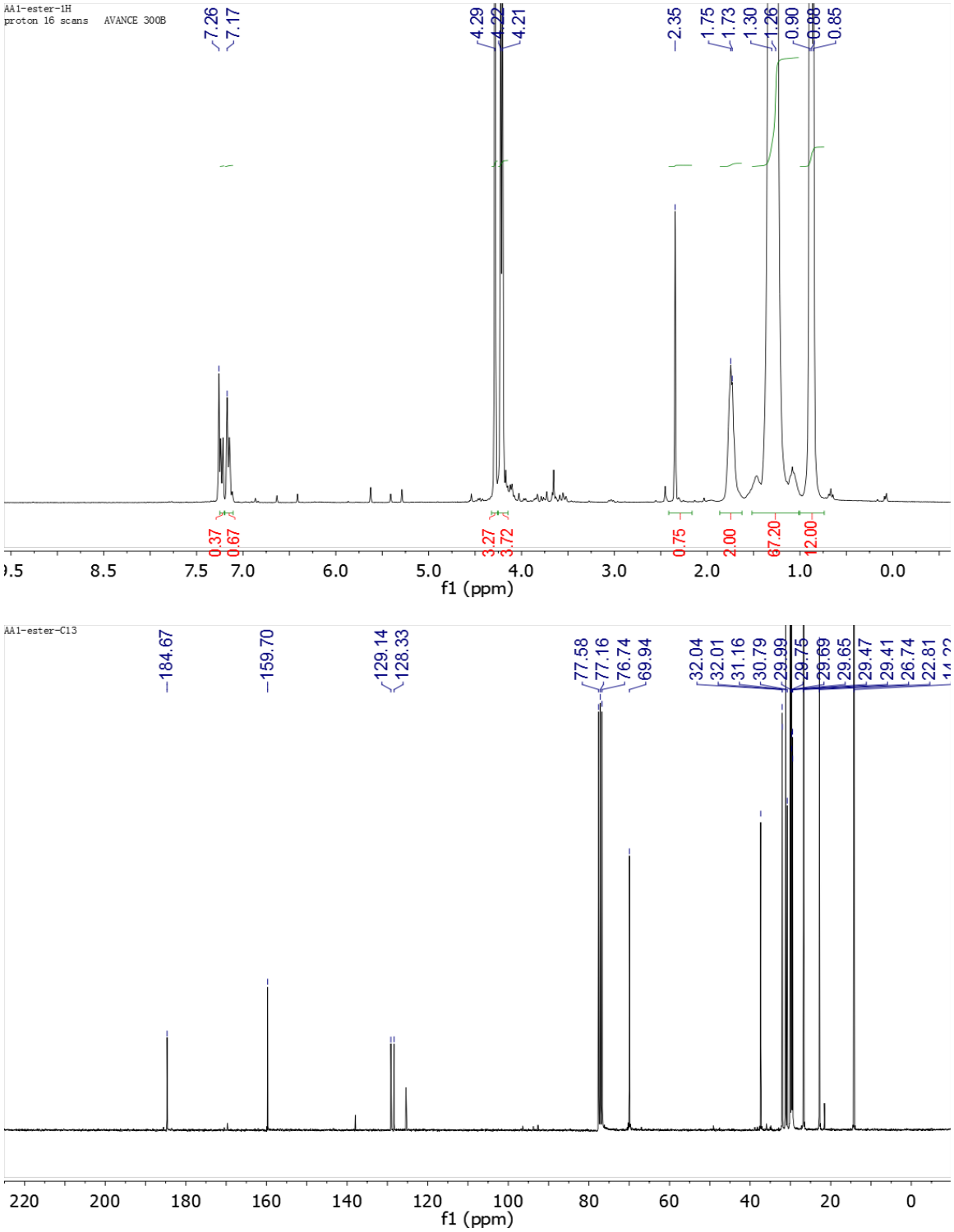

Figure A- 12: (a) 300 MHz ^{1}H NMR spectrum, and (b) 75 MHz ^{13}C NMR spectrum for 2-octyldodecyl 3-bromo-2-oxopropanoate **(14)** in $CDCl_3$

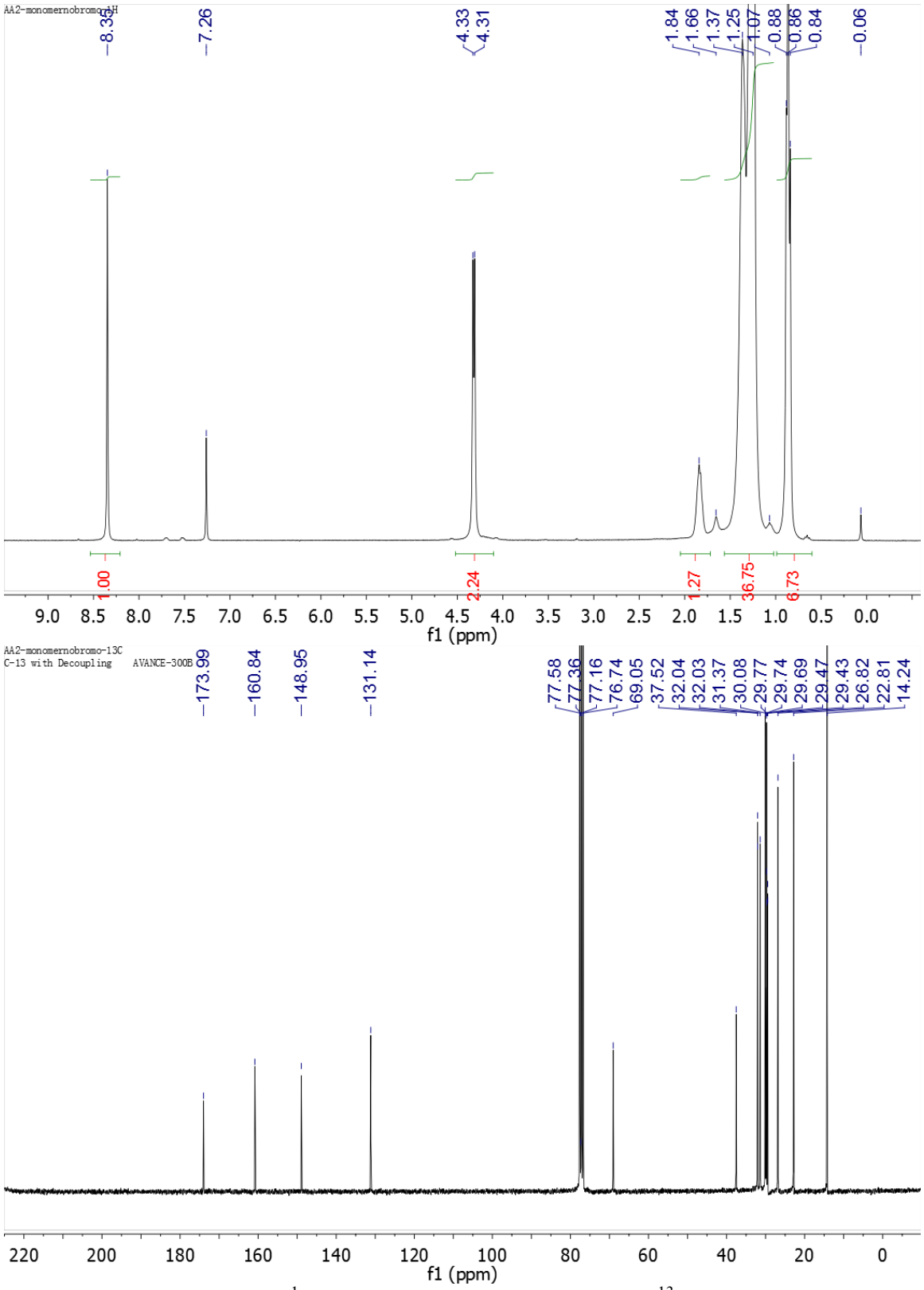

Figure A- 13: (a) 300 MHz ^{1}HNMR spectrum, and (b) 75 MHz ^{13}C NMR spectrum for (*E*)-bis(2-octyldodecyl) 2,2'-(diazene-1,2-diyl)bis (thiazole-4-carboxylate) (**DTAE**) **(15)** in $CDCl_3$

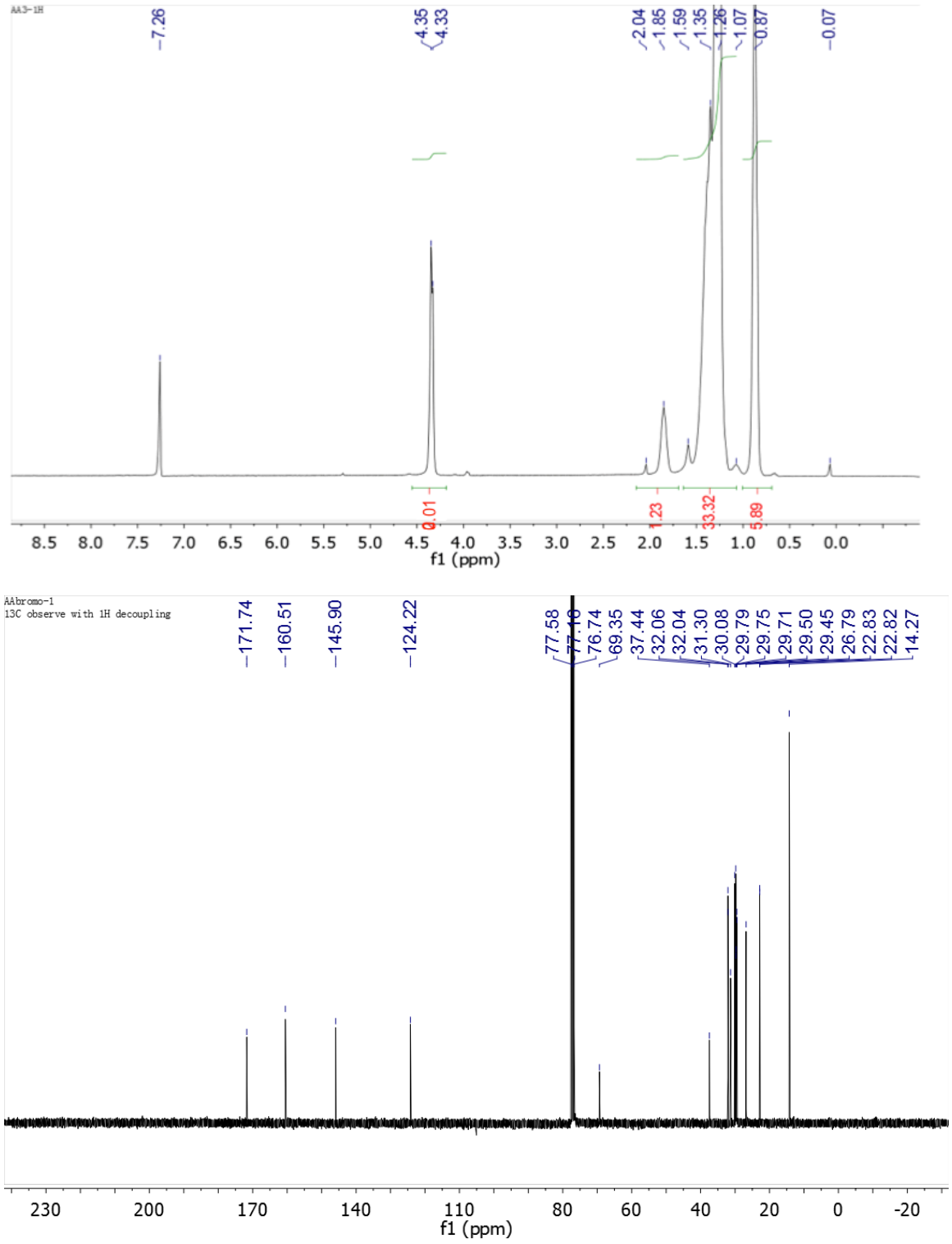

Figure A- 14: (a) 300 MHz ^{1}H NMR spectrum, and (b) 75 MHz ^{13}C NMR spectrum for (*E*)-bis(2-octyldodecyl) 2,2'-(diazene-1,2-diyl)bis(5-bromothiazole-4-carboxylate) (**DTAE-Br**) (**16)** in $CDCl_3$

Polymers:

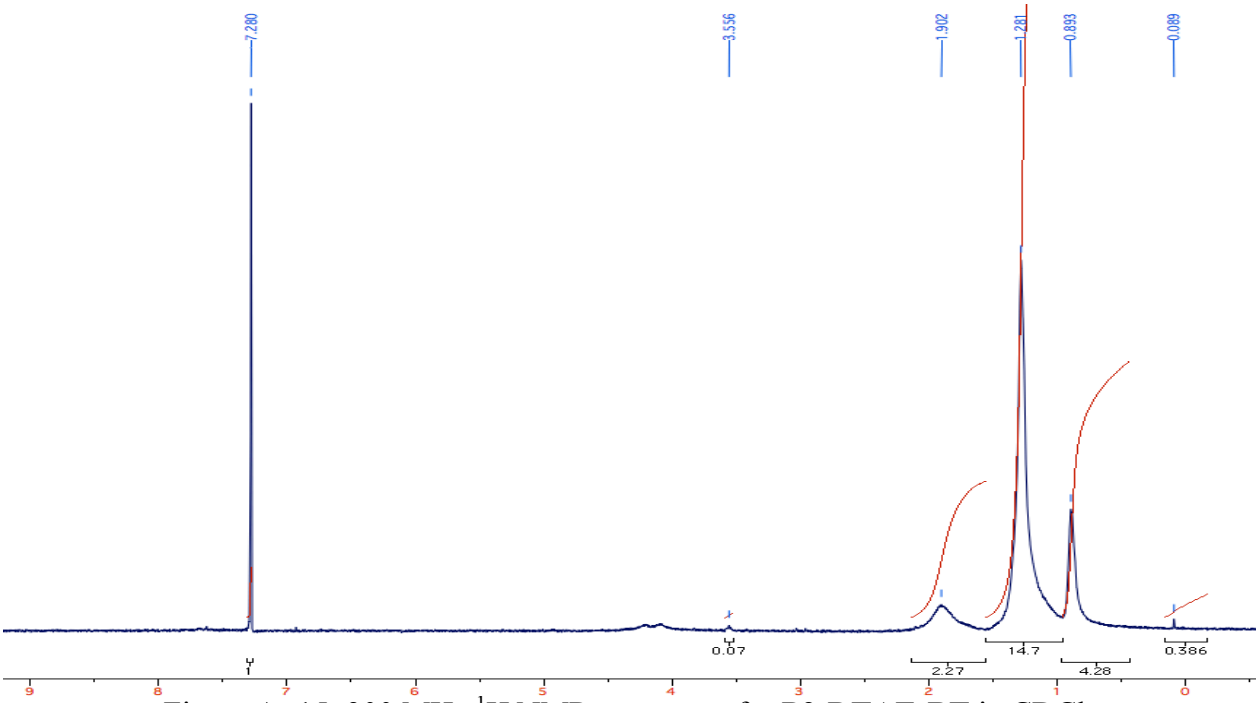

Figure A- 15: 300 MHz ^{1}H NMR spectrums for **P2-DTAE-BT** in $CDCl_3$

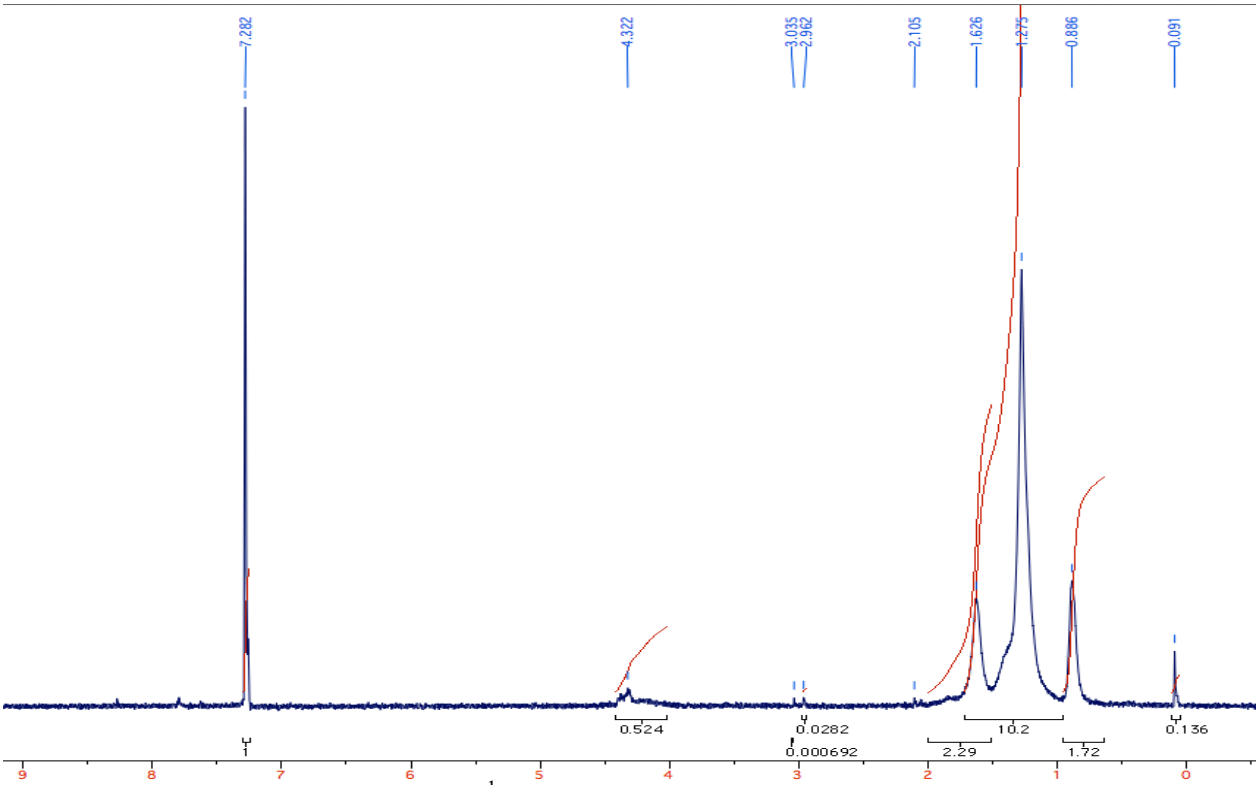

Figure A- 16: 300 MHz ^{1}H NMR spectrums for **P3-DTAE-B** in $CDCl_3$

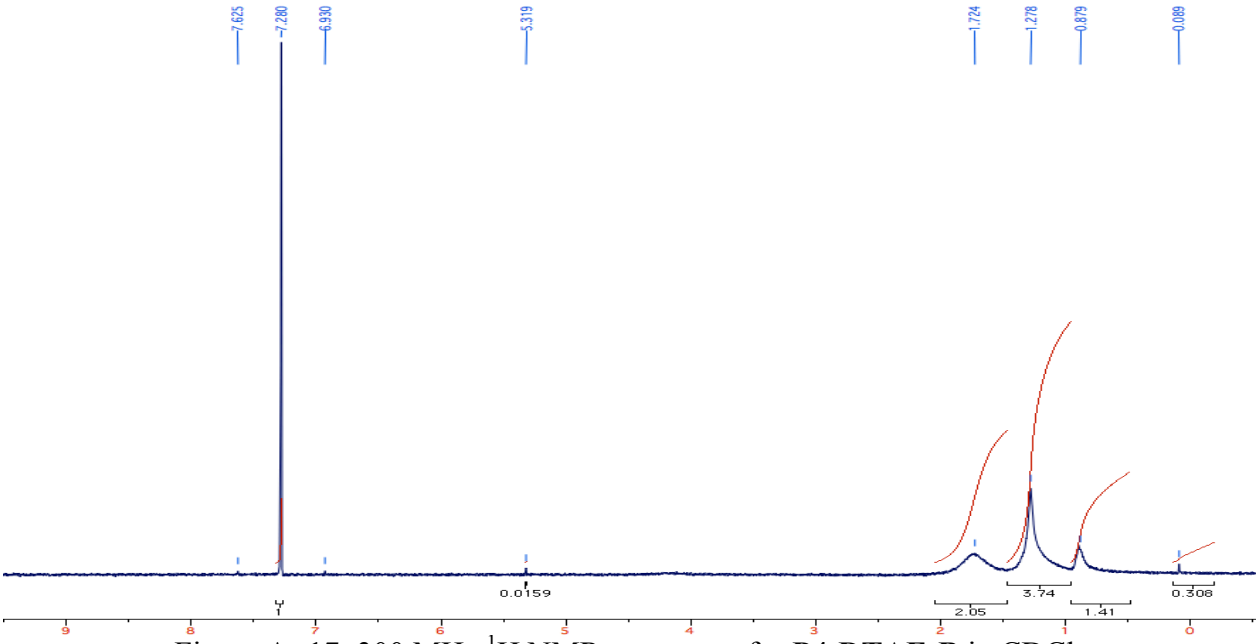

Figure A- 17: 300 MHz ^{1}H NMR spectrums for **P4-DTAE-B** in $CDCl_3$

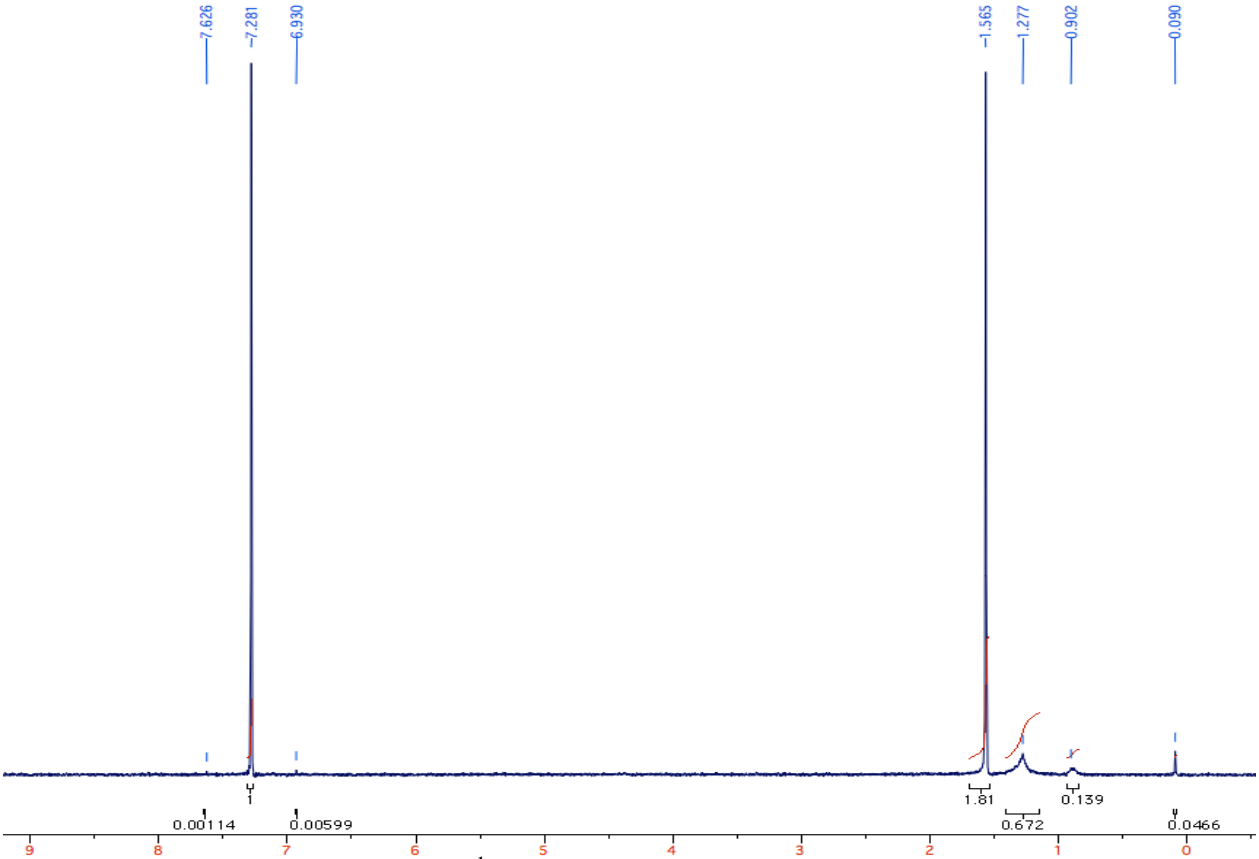

Figure A- 18: 300 MHz ^{1}H NMR spectrums for **P5-DTAE-BT** in $CDCl_3$

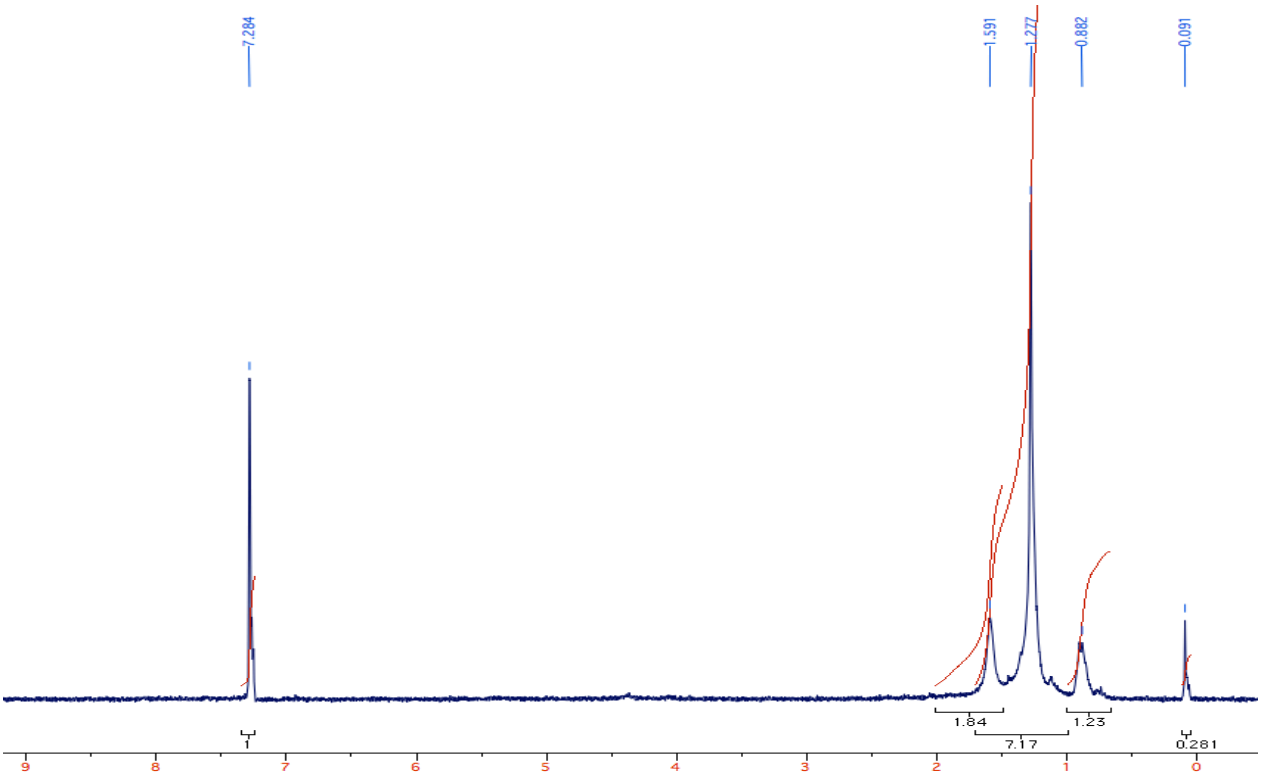

Figure A- 19: 300 MHz ^{1}H NMR spectrums for **P6-DTAE-TT** in $CDCl_3$

Appendix A-3 Chapter 4

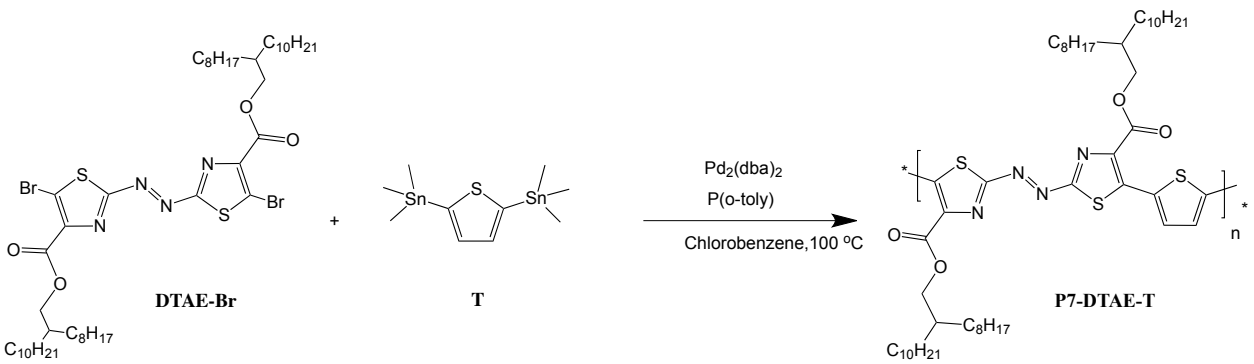

Synthesis of P7-DTAE-T: (0.160 g, 0.159 mmol, 1.0 equivalent) of brominated polymer was added to a clean, dry 25 ml RB flask. (0.0743 g, 0.159 mmol, 1.0 equivalent) of (dimethyl (5-(trimethylstannyl)thieno[3,2-b]thiophen-2-yl)stannyl)methylium was then added to the same flask with a small stir bar. (0.00388 g, 0.002 mmol, 2 % equivalent) was also added to the same flask. (0.0031 g, 0.0018 mmol, 80 % equivalent) was added to the same reaction flask under argon. 1 ml of chloroform was added to the reaction at 100 ºC, and it was stirred in the dark for 3 days (10 % yield).

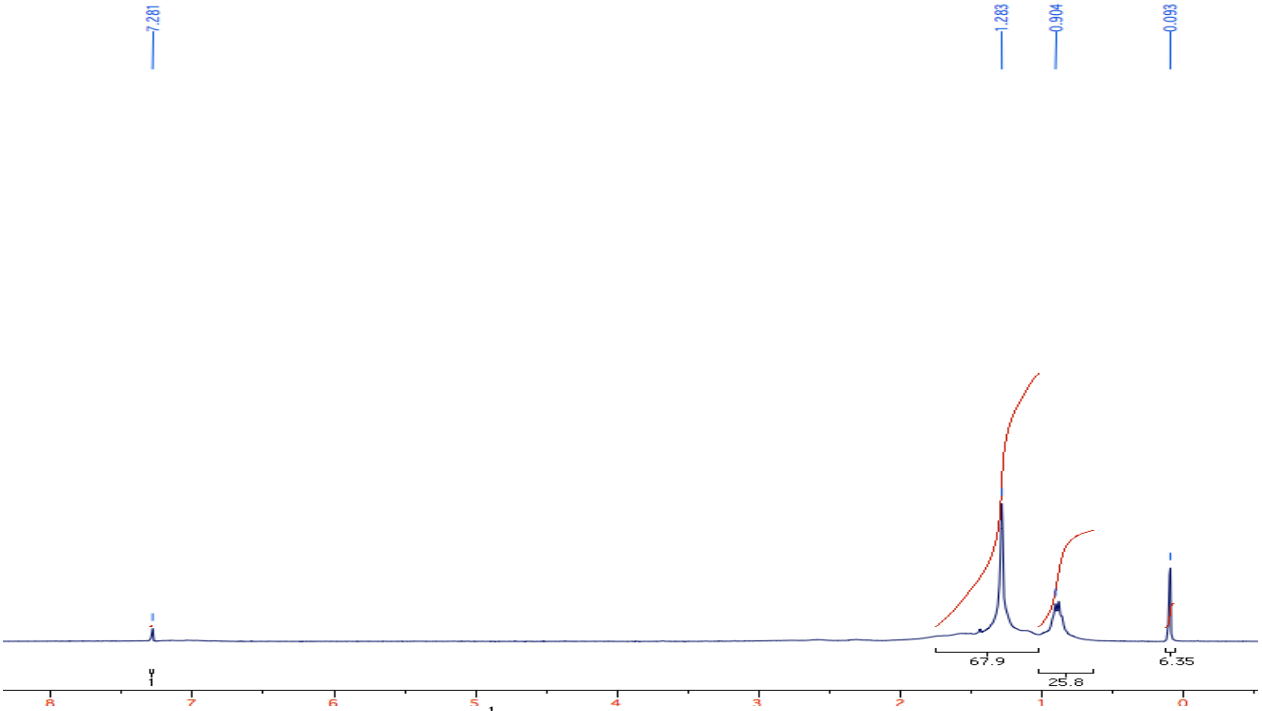

Figure A- 19: 300 MHz ^{1}H NMR spectrums for **P7-DTAE-T** in $CDCl_3$

Appendix B

Scientific Contributions

The following manuscript in preparation to be published based on aspects of the work contained in this thesis:

1. Alsam. A., Yan, Z., Sun. B., and Li. Y*., (2014). Novel (*E*)-1,2-bis(3-dodecyl-5-(trimethylstannyl) thiophen-2-yl) ethenebased donor–acceptor copolymer semiconductors for p-type organic thin film transistors.

2. Alsam. A., Quinn. J., Hong, W., Guo. C., and Li. Y*., (2014). Low band-gap of (*E*)-2-octyldodecyl 5-methyl-2-((5-(5-methylthieno[3,2-*b*]thiophen-2-yl)-4-(((2-octyldodecyl)oxy)carbonyl)thiazol-2-yl)diazenyl)thiazole-4-carboxylate azo polymers and their properties.

Abstract submitted:

Alsam. A., Li. Y., Low band-gap azo polymers as promising donors for organic photovoltaics, 5th National Scientific Conference, Canada, 2014.

Bibliography

1. Ackermann, L. (2009). Arylation Reactions: A Historical Perspective. Weinheim.

2. Ackermann, L. (2009). Modern Arylation Methods. Weinheim, Wiley-VCH Verlag GmbH & Co. KGaA.

3. Allard, S., Forster, M., Souharce, B., Thiem, H., Scherf, U. (2008). "Organic semiconductors for solution-processable field-effect transistors (OFETs)." Angewandte Chemie Intrnationl Edition **47**(22): 4070-4098.

4. Alupoaei, C. E., García-Rubio, Luis H. (2005). "An Interpretation Model For The UV-VIS Spectra Of Microorganisms." Chemical Engineering Communications **192**(2): 198-218.

5. Ames, D. E., Bull, B. (1982). Tetrahedron **38**: 383-387.

6. Aoyagi, Y., Inoue, A., Koizumi, I., Hashimoto, R., Tokunaga, K., Gohma, K., Komatsu, J., Sekine, K., Miyafuji, A., Kunoh, J., Honma, R., Akita Y., and Ohta, A. (1992). Heterocycles **33**: 257.

7. Berrouard, P., Najari, A., Pron, A., Gendron, D., Morin, P. O., Pouliot, J. R., Veilleux, J., Leclerc, M. (2012). "Synthesis of 5-alkyl[3,4-c]thienopyrrole-4,6-dione-based polymers by direct heteroarylation." Angewandte Chemie International Edition Impact Factor **51**(9): 2068-2071.

8. Beyer, H., Kreutzberger, A. (1952). "Über Thiazole, X. Mitteil.: Diazofarbstoffe aus 2.2′ -Diamino-Dithiazolylen-(5-5′) und Versuche zur benzidinartigen Umlagerung der in 4.4′ -Stellung unsubstituierten Hydrazothiazole-(2.2′)." Chemische Berichte **85**: 333‑337.

9. Bhadeshia, H. K. D. H. (2012). "Differential Scanning Calorimetry." University of Cambridge, Materials Science & Metallurgy.

10. Biesheuvel, P. M., Fu, Y., Bazant, M. Z. (2012). "Electrochemistry and capacitive charging of porous electrodes in asymmetric multicomponent electrolytes." Russian Journal of Electrochemistry **48**(6): 580-592.

11. Biniek, L., Chochos, C. L., Leclerc, N., Hadziioannou, G., Kallitsis, J. K., Bechara, R., Lévêque, P., Heiser, T. (2009). "A [3,2-b]thienothiophene-alt-benzothiadiazole copolymer for photovoltaic applications: design, synthesis, material characterization and device performances." Journal of Materials Chemistry **19**(28): 4946.

12. Binnig, G., Quate, C. F. (1986). "Atomic Force Microscope." Physical Review

Letters. **56**: 930.

13. Blouin, N., Michaud, A., Gendron, D., Wakim, S., Blair, E., Neagu-Plesu, R., Belletete, M., Durocher, G., Tao, Y., Leclerc, M. (2008). "Toward a Rational Design of Poly(2,7-Carbazole) Derivatives for Solar Cells." Journal of the American Chemical Society **130**: 732-742.

14. Braun, S., Salaneck, W. R., Fahlman, M (2009). "Energy-Level Alignment at Organic/Metal and Organic/Organic Interfaces." Advanced Materials **21**(14-15): 1450-1472.

15. Bürgi, L., Turbiez, M., Pfeiffer, R., Bienewald, F., Kirner, H-J., Winnewisser, C (2008). "High-Mobility Ambipolar Near-Infrared Light-Emitting Polymer Field-Effect Transistors." Advanced Materials **20**(11): 2217-2224.

16. Campeau, L. C., Fagnou, K. (2006). "Palladium-catalyzed direct arylation of simple arenes in synthesis of biaryl molecules." Chemical Communication (Camb)(12): 1253-1264.

17. Campeau, L. C., Parisien, M., Jean, A., Fagnou, K. (2006). "Catalytic Direct Arylation with Aryl Chlorides, Bromides, and Iodides: Intramolecular Studies Leading to New Intermolecular Reactions." Contribution from the Center for Catalysis Research and InnoVation American Chemical Society **128**(2).

18. Carsten, B., He, F., Son, H. J., Xu, T., Yu, L. (2011). "Stille polycondensation for synthesis of functional materials." Chemical Reviews **111**(3): 1493-1528.

19. Chen, H. Z., Ling, M. M., Mo, X., Shi, M. M., Wang, M., Bao, Z. (2007). "Air Stable n-Channel Organic Semiconductors for Thin Film Transistors Based on Fluorinated Derivatives of Perylene Diimides." Chemistry of Materials **19**: 816-824.

20. Chen, M. X., Perzon, E., Robisson, N., Jönsson, S. K. M., Andersson, M. R., Fahlman, M., Berggren, M. (2004). "Low band gap donor–acceptor–donor polymers for infra-red electroluminescence and transistors." Synthetic Metals **146**(3): 233-236.

21. Chen, Z., Lee, M. J., Shahid Ashraf, R., Gu, Y., Albert-Seifried, S., Meedom Nielsen, M., Schroeder, B., Anthopoulos, T. D., Heeney, M., McCulloch, I., Sirringhaus, H. (2012). "High-performance ambipolar diketopyrrolopyrrole-thieno[3,2-b]thiophene copolymer field-effect transistors with balanced hole and electron mobilities." Advanced Materials **24**(5): 647-652.

22. Chiang, C. K. D., M. A.; Gau, S. C.; Heeger, A. J.; Louis, E. J.; MacDiarmid, A. G.; Park, Y. W.; Shirakawa, H. (1978). "Synthesis of highly conducting films of derivatives of polyacetylene, (CH)x." Journal of the American Chemical Society

100: 1013-1015.

23. Cojocariu, C., Rochon, P. (2004). "Light-induced motions in azobenzene-containing polymers." Pure and Applied Chemistry **76**: 1479-1497.

24. Cooke, M. P. J. (1973). "Lithiotriphenylphosphinioacetonide as a convenient reagent for the introduction of the acetonyl synthon." The Journal of Organic Chemistry **38**: 4082-4084.

25. Corporation, P. (2012). "Organic Thin-Film Transistors - Polyera Corporation." Polymera Corporation. Retrieved September 5, 2012, 2012.

26. Corriu, R. J. P., Masse, J. P. (1972). "Activation of Grignard reagents by transition-metal complexes. A new and simple synthesis of trans-stilbenes and polyphenyls." Journal of the Chemical Society, Chemical Communications **144**.

27. Dahimi, O., Rahim, A. A., Abdulkarim, S. M., Hassan, M. S., Hashari, S. B., Mashitoh, A. S., Saadi, S. (2014). "Multivariate statistical analysis treatment of DSC thermal properties for animal fat adulteration." Food Chemistry **158**: 132-138.

28. Dandrade, B., Datta, S., Forrest, S., Djurovich, P., Polikarpov, E., Thompson, M. (2005). "Relationship between the ionization and oxidation potentials of molecular organic semiconductors." Organic Electronics **6**(1): 11-20.

29. Dietrich, W., Gerrit, K (1994). "Adaptive resonance theory based artificial neural networks for treatment of open-category problems in chemical pattern recognition - application to UV-Vis and IR spectroscopy." Chemometrics and Intelligent Laboratory Systems **23**: 309-329.

30. Dimitrakopoulos, C. D., Malenfant, P. R. L. (2002). "Organic Thin Film Transistors foe Larg Area Electronics." Advance Materials **14**(2): 99–117.

31. Dimitrakopoulos, C. D., Mascaro, D. J. (2001). "Organic thin- film transistors: A review of recent advances." International Business Machines Corporation **45**(1): 11.

32. Dong, M. W. (2006). Modern HPLC for Practicing Scientists. New Jersey, United States, A John Wiley & Sons.

33. Doyle, B. (2010). "Thiophene Based Donor/Acceptor Conjugated Polymers for Organic Photovoltaics." Rutgers University, **PhD Thesis**.

34. ElBatal, F. H., Marzouk, S. Y., Ezz-ElDin, F. M. (2011). "UV–visible and infrared spectroscopy of gamma-irradiated lithium diborate glasses containing SeO_2." Journal of Molecular Structure **986**(1-3): 22-29.

35. Espinet, P., Echavarren, A. M. (2004). "The mechanisms of the Stille reaction." Angewandte Chemie International Edition **43**(36): 4704-4734.

36. Facchetti, A. (2011). "π-Conjugated Polymers for Organic Electronics and Photovoltaic Cell Applications." Chemistry of Materials **23**(3): 733-758.

37. Facchetti, A. (2013). "Materials and Process Engineering for Printed and Flexible Optoelectronic Devices." Polyera Corporation and Northwestern University: 113-126.

38. Facchetti, A., Vaccaro, L., Marrocchi, A. (2012). "Semiconducting polymers prepared by direct arylation polycondensation." Angewandte Chemie International Edition **51**(15): 3520-3523.

39. Frisch, Æ. (2009). Gaussian 09W Reference: Wallingford, CT.

40. Frisch, Æ. H., H. P.; Dennington II, R. D.; Keith, T. A.; Millam, J.; Nielsen, A. B.; Holder, A. J.; Hiscocks, J. (2009). GaussView 5 Reference.

41. Frisch, M. J. T., G. W.; Schlegel, H. B.; Scuseria, G. E.; Robb, M. A.; Cheeseman, J. R.; Scalmani, G.; Barone, V.; Mennucci, B.; Petersson, G. A.; Nakatsuji, H.; Caricato, M.; Li, X.; Hratchian, H. P.; Izmaylov, A. F.; Bloino, J.; Zheng, G.; Sonnenberg, J. L.; Hada, M.; Ehara, M.; Toyota, K.; Fukuda, R.; Hasegawa, J.; Ishida, M.; Nakajima, T.; Honda, Y.; Kitao, O.; Nakai, H.; Vreven, T.; Montgomery, J. A. J.; Peralta, J. E.; Ogliaro, F.; Bearpark, M.; Heyd, J. J.; Brothers, E.; Kudin, K. N.; Staroverov, V. N.; Keith, T.; Kobayashi, R.; Normand, J.; Raghavachari, K.; Rendell, A.; Burant, J. C.; Iyengar, S. S.; Tomasi, J.; Cossi, M.; Rega, N.; Millam, J. M.; Klene, M.; Knox, J. E.; Cross, J. B.; Bakken, V.; Adamo, C.; Jaramillo, J.; Gomperts, R.; Stratmann, R. E.; Yazyev, O.; Austin, A. J.; Cammi, R.; Pomelli, C.; Ochterski, J. W.; Martin, R. L.; Morokuma, K.; Zakrzewski, V. G.; Voth, G. A.; Salvador, P.; Dannenberg, J. J.; Dapprich, S.; Daniels, A. D.; Farkas, O.; Foresman, J. B.; Ortiz, J. V.; Cioslowski, J.; Fox, D. J. Gaussian, Inc., (2010). Wallingford CT.

42. Fulmer, G. R., Miller, A. J. M., Sherden, N. H., Gottlieb, H. E., Nudelman, A., Stoltz, B. M., Bercaw, J. E., Goldberg, Karen I. (2010). "NMR Chemical Shifts of Trace Impurities: Common Laboratory Solvents, Organics, and Gases in Deuterated Solvents Relevant to the Organometallic Chemist." Organometallics **29**(9): 2176-2179.

43. Gottlieb, H. E., Kotlyar, V., Nudelman, A. (1997). "NMR Chemical Shifts of Common Laboratory Solvents as Trace Impurities." The Journal of Organic Chemistry **62**: 7512-7315.

44. Guo, C., Hong, W., Aziz, H., Li, Y. (2012). "Recent Progress in High Mobility

Polymer Semiconductors for Organic Thin Film Transistors." Reviews in Advanced Sciences and Engineering **1**(3): 200-224.

45. Guo, C., Sun, B., Quinn, J., Yan, Z., Li, Y (2014). "Synthesis and properties of indigo based donor–acceptor conjugated polymers." Journal of Materials Chemistry C **2**(21): 4289.

46. Guo, X. F., H.; Zhang, M.; Huang, Y.; Tan, S.; Li, Y. (2012). "Synthesis and Characterizations of Poly(4-alkylthiazole vinylene)." Journal of Applied Polymer Science **124**: 847–854.

47. Hebbar, N., Fiol-Petit, C., Ramondenc, Y., Plé, G., Plé, N. (2011). "A new series of rod-like conjugated molecules with a pyrazine or a bipyrazine core. Synthesis and light emitting properties." Tetrahedron **67**(12): 2287-2298.

48. Hennings, D. D., Iwasa, S., Rawal, V. H. (1997). "Anion-Accelerated Palladium-Catalyzed in Tramolecular Coupling of Phenols with Aryl Halides." Journal of Organic Chemistry **62**(2): 2-3.

49. Holt, P., Smith, A (1965). "Ultraviolet A bsorption of Some Substituted Azobenzene and Symmetric 1,1'- and 2,2'-Azonaphthalene Derivatives." Journal of the Chemical Society (Resumed): 5245–5248.

50. Houlgate, P., Lee, E (1999). Guide to Improving Analytical Quality in Chemistry.

51. Inganas, O., Zhang, F., Tvingstedt, K., Andersson, L. M., Hellstrom, S., Andersson, M. R. (2010). "Polymer photovoltaics with alternating copolymer/fullerene blends and novel device architectures." Advanced Materials **22**(20): E100-116.

52. Jana, D., Ghorai, B. K. (2012). "Pyridine-cored V-shaped π-conjugated oligomers: synthesis and optical properties." Tetrahedron **68**(36): 7309-7316.

53. Johnson, C. M. (2010). Differential scanning calorimetry: theory and practice. GE Healthcare Life Sciences.

54. Kakiuchi, T. (1998). "A theory of voltammetry of ion transfer across a liquid membrane in the absence of supporting electrolytes using the Nernst-Planck equation and electroneutrality assumption." Electrochimica Acta **44**.

55. Kang, E. S. H., Yuen, J. D., Walker, W., Coates, N. E., Cho, S., Kim, E., Wudl, F (2010). "Amorphous dithenylcyclopentadienone-carbazole copolymer for organic thin-film transistors." Journal of Materials Chemistry **20**(14): 2759.

56. Klauk, H. (2006). Organic Electronics: Materials, Manufacturing, and Applications. Wiley, John Wiley & Sons.

57. Kozłowski, R., Kubica, Z., Rzeszotarska, B., Smełka, L., Pietrzyński, G. (1989). "Lower Aliphatic 2-oxoacids and their Eteyl Esters from Ethyl Esters of 2-Hydroxy Acids." Organic Preparations and Procedures INT **21**: 75-82.

58. Kulkarni, A. P., Kong, X., Janekhe, S. A. (2006). "Polyfluorene Terpolymers Containing Phenothiazine and Fluorenone: Effects of Donor and Acceptor Moieties on Energy and Intrachain Charge Transfer Processes in the Photoluminescence and Electroluminescence of Multichromophore Copolymers." Macromolecules **39**(25): 8699-8711.

59. Kumada, M., Tamao, K. (1968). Advances in Organometallic Chemistry **6**: 19-117.

60. Lang, K. M., Hite, D. A., Simmonds, R. W., McDermott, R., Pappas, D. P., Martinis, J., M (2014). "Conducting atomic force microscopy for nanoscale tunnel barrier characterization." Review of Scientific Instruments **75**: 2726-2731.

61. Lee, C., Yang, W., Parr, R. G. (1988). "Development of the Colle-Salvetti correlation-energy formula into a function of the electron density." Physical Review B **37**: 785-789.

62. Lee, C. K., Gong, J (2011). "Fokker-Planck equation with arbitrary dc and ac fields: Continued fraction method." Physical Review E **84**(1).

63. Lee, K.-H., Morino, K., Sudo, A., Endo, T. (2010). "Synthesis and optical properties of π-conjugated polymers composed of diester-substituted bithiophene and dibenzothiophene or carbazole." Polymer Bulletin **67**(2): 227-236.

64. Li, Y., Singh, S. P., Sonar, P. (2010). "A high mobility P-type DPP-thieno[3,2-b]thiophene copolymer for organic thin-film transistors." Advanced Materials **22**(43): 4862-4866.

65. Li, Y., Sonar, P., Singh, S. P., Soh, M. S., Meurs, M. V., Tan, J. (2011). "Annealing-free high-mobility diketopyrrolopyrrole-quaterthiophene copolymer for solution-processed organic thin film transistors." Journal of the American Chemical Society **133**(7): 2198-2204.

66. Li, Y., Sonar, P., Singh, S. P., Zeng, W., Soh, M. S. (2011). "3,6-Di(furan-2-yl)pyrrolo[3,4-c]pyrrole-1,4(2H,5H)-dione and bithiophene copolymer with rather disordered chain orientation showing high mobility in organic thin film transistors." Journal of Materials Chemistry **21**(29): 10829.

67. Li, Y., Sun, B., Sonar, P., Singh, S. P. (2012). "Solution processable poly(2,5-dialkyl-2,5-dihydro-3,6-di-2-thienyl-pyrrolo[3,4-c]pyrrole-1,4-dione) for ambipolar organic thin film transistors." Organic Electronics **13**(9): 1606-1613.

68. Li. F., M., Nathan, A., Wu, Y., Ong, B. S. (2011). "Organic Thin Film Transistor Integration: A Hybrid Approach, First Edition. ." Wiley-VCH Verlag GmbH & Co. KGaA.

69. Liljas, A. (2013). "Background to the Noble Prize to the Braggs." Acta Crystallographica Section A **A69**: 10-15.

70. Liu, G., Pu, S., Wang, X (2010). "Photochromism of new 3,5-position hybrid diarylethene derivatives bearing both thiophene and thiazole moieties." Tetrahedron **66**(46): 8862-8871.

71. Mehta, V. P., Van der Eycken, E. V. (2011). "Microwave-assisted C-C bond forming cross-coupling reactions: an overview." Chemical Society Reviews **40**(10): 4925-4936.

72. Mercier, L. G., Leclerc, M. (2012). "Direct (Hetero) Arylation: A New Tool for Polymer Chemists." Accounts of chemical research **46**(7): 1597-1605.

73. Mishra, R., Jha, K. K., Kumar, S., Tomer, I. (2011). "Synthesis, properties and biological activity of thiophene: A review." Scholars Research **3**(4): 38-54.

74. Mumpton, F. A. (1960). "Clinoptilolite redefined." American Mineralogist **45**(3-4): 351-369.

75. Ohshita, J., Hwang, Y-M., Mizumo, T., Yoshida, H., Ooyama, Y., Harima, Y., Kunugi, Y. (2011). "Synthesis of Dithienogermole-Containing π-Conjugated Polymers and Applications to Photovoltaic Cells." Organometallics **30**(12): 3233-3236.

76. Ohshita, J., Kai, H., Kimura, K., Lee, K-H., Kunai, A. (2009). "Synthesis of Alternate Copolymers Composed of Dithienosilole and π-Conjugated Units." Polymer Journal **41**(6): 482-485.

77. Okamoto, K., Housekeeper, J. B., Michael, F. E., Luscombe, C. K. (2013). "Thiophene based hyperbranched polymers with tunable branching using direct arylation methods." Polymer Chemistry **4**(12): 3499.

78. Olivelli, P., Bandini, M. Bigi, A (2012). Thiophene-based Materials for Photovoltaic Applications. Chemical Science. CHIM/06-CHIMICA ORGANICA, University of Bologna. **PhD Thesis**.

79. Ortiz, R. P., Yan, H., Facchetti, A., Marks, T. J. (2010). "Azine- and Azole-Functionalized Oligo´ and Polythiophene Semiconductors for Organic Thin-Film Transistors." Materials **3**(3): 1553-1558.

80. Paszkowicz, W. (2006). "Ninety Years of Powder Diffraction: from Birth to Maturity." Synchrotron Radiation in Natural Science **5**(1-2): 115-126.

81. Peng, Q., Yan, H., Zhang, X., Wu, Y. D. (2012). "Conjugate addition vs Heck reaction: a theoretical study on competitive coupling catalyzed by isoelectronic metal (Pd(II) and Rh(I))." The Journal of Organic Chemistry **77**(17): 7487-7496.

82. Peyrard, L., Dumartin, M. L., Chierici, S., Pinet, S., Jonusauskas, G., Meyrand, P., Gosse, I. (2012). "Development of functionalized cyclotriveratrylene analogues: introduction of withdrawing and pi-conjugated groups." The Journal of Organic Chemistry **77**(16): 7023-7027.

83. Prevatt, J. (2004). "Modern UV-VIS Spectroscopy: A Decade of Fiber-Optic CCD Array Spectrophotometers." American Laboratory, Application Note.

84. Privalov, P. L., Plotnikov, V. V., Filmonov, V. V. (1975). "Precision scanning microcalorimeter for the study of liquids." The Journal of Chemical Termodynamics **7**: 41-47.

85. Pu, S., Li, H., Liu, G., Liu, W. (2010). "Photochromism of new diarylethenes bearing both thiazole and benzene moieties." Tetrahedron Letters **51**(27): 3575-3579.

86. Qi, D., Zhang, L., Zhang, Y., Bian, Y., Jiang, J. (2010). "Nature of the Intense Near-IR Absorption and Unusual Broad UV-Visible-NIR Spectra of
87. Azulenocyanines: Density Functional Theory Studies." The Journal of Physical Chemistry A **114**: 13411-13417.

88. Ramirez, F., Dershowitz, S. (1956). "Phosphinemethylenes. 11.Triphenylphosphineacylrnethylenes." The Journal of Organic Chemistry **22**: 41-45.

89. Razus, A. C., Birzan, L., Nae, S., Surugiu, M. N., Cimpeanu, V. (2003). "Azulene-1-azo-2'-thiazoles.a Synthesis and Properties." Journal of Heterocyclic Chemistry **40**: 995.

90. Robert, A., Wilson, Bullen, H. A. (2007). "Introduction to Scanning Probe Microscopy (SPM). Basic Theory Atomic Force Microscopy (AFM)." Creative commons Attribution-NonCommercial-ShareAlike 2.5 Generic: 859-572-5411.

91. Rudenko, A. E., Wiley, C. A. Tannaci, J. F. Thompson, B. C. (2013). "Optimization of direct arylation polymerization conditions for the synthesis of poly(3-hexylthiophene)." Journal of Polymer Science Part A: Polymer Chemistry **51**(12): 2660-2668.

92. Scharber, M. C., Mühlbacher, D., Koppe, M., Denk, P., Waldauf, C., Heeger, A.

J., Brabec, C. J (2006). "Design Rules for Donors in Bulk-Heterojunction Solar Cells—Towards 10 % Energy-Conversion Efficiency." Advanced Materials **18**(6): 789-794.

93. Schipper, D. J., Fagnou, K (2011). "Direct Arylation as a Synthetic Tool for the Synthesis of Thiophene-Based Organic Electronic Materials." Chemistry of Materials **23**(6): 1594-1600.

94. Shafiee, A., Salleh, M. M., Yahaya, M. (2011). "Determination of HOMO and LUMO of [6,6]-Phenyl C61-butyric Acid 3-ethylthiophene Ester and Poly (3-octyl-thiophene-2, 5-diyl) through Voltametry Characterization." Sains Malaysiana **40**(2).

95. Shirakawa, H., Louis, E. J., MacDiarmid, A. G., Chiang, C. K., Heeger, A. J. (1977). Journal of the Chemical Society, Chemical Communications **578**.

96. Skoog, D. A., Holler, F. J., Nieman, T. A (1998). Principles of instrumental analysis. Philadelphia: Saunders College Pub.

97. Soderberg, T. (2010). Organic Chemistry with a Biological Emphasis, Section 2.1: Molecular orbital theory: conjugation and aromaticity. ChemWiki.

98. Song, S.-H., Park, S-H., Jin, Y-E., Kim, I., Lee, K-H., Suh, H-S (2011). "Synthesis and Characterization of Novel Conjugated Polymer with Thiophene and Benzimidazole." Bulletin of the Korean Chemical Society **32**(8): 3045-3050.

99. Spectronic, T. (2012). "Basic UV-Vis Theory, Concepts and Applications." Thermo Spectronic 1-28.

100. Steckler, T. T., Zhang, X., Hwang, J., Honeyager, R., Ohira, S., Zhang, X.-H., Grant, A., Ellinger, S., Odom, S., Sweat, D., Tanner, D. B., Rinzler, A. G.,Barlow, S., Brédas, J.-L., Kippelen, B., Marder, S. R., Reynolds, J. R. (2009). "A spray-processable, low bandgap, and ambipolar donor-acceptor conjugated polymer." Journal of the American Chemical Society **131**(8): 2824-2826.

101. Stille, J. K., Angew (1986). "The Palladium-Catalyzed Cross-Coupling Reactions of Organotin Reagents with Organic Electrophiles [New Synthetic Methods (58)]." Angewandte Chemie International Edition **25**(6): 508 – 524.

102. Sun, B., Hong, W., Aziz, H., Li, Y (2012). "Diketopyrrolopyrrole-based semiconducting polymer bearing thermocleavable side chains." Journal of Materials Chemistry **22**(36): 18950.

103. Tanaka, K., Tateishi, Y., Nagamura, T (2004). "Photoisomerization of Azobenzene Probes Tagged to Polystyrene in Thin Films." Macromolecules **37**(22): 8188-8190.

104. Tarkuc, S., Udum, Y. A., Toppare, L. (2012). "Tailoring the optoelectronic properties of donor–acceptor–donor type π-conjugated polymers via incorporating different electron-acceptor moieties." Thin Solid Films **520**(7): 2960-2965.

105. Tecklenburg, R., Paasch, G., Scheinert, S. (1998). "Theory of Organic Field Effect Transistors." Advance Materials for Optics and Electronics **8**: 285-294.

106. Thompson, B. C., Frechet, J. M. (2008). "Polymer-fullerene composite solar cells." Angewandte Chemie International Edition **47**(1): 58-77.

107. Tseng, C. W., Huang, D. C., Tao, Y. T. (2013). "Azobenzene-functionalized gold nanoparticles as hybrid double-floating-gate in pentacene thin-film transistors/memories with enhanced response, retention, and memory windows." ACS Applied Materials & Interfaces **5**(19): 9528-9536.

108. Vachal, P., Toth, Leslie M. (2004). "General facile synthesis of 2,5-diarylheteropentalenes." Tetrahedron Letters **45**(38): 7157-7161.

109. Wang, K., Wang, M. (2013). "Direct Arylation Polymerization: A Green, Streamlining Synthetic Approach to -conjugated Polymers." Current Organic Chemistry **17**.

110. Wunderlich, B. (1990). Thermal Analysis of polymeric Materials New York: Academic Press.

111. Yan, H., Chen, Z., Zheng, Y., Newman, C., Quinn, J. R., Dotz, F., Kastler, M., Facchetti, A (2009). "A high-mobility electron-transporting polymer for printed transistors." Nature **457**: 679-686.

112. Yan, Z. (2013). Development of New Building Blocks for Constructing Novel Polymer Semiconductors for Organic Thin Film Transistors Chemical Engineering University of Waterloo. **Master Thesis**.

113. Yan, Z., Sun, B., Guo, C., Li, Y. (2014). "Synthesis and properties of azothiazole based π-conjugated polymers." Journal of Materials Chemistry C **21**: 22-46.

114. Yan. Z., S., B., Li, Y. (2013). "Novel stable (3E,7E)-3,7-bis(2-oxoindolin-3-ylidene)benzo[1,2-b:4,5-b']difuran-2,6(3H,7H)-dion e based donor-acceptor polymer semiconductors for n-type organic thin film transistors." Chemical Communications (Camb) **49**(36): 3790-3792.

115. Zhao, X., Zhan, X. (2011). "Electron transporting semiconducting

polymers in organic electronics." Chemical Society Reviews **40**(3728–3743).

116. Zhu, Y., Champion, R. D., Jenekhe, S. A. (2006). "Conjugated donor-acceptor copolymer semiconductors with larg intramolecular charg transfer: synthesis, optical properties, electrochemistry, and field effect carrier mobility of thienopyrazine-based copolymers." Macromolecules **39**(25): 8712-8719.

117. Zollinger, H. (1987). "Colour Chemistry. Synthesis, Properties, and Applications of Organic Dyes." VCH, Weinheim.